U.S. DEPARTMENT OF ENERGY

Evaluation of Gas Retention in Waste Simulants: Intermediate-Scale Column and Open-Channel-Depth Tests

MR Powell
PA Gauglitz
KM Denslow
CM Fischer
DJ Heldebrant

MS Prowant
SA Sande
JM Davis
MR Telander

February 2014

Pacific Northwest
NATIONAL LABORATORY

Proudly Operated by **Battelle** *Since 1965*

DISCLAIMER

This report was prepared as an account of work sponsored by an agency of the United States Government. Neither the United States Government nor any agency thereof, nor Battelle Memorial Institute, nor any of their employees, makes **any warranty, express or implied, or assumes any legal liability or responsibility for the accuracy, completeness, or usefulness of any information, apparatus, product, or process disclosed, or represents that its use would not infringe privately owned rights**. Reference herein to any specific commercial product, process, or service by trade name, trademark, manufacturer, or otherwise does not necessarily constitute or imply its endorsement, recommendation, or favoring by the United States Government or any agency thereof, or Battelle Memorial Institute. The views and opinions of authors expressed herein do not necessarily state or reflect those of the United States Government or any agency thereof.

Evaluation of Gas Retention in Waste Simulants: Intermediate-Scale Column and Open-Channel-Depth Tests

MR Powell   MS Prowant
PA Gauglitz   SA Sande
KM Denslow   JM Davis
CM Fischer   MR Telander
DJ Heldebrant

February 2014

Pacific Northwest National Laboratory
Richland, Washington 99352

Summary

Gas generation in Hanford's radioactive waste storage tanks can lead to gas accumulation within the layers of settled solids (sludge) at the tank bottoms. The gas is formed principally by radiation-driven chemical reactions. Accumulation of gas within the sludge increases the sludge-layer volume, which decreases the available tank volume for waste storage. Further, accumulation of large amounts of gas in the sludge can potentially result in a relatively rapid release of the accumulated gas if the sludge-layer density is reduced to less than that of the overlying sludge or that of the supernatant liquid. Accordingly, a thorough understanding is needed of the circumstances that can lead to problematic gas accumulation in sludge layers. The Deep-Sludge Gas-Release Event Project (DSGREP) has been tasked with developing an improved understanding of these gas-release events.

Work by van Kessel and van Kesteren[1] implies that, for sludge of sufficient shear strength, a theoretical sludge depth (d_{max}) exists above which connected cracks and channels will develop that allow gas to escape. However, at depths below d_{max}, the overburden pressure is sufficient to prevent formation of the connected-channel network and any generated gas will tend to accumulate in the sludge until the sludge bulk density is low enough that the layer becomes unstable and the gas is released.

The tests described in this document were specifically designed to evaluate the accuracy of the d_{max} theory presented by van Kessel and van Kesteren. The d_{max} theory was tested with two sets of experiments. In one set of experiments, an 18.4-cm (7.25-in.)-diameter, 4.3-m (14-ft)-high (approximate dimensions) column of simulated sludge was used to directly test the prediction that increased gas retention occurs at depths below d_{max}. The sludge simulant was sufficiently deep that if the gas-retention behavior changed significantly at depths below d_{max} then those changes should have been detected. This test was performed twice, and in both cases no increase was noted in the retained-gas fraction at depths below d_{max}. Physical property measurements on simulant samples collected after each test showed relatively little consolidation/dewatering of the simulant; thus, the test results were not significantly impacted by water flow through the gas channels or by changes in simulant properties.

The second set of tests designed to evaluate the d_{max} theory involved measuring the maximum open channel depth for kaolin/water mixtures with shear strengths ranging from 80 to 2000 Pa. A 2-cm-diameter cylindrical channel was formed in the center of a container of kaolin-based sludge simulant and the depth at which the overburden pressure forced the channel closed was measured using an electrical-resistance-based probe. The d_{max} theory predicts a specific relationship between open channel depth and shear strength. For the case where simulant dewatering does not contribute to channel formation, the test results show that d_{max} theory over-predicts the open channel depth by roughly an order of magnitude.

None of the tests described in this document support the central prediction of the d_{max} theory that overburden pressure closes off gas-release channels at depths below d_{max}, thereby leading to elevated gas

---

[1] van Kessel T and WGM van Kesteren. 2002. "Gas Production and Transport in Artificial Sludge Depots." *Waste Management.* **22**:19-28.

retention and eventually an instability causing gas release. Test results indicate that the d_{max} theory is not a reliable predictor of the effect of sludge-layer depth on gas release from gas-generating sludge layers.

Acronyms and Abbreviations

DSGREP	Deep-Sludge Gas-Release Event Project
EPK	Edgar Plastic Kaolin
GVF	gas-void fraction
PNNL	Pacific Northwest National Laboratory
QA	quality assurance
QAP	Quality Assurance Program
WRPS	Washington River Protection Solutions
wt%	weight percent
WWFTP	WRPS Waste Form Testing Program

Nomenclature

d_f	average floc size, m
d_{max}	maximum sludge depth in which a channel remains open, m
E	modulus of elasticity, Pa
e	void ratio
g	gravitational acceleration, 9.81 m/s^2
h	elevation above bottom of the intermediate-scale column, m
h_s	simulant depth before compression, m
Δh_c	measured elevation change of simulant surface upon compression, m
h_{init}	initial elevation above the bottom of the intermediate-scale column, m
K_0	ratio between horizontal and vertical effective stress
ΔP	change in pressure at simulant surface upon compression, Pa
P_{atm}	atmospheric pressure, Pa
P_{hyd}	hydrostatic head above simulant surface before compression, Pa
r_0	radius of the undisturbed channel, m
t	time
x	retained gas fraction calculated by correlation with ultrasonic attenuation
x_i	mass fraction zerovalent iron
x_k	mass fraction dry kaolin clay
x_w	mass fraction water
y	measured ultrasonic signal attenuation
ν	Poisson's ratio
ρ_{gas}	density of the retained gas, kg/m^3
ρ_{gf}	gas-free simulant density, kg/m^3
ρ_s	dry density of the sediment particles, kg/m^3
ρ_w	water density, kg/m^3
τ_s	undrained shear strength, Pa
ϕ_{avg}	average retained gas fraction
ϕ_g	retained gas fraction
ϕ_{init}	initial retained gas fraction
ϕ_{local}	local retained gas fraction

Contents

Figures

Tables

1.0   Introduction

Gas generation in Hanford's radioactive waste storage tanks can lead to gas accumulation within the layers of settled solids (sludge) at the tank bottoms. The gas is formed principally by radiation-driven chemical reactions. Accumulation of gas within the sludge increases the sludge-layer volume, which decreases the available tank volume for waste storage. Further, accumulation of large amounts of gas in the sludge can potentially result in a relatively rapid release of the accumulated gas if the sludge-layer density is reduced to less than that of the overlying sludge or that of the supernatant liquid. Accordingly, a thorough understanding is desired of the circumstances that can lead to problematic gas accumulation in sludge layers. The Deep-Sludge Gas-Release Event Project (DSGREP) has been tasked with developing an improved understanding of these gas-release events.

In an evaluation of gas retention and release in sludge depots (i.e., large, dike-walled reservoirs filled with dredging spoils), van Kessel and van Kesteren (2002) discussed the role of channel formation above and below a critical depth (d_{max}) and stated:

"In the upper part of an artificial sludge depot, channel formation has an important contribution to drainage of gas; at depths below d_{max} this mechanism is not relevant, however."

"In the lower part of a depot, outflow of gas will only occur when the gas content is increased up to a level at which the sediment matrix becomes unstable."

However, DSGREP found no appropriately controlled experiment to corroborate the d_{max} theory hypothesized by van Kessel and van Kesteren. Wichman et al. (2000) studied gas retention in a 30-m-deep sludge depot and did not observe an increase in gas retention at lower depths as would be predicted by the d_{max} theory. The principal goal of the work described in this report is to conduct experiments designed specifically to determine whether the change in gas-retention behavior predicted by van Kessel and van Kesteren's d_{max} theory actually occurs and is a relevant concern for the Hanford radioactive waste storage tanks.

1.1   Description of d_{max} Theory

Work by van Kessel and van Kesteren (2002) implies that, for sludge of sufficient shear strength, a theoretical sludge depth (d_{max}) exists above which connected cracks and channels will develop that allow gas to escape. According to this d_{max} theory, for depths shallower than d_{max}, the gas generated within the sediment forms small bubbles which grow and eventually coalesce and form a network of connected channels. The generated gas moves through this channel network and eventually reaches the sludge surface, where it is released. For sludge-layer thicknesses greater than d_{max}, however, the overburden pressure is too high to allow formation of the connected-channel network and gas is retained in the sludge below d_{max} until a density-driven instability results in bulk movement of the sludge that releases gas upward and into the network of connected channels.

The value of d_{max} is predicted by the following equation from van Kessel and van Kesteren (2002):

$$d_{max} = \frac{\tau_s(1+e)}{K_0(\rho_s-\rho_w)g} \times \left[1 + \ln\left(\frac{r_0^2-d_f^2}{d_f^2}\right) + \ln\left(\frac{E}{2\tau_s(1+v)}\right)\right] \tag{1.1}$$

where τ_s = undrained shear strength, Pa
      e = void ratio
      K_0 = ratio between horizontal and vertical effective stress
      ρ_s = dry density of the sediment particles, kg/m^3
      ρ_w = water density, kg/m^3
      g = gravitational acceleration, 9.81 m/s^2
      r_0 = radius of the undisturbed channel, m
      d_f = average floc size, m
      E = modulus of elasticity, Pa
      ν = Poisson's ratio

Water flow through the interconnected, gas-channel network can result in the effective d_{max} being deeper than predicted by Equation 1.1. Sludge materials can dewater/consolidate in response to overburden pressure (also known as "self-weight") and the resulting water is released into the gas channels where it is driven by the gas flow toward the surface. The moving water erodes channel walls and maintains the channels open at depths that would otherwise not be expected to remain open based on d_{max} theory predictions. Because of this water-flow effect, the d_{max} predictions from Equation 1.1 apply specifically to cases where either sludge consolidation is complete (i.e., water flow has ceased) or the sludge experiences no significant consolidation (i.e., sludge dewatering is insignificant). For the kaolin-clay-based simulants used in the tests described in this report, consolidation/dewatering resulted in insignificant quantities of water production (see Section 3.1.2).

Two sets of tests were performed to directly evaluate the reliability of the d_{max} theory:
(1) intermediate-scale column d_{max} tests; and (2) open-channel-depth tests. Each set of tests is described briefly in the subsections below. Detailed descriptions of each set of tests are provided in Section 2.0.

1.1.1 Intermediate-Scale Column d_{max} Tests for Evaluation of d_{max} Theory

In the intermediate-scale column d_{max} tests, simulated tank sludge was prepared using kaolin clay, water, and zerovalent iron. This sludge simulant was loaded into an acrylic column (18.4-cm [7.25-in] inside diameter) to an initial depth of 4.3 m (14 ft). Over several days, the iron reacted to generate gas within the simulant matrix and form bubbles, slits, and cracks. Gas generation was allowed to continue until a steady-state gas-retention condition was reached (i.e., the retained-gas fraction in the simulant reached a maximum while the additional gas generated was continually released to the column headspace). The vertical, retained-gas-fraction profile was then determined to compare with the d_{max} theory prediction that the retained gas fraction should markedly increase at depths below d_{max}. This intermediate-scale column d_{max} test was performed twice. These tests are referred to as intermediate-scale column d_{max} tests to distinguish them from the tall column d_{max} tests that were performed in a 5-ft-diameter, 45-ft-high steel column and described in a separate document. The tall column d_{max} tests were performed after the intermediate-scale tests and are described in a separate document.

The target shear strength for both intermediate-scale column d_{max} tests was 350 Pa. The void ratio (e) equals the volume of water in the sludge divided by the volume of particulate and is calculated based on the known weight fraction of solids and the densities of kaolin particles and water. According to Wells et al. (2010, Figure 3.1), values for kaolin/water K_0 range from about 0.4 to 0.75, depending on the simulant shear strength. For τ_s=350 Pa the data predicts $K_0 = 0.55$ to 0.75 with a best-estimate value of about 0.65. The dry density of kaolin particles (ρ_s) is 2650 kg/m^3 (Wells et al. 2010) and the density of water at room

temperature (ρ_w) is 998 kg/m^3 (Lide 2003). The radius of the undisturbed channel is taken to be 0.5 cm based on visual observations of typical gas-channel sizes (Gauglitz et al. 2012) and on the r_o used by Crosato (1998) for d_{max} calculations.

The average floc size (d_f) is not accurately known for kaolin/water mixtures. However, d_f must clearly be larger than the mean particle size of kaolin[1], which is approximately 5.5×10^{-6} m (Bontha et al. 2010). For the purposes of estimating d_{max} for the testing, $d_f = 5.5×10^{-6}$ m is used. This approach is expected to be conservative with respect to d_{max} test design[2] since smaller values of d_f result in increased values for d_{max}. The floc size used by Crosato (1998) was 200×10^{-6} m.

Values for E and ν are estimated from τ_s using a correlation given in Wells et al. (2010) for shear modulus. The quantity $E/(2(1+\nu))$ is equal to the shear modulus, so the shear modulus estimate from Wells et al. (2010) is used in place of this expression in Equation 1.1. Extrapolating the data in Figure 3.5 of Wells et al. (2010) gives an estimate for the shear modulus for a $\tau_s = 350$ Pa kaolin/water mixture of about 67 kPa. A more conservative extrapolation approach yields a conservatively high estimate for the shear modulus of approximately 116 kPa. Both of these values are used in the calculations described below.

Table 1.1 shows various calculated values for d_{max} based on different assumptions for the various parameters in Equation 1.1. Calculations are included using $K_0 = 0.55$ (approximately the most conservative possible value for 350 Pa kaolin), $K_0 = 0.65$ (most likely value based on the data in Wells et al. 2010.), and $K_0 = 0.75$ (approximately the least conservative possible value for 350 Pa kaolin). A value for d_f of 5.5×10^{-6} m is included to represent the most conservative possible value. A value of 200×10^{-6} m is included as well to reflect the d_f used by van Kessel and van Kesteren (2002). Finally, values for the shear modulus of 116 kPa (most conservative) and 67 kPa (most likely) are used. Parameters held constant for the Table 1.1 calculations are $\tau_s = 350$ Pa, $e = 2.49$, $\rho_s = 2650$ kg/m^3, $\rho_w = 998$ kg/m^3, and $r_o = 0.5$ cm. Calculated d_{max} values range from about 1.28 m (4.2 ft) to as high as 2.80 m (9.2 ft). The 2.80-m (9.2 ft) d_{max} represents the most conservatively high estimate and this value was used to establish the required initial simulant depth in the intermediate-scale column. The sludge simulant depth used for the intermediate-scale column tests was 4.3 m (14 ft), which is greater than all the d_{max} values in Table 1.1; thus the simulant should have been sufficiently deep to allow observation of a change in gas-retention behavior at depths deeper than d_{max}. Using the best-estimate values for K_0 and shear modulus along with $d_f = 200×10^{-6}$ m predicts $d_{max} = 1.47$ m (4.8 ft).

The intermediate-scale column d_{max} tests were designed to ensure that the initial sludge simulant height is significantly greater than d_{max}. Thus, if d_{max} theory is correct, these tests should have revealed a significant increase in the retained gas fraction at depths below d_{max}. However, as is discussed in Section 3.0, no such increase was observed.

---

[1] EPK Pulverized kaolin clay from Edgar Minerals Inc. (Edgar, Florida).

[2] The principal test design consideration for the d_{max} tests is the depth of the simulant. The tests had to be conducted with an initial simulant depth greater than the largest expected d_{max}. A conservative approach was used in the selection of values for the parameters in Equation 1.1 to ensure the simulant depth used for the d_{max} tests was deeper than the largest expected d_{max}.

Table 1.1. Calculated d_{max} for Various Assumed Input Parameter Values

K_0	d_f (μm)	Shear Modulus (kPa)	Predicted d_{max} [a]
0.55	5.5	67	2.72 m (8.9 ft)
0.55	5.5	116	2.80 m (9.2 ft)
0.55	200	67	1.74 m (5.7 ft)
0.55	200	116	1.81 m (5.9 ft)
0.65	5.5	67	2.30 m (7.6 ft)
0.65	5.5	116	2.37 m (7.8 ft)
0.65	200	67	1.47 m (4.8 ft)
0.65	200	116	1.53 m (5.0 ft)
0.75	5.5	67	2.00 m (6.6 ft)
0.75	5.5	116	2.05 m (6.7 ft)
0.75	200	67	1.28 m (4.2 ft)
0.75	200	116	1.33 m (4.4 ft)

(a) To better illustrate the magnitude of the effects for various parameter changes, three significant figures are shown for the d_{max} values calculated in meters. Given the uncertainty in the input parameters, the d_{max} values should not be considered accurate to three significant figures. The values provided in Table 1.1 are intended simply to illustrate the range of likely d_{max} values for the sludge simulant used for the d_{max} column tests.

1.1.2   Open-Channel-Depth Tests for Evaluation of d_{max} Theory

The second set of tests designed to evaluate d_{max} theory involved making cylindrical, vertical holes through simulated tank sludge samples composed of kaolin clay and water. The depth at which the holes closed off due to the force of the overburden pressure is a direct measure of d_{max}. Sludge simulants covering a range of shear strengths from about 80 to 2000 Pa were tested in this manner. The predictions of d_{max} from Equation 1.1 for these simulants are compared with the observed maximum open channel depths to provide a direct check on the accuracy of the d_{max} equation. For the open-channel-depth tests, r_o in Equation 1.1 is taken to be 1 cm instead of 0.5 cm as was used in Section 1.1.1 for the intermediate-scale column d_{max} tests because of the need in the open-channel-depth tests to form the initial channel large enough to allow space for the sludge-detection probe.

Equation 1.1 predicts the maximum depth to which a channel in the sludge layer can remain open. According to d_{max} theory, at depths deeper than d_{max} the overburden pressure from the sludge above the channel is sufficient to overcome the sludge mechanical strength and force the channel closed. Small-scale laboratory tests were performed to directly determine the accuracy of the d_{max} predictions for a range of different sludge strengths. A 2-cm-diameter vertical channel was formed in each simulant sample from the surface down to the bottom of the 18.4-cm-diameter container. The total simulant depth was sufficient to ensure that the simulant would flow in and close off the channel. The depths at which the channels closed off were measured and compared with the d_{max} predicted by Equation 1.1. Figure 1.1 shows the variation of open channel depth, which is equal to d_{max}, with shear strength over the range of strengths used in the open-channel-depth testing. The predictions using "conservative parameter values" follow a similar approach to those used to develop the values in Table 1.1 (i.e., floc diameter is set to 5.5 μm, the shear modulus is set equal to the largest value implied by the data in Wells et al. [2010], and

K_0 is set to the smallest value implied by the data in Wells et al. [2010]). For the "expected parameter values," floc diameter is set to 200 μm and K_0 and the shear modulus are set equal to typical values based on the data in Wells et al. (2010).

To evaluate the d_{max} theory, the predictions in Figure 1.1 were compared with the experimentally determined, maximum open channel depths. As described in Section 3.0, d_{max} theory was found to significantly over-predict the actual maximum open channel depth (i.e., the measured maximum open channel depths are significantly shallower than predicted by d_{max} theory). The significant disagreement between measured open channel depths and those predicted by Equation 1.1 calls into question the accuracy of d_{max} theory as well as its usefulness for predicting changes in gas-retention behavior with increased sludge depth in Hanford's radioactive waste tanks.
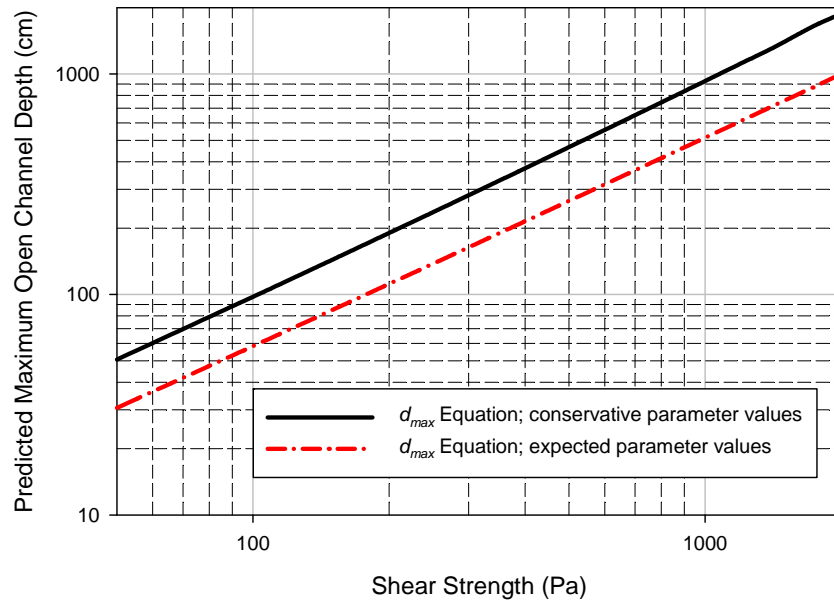
Figure 1.1. Predicted d_{max} for Kaolin Clay Sludge Simulant vs. Shear Strength

1.2 Test Objectives and Assumptions

The principal objective of the testing described in this document was to evaluate the accuracy of the d_{max} theory described by van Kessel and van Kesteren (2002). In the intermediate-scale column d_{max} tests, the d_{max} theory was directly tested by determining whether a significant increase in gas retention occurs at sludge depths deeper than d_{max}. In the open-channel-depth tests, the relationship between sludge simulant strength and the open channel depth was determined experimentally and then compared with predictions from the d_{max} theory.

1.3 Quality Requirements

This work is required to comply with all NQA-1 requirements and quality clauses as specified in the Statement of Work.

Pacific Northwest National Laboratory's (PNNL's) Quality Assurance Program (QAP) is based on requirements defined in the U.S. Department of Energy Order 414.1D, "Quality Assurance" and Title 10 *Code of Federal Regulations* Part 830, "Nuclear Safety Management,"
Subpart A – "Quality Assurance Requirements" (a.k.a. the Quality Rule). PNNL has chosen to implement the following consensus standards in a graded approach:

- ASME NQA-1-2000, Quality Assurance Requirements for Nuclear Facility Applications, Part I, Requirements for Quality Assurance Programs for Nuclear Facilities.

- ASME NQA-1-2000, Part II, Subpart 2.7, Quality Assurance Requirements for Computer Software for Nuclear Facility Applications.

- ASME NQA-1-2000, Part IV, Subpart 4.2, Guidance on Graded Application of Quality Assurance (QA) for Nuclear-Related Research and Development.

The procedures necessary to implement the requirements are deployed through PNNL's "How Do I…?" (HDI) system for delivering requirements to PNNL staff.

The work contained herein was performed in accordance with 64405-QA-001, *Support to Evaluation of Gas-Release Mechanisms in Deep Sludge Project Quality Assurance Plan*. The DSGREP uses the Washington River Protection Solutions (WRPS) Waste Form Testing Program (WWFTP) QAP (QA-WWFTP-001) at the Applied Research level as the basis for performing work. The WWFTP QAP implements an NQA-1-2000 QAP, graded on the approach presented in NQA-1-2000, Part IV, Subpart 4.2. This QAP and implementing procedures meet the quality requirements of NQA-1-2004, NQA-1a-2005, and NQA-1b-2007 as provided in the Statement of Work authorizing PNNL to conduct these studies.[1]

---

[1] This program has been independently evaluated by Acquisition Verification Services of Mission Support Alliance to specified requirements of NQA-1-2004 (including NQA-1a-2005 and NQA-1b-2007 Addenda) and is operating under WRPS-approved Supplier Quality Assurance Program Implementation Plan QA-WWFTP-002.

2.0   Experimental Approach

The purpose of this section is to provide a detailed description of the tests performed to evaluate d_{max} theory. Section 2.1 describes the procedure used for the intermediate-scale column d_{max} tests. Section 2.2 describes the procedure used for the open-channel-depth tests.

2.1   Test Procedure for Intermediate-Scale Column d_{max} Tests

The intermediate-scale column d_{max} tests involved filling an acrylic column (18.4-cm [7.25-in.] inside diameter) with gas-generating sludge simulant to an initial depth of 4.3 m (14 ft). As gas bubbles formed in the simulant, the sludge simulant expanded and the column height increased beyond its initial 4.3-m level. The column height increased until the rate of gas release from the top surface of the simulant column equaled or exceeded the rate of gas generation in the simulant. Periodically during the test, ultrasonic attenuation measurements were made at selected vertical locations to allow estimation of the retained gas fraction at each location. In addition, digital photographs of the column were taken periodically to document bubble shapes and to assist in the estimation of the volume fraction gas profile.

After a steady-state retained gas fraction was achieved and maintained, a compression test was performed in which the bubble-laden simulant was compressed by either adding water or compressed nitrogen to the column headspace. The resulting movement of the simulant throughout the column was recorded by digital photographs and time-lapse video. Upon completion of the compression tests, the simulant was removed from the column and samples taken for analysis to determine the extent of physical property changes in the simulant during the test.

The intermediate-scale column d_{max} test described above was repeated with only minor changes in experimental procedure to demonstrate replication of the results.

The following subsections provide detailed descriptions of the experimental apparatus, sludge simulant, and testing procedures.

2.1.1   Experimental Apparatus

The intermediate-scale column d_{max} tests used the experimental apparatus shown in Figure 2.1. The intermediate-scale column was composed of flanged sections of acrylic tubing. Each section was 70 cm (2.3 ft.) long with an outer diameter of 20.3 cm (8 in.) and an inner diameter of 18.4 cm (7.25 in.). Figure 2.1(a) shows one of the column segments. A ruler with millimeter-scale resolution was installed vertically on opposite sides of each column segment. The rulers were used to measure the level of simulant and water during the tests as well as the level of individual bubbles and cracks.

Figure 2.1(b) shows the intermediate-scale column, which was composed of nine individual segments. The photograph in Figure 2.1(b) was taken during column assembly with eight column segments shown. An elastomeric O-ring was installed in a groove between each set of flanges to provide a water-tight, gas-tight seal. When fully assembled, the column height is 6.3 m (20.7 ft). The column was surrounded by a metal support structure that served to keep the column vertically oriented over the platform scale at the bottom of the column. The platform scale at the base of the column was an Arlyn Scales Model 320M with a 455 kg (1000 lb) capacity. At each flange junction elevation, metal supports

with soft rubber pads on their ends extended inward from the support frame to within approximately 5 mm of the flange edges. These pads ensured that the column remained vertical but did not provide any vertical support that would affect the accuracy of the scale readings. Mass measurements from the scale were used to determine the quantities of sludge simulant and water loaded into the column. The scale is not visible in Figure 2.1(b) because the base of the column is surrounded by a 1-ft-high secondary containment vessel, which was installed to capture simulant and water in the event of a leak in the column. Access to the column was provided by a combination of ladders and an electrically powered scissor lift.

(a)   (b)
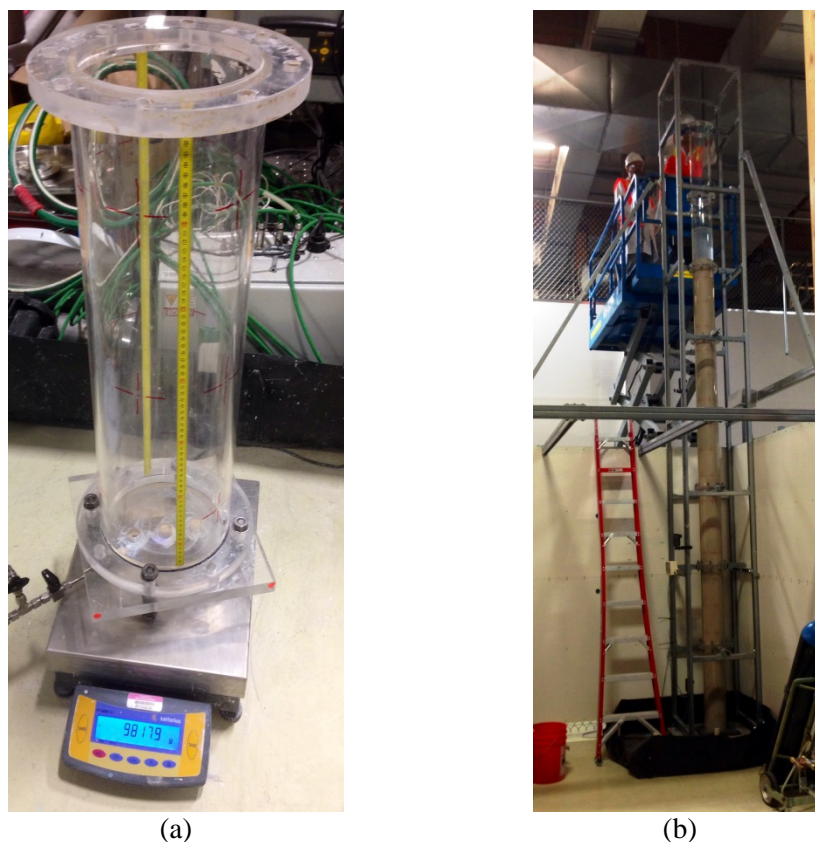
Figure 2.1. (a) Individual Acrylic Column Segment and (b) Assembled Intermediate-Scale Column

Before the d_{max} tests, a level/volume correlation was performed on the assembled intermediate-scale column. Measured quantities of room-temperature (21°C) water were added to the column and the water level determined by reading the rulers affixed to both sides of the column. These data were used to determine the volume of material contained in the column based on the ruler readings. Initial simulant bulk density was calculated using the simulant mass as indicated by the platform scale under the column along with the simulant volume as indicated by the ruler readings.

Figure 2.2 shows a schematic representation of the assembled intermediate-scale test column and gas-collection apparatus. Only six column segments are shown in the diagram, but nine were used for the testing. Once filled with the appropriate quantity of sludge simulant and water, a gas-tight, 2.5-cm (1-in.)-thick lid was installed on the top-most column segment. Valves on the lid allowed for introduction of nitrogen gas to purge the column headspace of air at the beginning of the test and hydrogen at the end of the test.
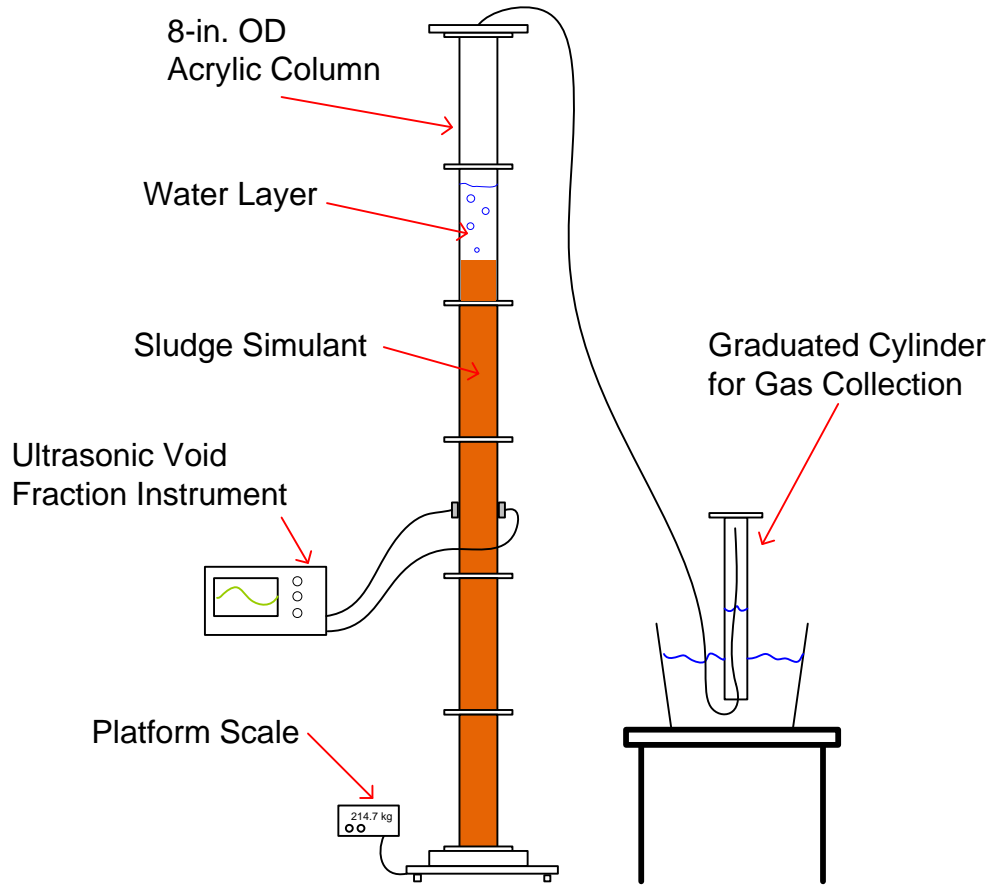
Figure 2.2. Schematic of Initial d_{max} Column Test Apparatus

Ultrasonic transducers were used to measure the ultrasonic attenuation of the sludge simulant at multiple vertical and azimuthal locations. The ultrasonic attenuation measurements are described in Section 2.1.3.

A polyethylene tube with an outside diameter of ¼-in. was connected to a valve on the column lid at one end and then routed inside an inverted, water-filled 1000-mL graduated cylinder. This graduated cylinder was used to collect and measure the volume of gas generated during the test. As the cylinder filled with generated gas, a small syringe was used to remove the accumulated gas; the cylinder readings before and after each gas removal were recorded.

The graduated-cylinder arrangement shown in Figure 2.2 was used for most of the first intermediate-scale column d_{max} test (Test #1). However, near the end of Test #1, relatively small, but significant variations in pressure were noted as the graduated cylinder filled and emptied. Because the headspace volume was much larger than the gas volume contained in the graduated cylinder, whenever gas was removed from the graduated cylinder using the syringe the amount of gas actually removed was significantly greater than implied by the difference between the "before" and "after" volume readings on the cylinder. The gas-collection rate could still be determined, but pressure corrections were required. To avoid the complication of applying these corrections to all the remaining test data, the gas-collection apparatus was changed to remove the pressure-variation effect. For the final two days of Test #1 and all of Test #2, the gas-collection approach shown in Figure 2.3 was used instead of that shown in Figure 2.2.

The generated gas was first collected in an inverted, 10-L water-filled beaker. Periodically, a mechanical pump was used to transfer gas out from the beaker and then into the 1-L graduated cylinder. Gas was then pumped out of the 1-L cylinder and vented to ambient. The "before" and "after" readings on the 1-L graduated cylinder could then be used as a direct measure of the gas-generation rate and a complicated pressure correction was not required.

8-in. OD
Acrylic Column

Water Layer

Sludge Simulant

Graduated Cylinder
for Gas Collection

Ultrasonic Void
Fraction Instrument

Platform Scale

214.7kg
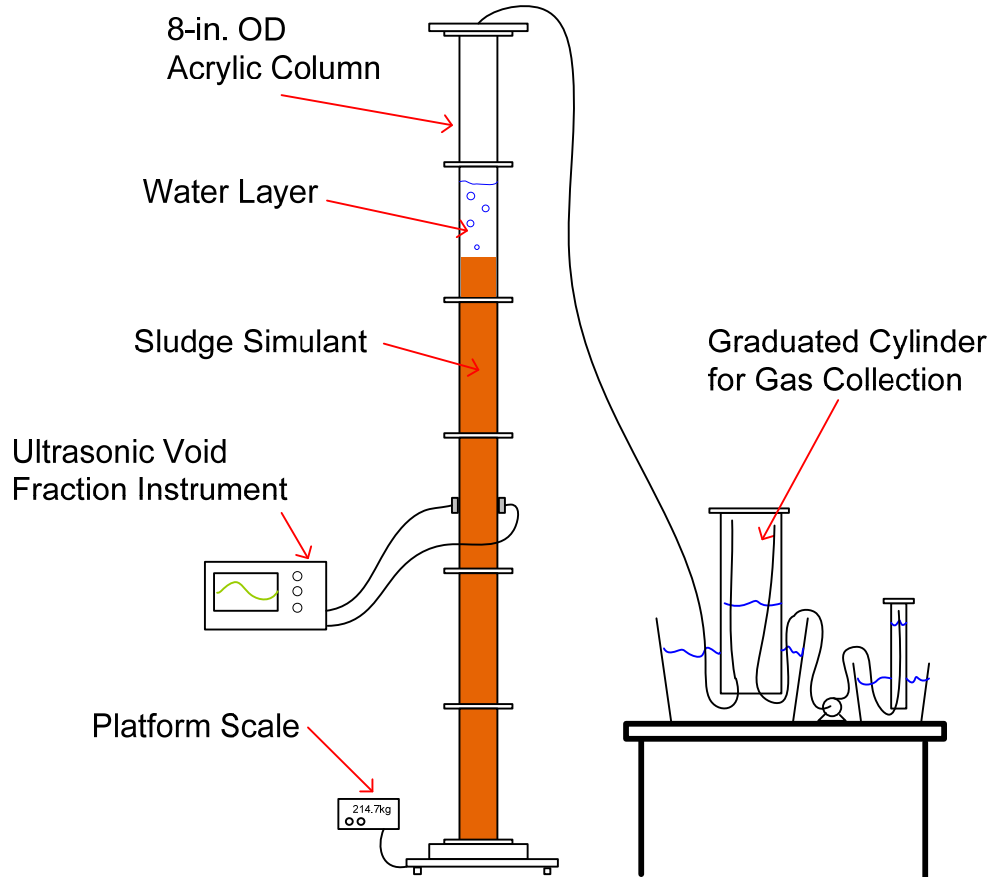
Figure 2.3. Schematic of Final d_{max} Column Test Apparatus with Modified Gas-Collection System

2.1.2   Kaolin-Based Sludge Simulant

Sludge simulant for the intermediate-scale column d_{max} tests was composed of kaolin clay, water, zerovalent iron, and a small quantity of biocide to inhibit biological activity within the clay mixture. The simulant used for the open-channel-depth tests was similar to the d_{max} simulant except that no iron was added. The kaolin clay used for all tests was EPK Pulverized kaolin clay from Edgar Minerals, Inc. (Edgar, Florida). The clay was packaged as a dry powder in 50-lb bags. All bags used in the tests were obtained from the same pallet to reduce the potential impact of batch-to-batch variability in clay properties.

Zerovalent iron was added to the simulant mixture for the intermediate-scale column d_{max} tests. After an induction period, the iron reacts with water to form gas (principally hydrogen), which creates the desired bubbles, slits, and cracks. The induction-period duration typically ranges from between 1 and 4 days. The zerovalent iron used for all the tests was Grade S-3700 Micropowder Iron from ISP

Technologies, Inc. (Wayne, New Jersey). Mt. Hood #480 Biocide from Mt. Hood Chemical Corporation (Portland, Oregon) was added to the water before the resulting mixture was mixed with kaolin clay and then zerovalent iron added, if necessary. Room temperature (~21°C), tap water from the City of Richland was used to prepare all sludge simulants.

Both intermediate-scale column d_{max} tests used the same sludge simulant composition: 52.30 wt% kaolin clay powder ("as is" from the bag), 47.44 wt% water, 75 ppm (by weight) of biocide, and 0.25 wt% zerovalent iron. The clay powder typically contained about 1.85 wt% water, so the measured weight percent solids of the simulant mixture should have been be 51.6 wt% when mixed according to the specified composition. In practice, however, some moisture loss occurred during mixing; thus the solids content was typically about 51.9 wt%.

The d_{max} sludge simulants were prepared by first mixing the kaolin clay and biocide-treated water in a mortar mixer (IMER Readyman 20) for approximately 2 hours until the clay/water mixture was visibly smooth (i.e., free of unmixed lumps). A plastic sheet covered the mixer during this process to reduce moisture loss. The mixture was then transferred into buckets and allowed to sit overnight to allow equalization of the moisture content within the clay. After equalization, the vane shear strength was measured on a 500-mL sample of the simulant to verify that its shear strength was within the target range of 330 to 400 Pa. The simulant was then transferred back into the mortar mixer for addition and mixing of the zerovalent iron. The iron powder was slowly added while the mixer continuously operated. To reduce clumping of the iron powder and ensure a more uniform final mixture, the iron was passed through a 100-mesh sieve placed above the mixing sludge simulant. Mixing continued for approximately 20 minutes after the last of the iron was added. Mixing was stopped once there was no longer visible evidence of inhomogeneity (e.g., variation in color and/or streaks of darker material indicating increased iron concentration).

In the first intermediate-scale column d_{max} test, the simulant loaded into the column was prepared in two batches. Two batches were required because the mortar mixer lacked sufficient capacity to mix all of the required simulant in a single batch. Both batches were prepared using the same composition as specified above. Once iron was mixed into the first batch, that batch was loaded into the intermediate-scale column while the second batch was loaded into the mixer and iron was added. Variation in composition between the two batches was small as determined by moisture-content analyses. However, concerns were raised that because the batch loaded in the bottom half of the column had its iron added approximately 3 hours before iron was added to the second batch, then gas generation would begin in the lower half of the column about 3 hours before it began in the upper half of the column. This difference in gas-generation start times could result in greater gas accumulation in the lower half of the column than would be obtained if gas generation began simultaneously throughout the column.

In the second intermediate-scale column d_{max} test, the simulant was again prepared in two separate batches, but both batches were completely mixed and loaded into buckets before loading of the intermediate-scale column began. As the column was loaded, ~1-L scoops of simulant were added from each batch in an alternating fashion. This approach ensured a reasonably uniform gas-generation start time throughout the column.

The sludge simulants used for the open-channel-depth tests were composed of kaolin clay, water, and biocide. The biocide concentration was maintained constant at approximately 75 ppm, but the fraction of kaolin clay was varied from 45.5 to 60.0 wt% to achieve a shear strength range of 100 to 2000 Pa. The

open-channel-depth simulants were mixed in a manner similar to that used for the d_{max} tests with the exception that no zerovalent iron was added.

Laboratory characterization of sludge simulant samples consisted of vane shear strength measurements and moisture-content analysis. Vane shear strength was measured according to a standard procedure[1] using a Haake Viscotester Model 550 fitted with a shear vane. Moisture-content analyses were performed using a Mettler-Toledo Model HR83 moisture analyzer. A small quantity of each sample (i.e., 5 to 8 g) was loaded into the moisture analyzer and then dried to 105°C. The mass loss upon drying was used to calculate the weight percent solids.

Sludge simulant bulk density was measured at the beginning of each intermediate-scale column d_{max} test by dividing the measured mass of simulant loaded into the column by the total volume of simulant loaded. This initial bulk density (ρ_{bulk}) of the simulant was used to estimate the initial volume fraction of gas contained in the simulant. Invariably, during the simulant mixing process some gas was entrained. This entrained gas reduced the bulk density to a value less than that expected based on the known densities of water, kaolin, and iron. By comparing the calculated gas-free density with the actual initial bulk density, the initial fraction of entrained gas was estimated. The density of kaolin clay particles is 2650 kg/m^3 (Wells et al. 2010) and the density of iron is 7870 kg/m^3 (Lide 2003). Water density varies significantly with temperature, but at the typical laboratory temperature of 20°C, its density is 998 kg/m^3. The gas-free density of sludge simulant at 20°C is given by:

$$\rho_{gf} = \frac{1}{\frac{x_k}{2650 \text{ kg/m}^3} + \frac{x_w}{998 \text{ kg/m}^3} + \frac{x_i}{7870 \text{ kg/m}^3}} \tag{2.1}$$

where ρ_{gf} = gas-free simulant density (kg/m^3)
          x_k = mass fraction dry kaolin clay
          x_w = mass fraction water
          x_i = mass fraction zerovalent iron

The gas-free simulant density and the observed initial bulk density were used to estimate the initial volume fraction of gas retained in the simulant using the equation:

$$\phi_g = \frac{(\rho_{gf} - \rho_{bulk})}{(\rho_{gf} - \rho_{gas})} \tag{2.2}$$

where ϕ_g = volume fraction retained gas
         ρ_{gas} = density of the retained gas (kg/m^3)

The retained gas was presumably air, which has a density of about 1.2 kg/m^3 at 20°C and 1 atm of pressure (Lide 2003). The average pressure experienced by the entrained air can be estimated based on the average lithostatic/hydrostatic head in the simulant column, which implies an average gas pressure of about 1.33 atm. The average retained-gas density is then estimated to be about 1.6 kg/m^3. The calculated

---

[1] Shear strength measurements are made according to PNNL Technical Procedure RPL-COLLOID-02, *Measurement of Physical and Rheological Properties of Solutions, Slurries and Sludges.*

volume fraction of retained gas is relatively insensitive to the estimated value for ρ_{gas}, so for the d_{max} testing described in this document it is not necessary to precisely determine the average air density.[1]

2.1.3 Ultrasonic Attenuation Measurements for Quantifying Gas Fraction

Ultrasound is a high-frequency, oscillating sound pressure wave that can be transmitted through opaque or transparent media that include solids, liquids, gases, or a combination thereof. Ultrasonic measurements are often performed in process-monitoring applications to non-invasively probe fluids in vessels and pipes to measure the physical properties of the fluid or detect certain physical phenomena. The sound field properties of ultrasonic velocity and attenuation are commonly measured via ultrasound and used to characterize concentration, density, and other physical properties for fluid mixtures and slurries.

Ultrasonic velocity is calculated by measuring the time required for an ultrasonic pulse to traverse a known distance (e.g., pipe diameter) and dividing it by the known distance. Ultrasonic attenuation is calculated by measuring the reduction in ultrasonic signal amplitude over a known distance and quantifying the change in amplitude relative to the starting material (e.g., gas-free sludge simulant) or a reference fluid (e.g., water). Ultrasonic attenuation measurements were ultimately used to quantify gas-void fraction (GVF) in the intermediate-scale column due to the sensitivity of attenuation to changes in GVF and the practicality of their application. The bubble-laden kaolin slurries did not lend themselves to ultrasonic velocity measurements due to the large gas bubble geometries and their sizes relative to the intermediate column diameter.

2.1.3.1 Background

Ultrasound can be very sensitive to the presence of gas bubbles in a liquid and this sensitivity can be used to characterize bubble-laden media. However, great care must be taken when selecting the ultrasonic measurement frequency or frequencies used to meet the measurement objective. Gas bubbles have resonance frequencies that, when excited by a sound wave of equivalent frequency, result in vibratory motion of the bubbles with a sharply peaked resonance at the fundamental pulsation frequency. Measurements performed over the resonance frequency or frequencies of gas bubbles in a liquid result in non-linear ultrasonic attenuation and velocity measurements. Figure 2.4 shows an example of the effect of bubble resonance on ultrasonic attenuation over a range of ultrasonic frequencies for gas bubbles in water. Bubble resonance is clearly achieved between 25 and 30 kHz, although the range of frequencies affected is broader than this.

Figure 2.5 shows an example of the effects of bubble resonance on ultrasonic velocity for a range of ratios of ultrasonic frequency to bubble resonance frequency. The ultrasonic measurement frequency equals the bubble resonance at a frequency ratio of 1.0 along the plot's abscissa. At ultrasonic frequencies well below the bubble resonance (i.e., frequency ratio is << 1.0), the velocity is independent of ultrasonic frequency, is less than that of bubble-free water, and can be accurately predicted by Wood's emulsion equation; at ultrasonic frequencies in the range of bubble resonance (i.e., frequency ratio ~1.0), the velocity first decreases and then rapidly increases to a value above that for bubble-free water; and at frequencies above resonance (frequency ratio is >> 1.0), the velocity decreases until it reaches the value for bubble-free water.

---

[1] For example, using values from Test #2, ρ_{gf} = 1.4764 kg/m^3 and ρ_{bulk} = 1.4673 kg/m^3 gives ϕ = 0.621% when ρ_{gas} = 0.0 kg/m^3, ϕ = 0.621% when ρ_{gas} = 0.0016 kg/m^3, and ϕ = 0.622% when ρ_{gas} = 0.0032 kg/m^3.
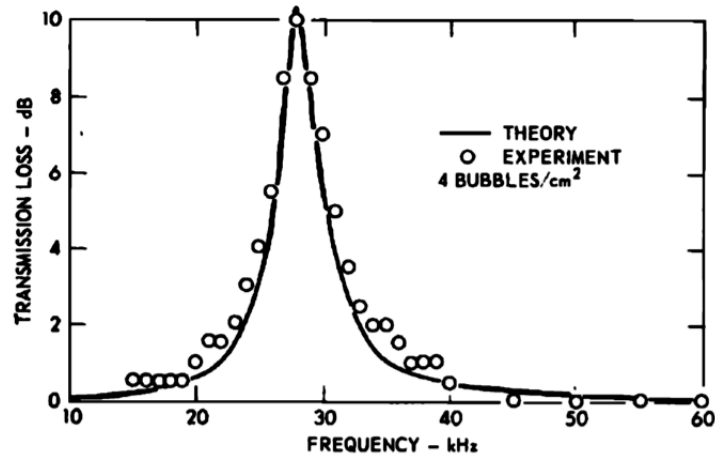
Figure 2.4. The Attenuation of Sound through a Screen of Bubbles (4 per square centimeter) of Uniform Size for Frequencies Ranging from 10 to 60 kHz (Anderson and Hampton 1980)
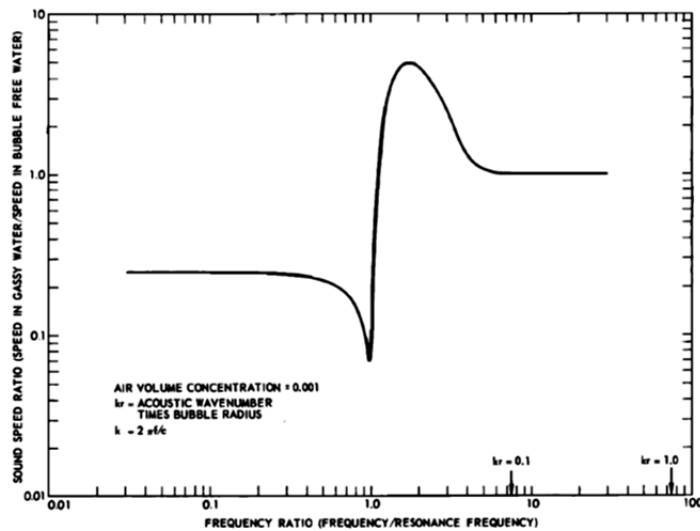
Figure 2.5. Ultrasonic Velocity for a Range of Ultrasonic Frequencies in Water Containing Bubbles of Uniform Size (Anderson and Hampton 1980)

The non-linear effects of bubble resonance on ultrasonic velocity and attenuation can be valuable for characterizing bubble sizes (or particle sizes) when that is the objective of the measurement. However, when the objective of ultrasonic velocity or attenuation measurements is to quantify gas concentration, then great care must be taken to select ultrasonic measurement frequencies that are either well below or well above the range of bubble resonances in the bubble-laden medium for a monotonic relationship to exist between gas concentration and these sound field properties.

Ultrasonic attenuation is the reduction of the pulse amplitude due to the absorption, scattering, and/or reflection of sound energy by the gas bubbles as the pulse propagates through the bubbly medium. In general, attenuation increases with increasing gas concentration. In addition, a monotonic relationship exists between attenuation and gas concentration at ultrasonic frequencies well below and well above the bubble resonances in a bubble-laden medium. The velocity of an ultrasonic pulse in a bubbly medium

can either be affected by the change in bulk compressibility when gas is added to a liquid or not affected at all. The ultrasonic velocity will only be influenced by the gas concentration if the ultrasonic measurement frequency is well below the lowest bubble resonance frequency in a bubbly medium; the velocity will remain essentially constant if the ultrasonic measurement frequency is above the highest bubble resonance frequency.

Previous investigators have developed theoretical models for ideal bubbly media that allow gas concentrations to be determined based on ultrasonic measurements. The bubbly media contained bubbles that had spherical or spheroidal shapes, uniform gas bubble sizes, and uniform distribution in the supporting liquid. For example, Wilson et al. (2008) performed ultrasonic measurements at ultrasonic frequencies below gas-bubble-resonance frequencies in kaolinite sediment. The gas concentrations of the gassy kaolinite sediment could be accurately predicted based on the ultrasonic velocity measurements and a simplified version of Wood's equation. However, the predictions were much less accurate for real gas-bearing media having non-spherical bubble shapes and heterogeneous bubble distributions. A working theory for non-ideal slurries with non-spherical bubbles has not been developed, rendering currently available direct inversion algorithms for ideal slurries unreliable.

Non-ideal bubbly media require empirically derived correlations between gas concentration and ultrasonic measurements with test configurations that represent the fluid mixture and the pipe or vessel characteristics. Investigators have developed empirically derived correlations between gas concentration and ultrasonic measurements for bubbly mixtures and gas-bearing sediments, sands, and muds. Kepkay and Cooke (1978) measured ultrasonic velocity through gas-bearing silty clay at frequencies below bubble resonance and generated a decreasing step-down relationship between acoustic velocity and GVF; Wilkens and Richardson (1998) performed measurements of ultrasonic velocity and attenuation over a wide range of acoustic frequencies in gassy seafloor sediments. They reported the sensitivity of ultrasonic velocity to the presence of gas bubbles only at ultrasonic frequencies below bubble resonance and the high sensitivity of attenuation to the presence of gas at frequencies well above and below the range of bubble resonance frequencies.

An example of an empirical relationship developed between ultrasonic attenuation and a 25-wt% kaolin/bentonite slurry during oxygen bubble generation from hydrogen peroxide decomposition[1] is provided in Figure 2.6.

2.1.3.2   Technical Approach

Gassy kaolin mixtures are known to yield non-ideal gas bubbles with a wide range of shapes and dimensions that include relatively small-diameter spheroidal bubbles to large gas-filled cracks/slits that are several inches wide. See Figure 2.7 for an example of the gas-void sizes and geometries in 300-400 Pa kaolin.

---

[1] The data in the figure are from Panetta PD, BJ Tucker, KM Judd, and AA Diaz. 2004. *Ultrasonic determination of gas volume fraction (proof of principle results).* Unpublished data, Pacific Northwest National Laboratory.
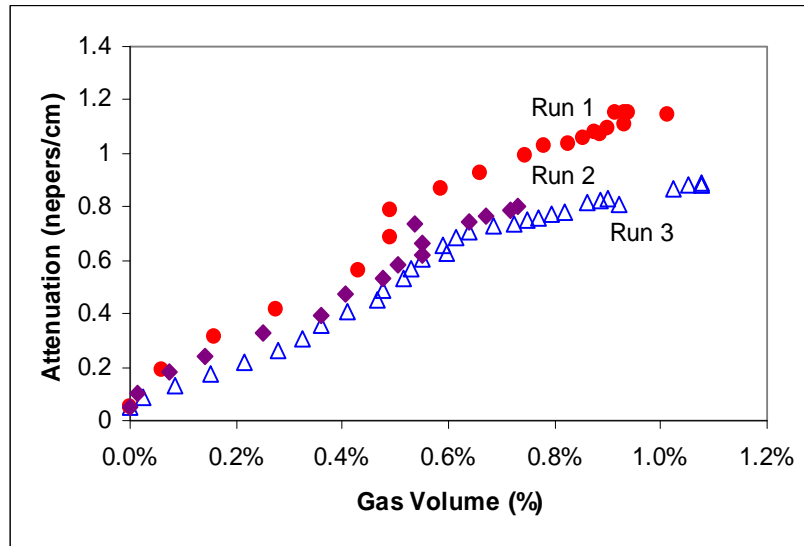
Figure 2.6. Example of a Trend between Ultrasonic Attenuation and GVF in a Kaolin/Bentonite Slurry

Figure 2.7. Photograph of Gas-Void Sizes and Geometries in 300-400 Pa Kaolin Clay Sludge Simulant

The wide range of possible bubble sizes is accompanied by a wide range of possible bubble resonance frequencies that have to be avoided when selecting ultrasonic measurement frequencies. The larger bubbles preclude the use of practical low ultrasonic measurement frequencies for ultrasonic velocity measurements given the relatively small diameter of the intermediate-scale column. A measurement frequency that would be well below the lowest bubble resonance frequency would have a wavelength larger than the diameter of the intermediate-scale column acrylic tube and be impractical to use.

Therefore, the combination of large gas voids and small tube geometry relative to below-resonance ultrasonic wavelengths resulted in the dismissal of ultrasonic velocity as a parameter for measuring GVF. Ultrasonic attenuation measurements that could be performed above the range of bubble resonance frequencies were determined to have a good likelihood of success based on research published in the scientific literature and previous laboratory testing at PNNL. For these reasons, ultrasonic-attenuation measurements were selected to quantify the GVF in the intermediate-scale column.

Additional considerations made when selecting the ultrasonic frequency for attenuation measurements were 1) the total attenuation of the sound field by the bubbly kaolin medium at its highest gas concentration and 2) the geometry of the intermediate-scale column tube diameter. The ultrasonic frequency selected for measurement had to be sensitive to changes in gas concentration without being completely attenuated by the bubbly medium at its highest gas concentration and had to result in at least three wavelengths across the measurement path (tube diameter). Early testing was performed to evaluate three candidate frequencies (i.e., 54, 150, and 500 kHz) for their abilities to meet these measurement requirements. A frequency of 500 kHz was ultimately selected for yielding the highest attenuation change per change in GVF.

In the absence of an available working theory to facilitate direct inversion analysis, i.e., a direct determination of GVF based on attenuation measurements, a relationship between ultrasonic attenuation and GVF had to be empirically developed through laboratory testing. The "calibration standard" used to develop the relationship between ultrasonic attenuation and GVF was kaolin slurry with the same composition as was used in the intermediate-scale column d_{max} tests. Details on the correlation development tests are provided in Section 2.1.3.3.

2.1.3.3   Measurement Description

Laboratory testing was performed to develop a mathematical correlation between GVF of the kaolin test slurry and ultrasonic attenuation. Testing was performed in a test section constructed of one segment of the intermediate-scale column. The 70-cm-long column segment was oriented vertically with the bottom end of the segment sealed to a 0.3-m × 0.3-m acrylic base plate. Two vertically aligned measuring tapes that spanned the length of the acrylic tube were adhered to the outside surface of the tube 180 degrees apart along the circumference. The test section vessel was filled to approximately 48 cm with the same sludge simulant as was used for d_{max} Test #2 (see Section 2.1.2). Approximately 5 cm of water was added to the top of the kaolin layer before the top end of the test section was sealed against a 0.3-m × 0.3-m square acrylic plate using a rubber O-ring. Plastic tubing placed between the head space of the test section and an immersed, inverted, and water-filled graduated cylinder were used to vent the test section and monitor gas evolution in the graduated cylinder. A drawing of the test section is provided in Figure 2.8.

The GVF generated by the oxidation of dispersed zerovalent iron particles in the kaolin slurry was quantified by measuring changes in the level of the water layer placed above the kaolin layer. These level measurements were made using the two rulers affixed to the outside wall of the test section. The water level measurements were used to define the reference "true-state" GVF of the kaolin slurry, which was assumed to be evenly distributed in the test section. The bulk GVF data are half the data required for the mathematical correlation between GVF and ultrasonic attenuation.
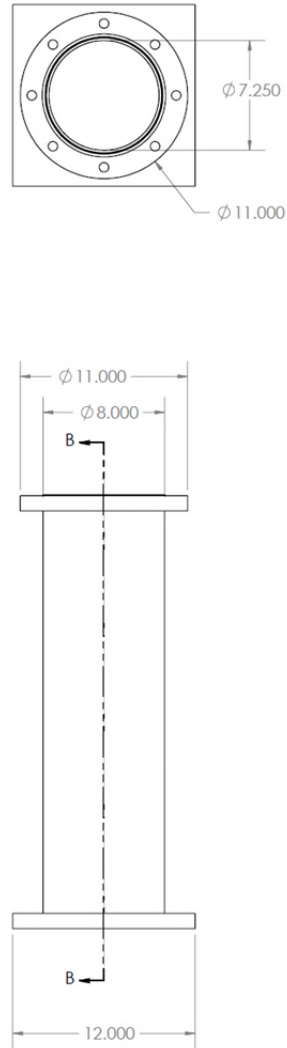
Figure 2.8. Drawing of the Test Section Used for Ultrasonic Correlation Testing (dimensions shown are in inches)

Ultrasonic measurements were performed immediately after the water level measurements to facilitate the correlation of the true state GVF with an ultrasonic response as accurately as possible. Ultrasonic measurements were performed with two identical 500-kHz, 6-mm diameter ultrasonic transducers circumferentially positioned 180 degrees apart at the same elevation on the outside wall of the test section. The transducers operated in thru-transmission mode (i.e., one transducer transmits an ultrasonic pulse that traverses the acrylic tube and is received by the opposite transducer). The transducers were aligned and held in position on the test section by a fixture strapped to the test section during measurements. The fixture minimized coupling and alignment errors by the operator and provided a means for applying consistent pressure to the transducers during the measurement process. Ultrasonic measurements were performed at three different circumferential locations at 15- and 30-cm elevations above the bottom of the test section. Ultrasonic pulses were generated by an Olympus 5058PR ultrasonic pulser-receiver unit. The same unit was used to amplify and filter the received pulse. The ultrasonic signals from the pulser-receiver were digitized, displayed, and saved to a LeCroy waveRunner 64Xi digital oscilloscope. Photographs of the test section with rulers and red crosshairs marking transducer measurement locations, the transducers, transducer fixture, and the test setup are provided in Figure 2.9.
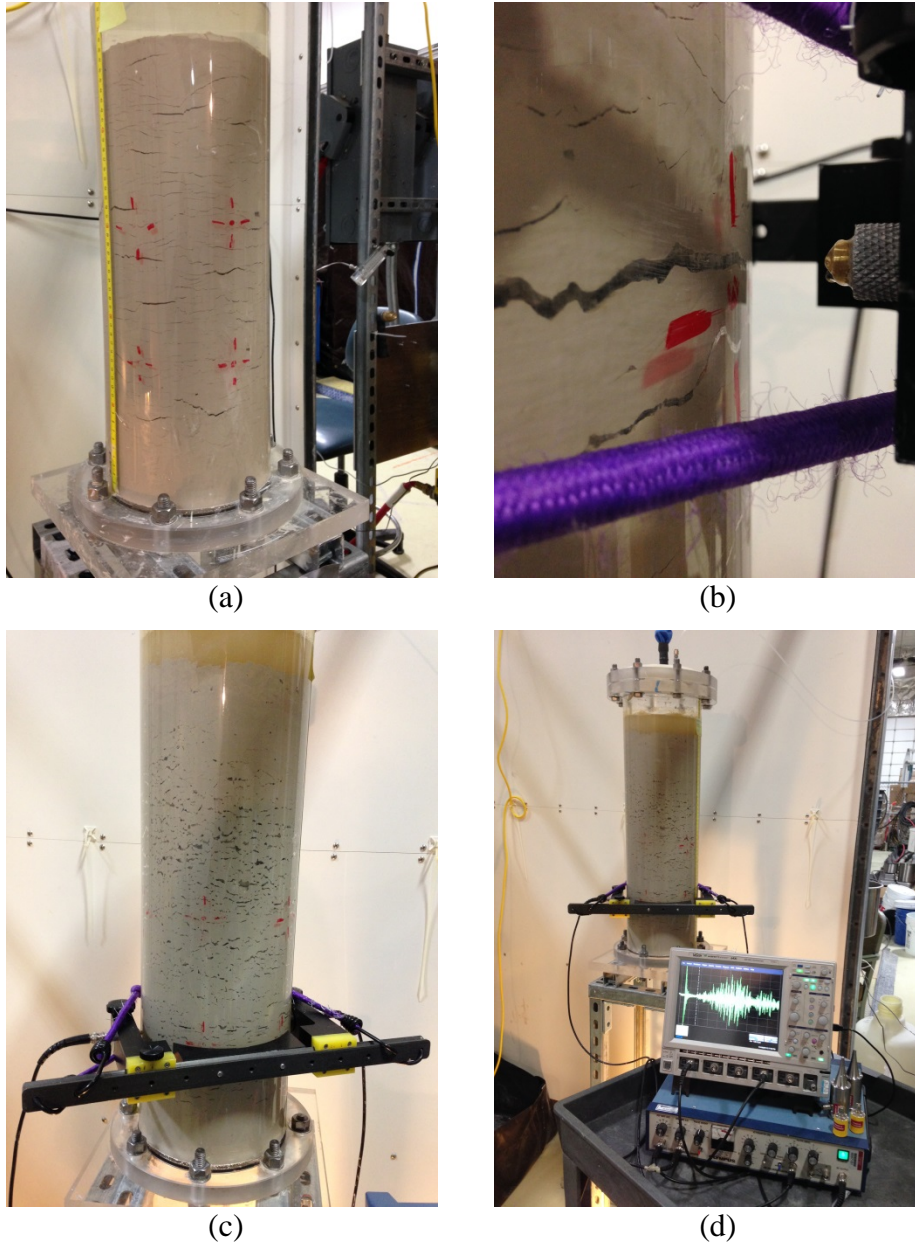
Figure 2.9. Photographs of (a) the Test Section with Red Cross-Hair Marks for Transducer Placement, (b) a 500-kHz Ultrasonic Transducer with Gel Couplant, (c) the Transducer Alignment Fixture Strapped to the Outside Wall of the Test Section, and (d) the Complete Measurement Setup

The ultrasonic signals collected at the three circumferential positions at the 15-cm elevation were averaged and the three signals collected at the 30-cm elevation were averaged for each measurement interval in time. Ultrasonic attenuation was calculated for each measurement interval in time relative to the gas-free sludge simulant measured at time=0. Attenuation is expressed in units of decibels (dB) using Equation 2.3:

$$\text{Attenuation (dB)} = 20 \log_{10} \frac{A_1}{A_2} \qquad\qquad (2.3)$$

where A_1 denotes the amplitude of the signal through the gas-free kaolin at time=0 and A_2 denotes the amplitude of a signal through the kaolin at a measurement interval after time=0. The attenuation data were subsequently time-correlated with the GVF values calculated from the water level measurements made immediately before the ultrasonic measurements. The time-correlated data were plotted as attenuation versus GVF. The 15- and 30-cm data were plotted separately and the data trend for each elevation was fit with a trendline. A nominal correlation equation to relate attenuation to GVF was calculated by averaging the two closely matched trendlines for the two elevations. The results of the ultrasonic correlation test data are presented in Section 3.1.3.2.

The same measurement apparatus and test setup were used for collecting ultrasonic data during the d_{max} tests in the intermediate-scale column. A photograph of the transducer fixture on the intermediate-scale column during a measurement is provided in Figure 2.10. The ultrasonic signals collected during the d_{max} tests were analyzed to obtain the signal amplitudes. The amplitude data at time=0 in the intermediate-scale column were averaged and used to generate A_1. The attenuation data from the d_{max} tests and the nominal correlation equation generated from the ultrasonic correlation tests were used to calculate GVF for the d_{max} tests. The results of the ultrasonically determined GVF data are presented in Section 3.1.3.2 as GVF versus time and column height versus GVF.
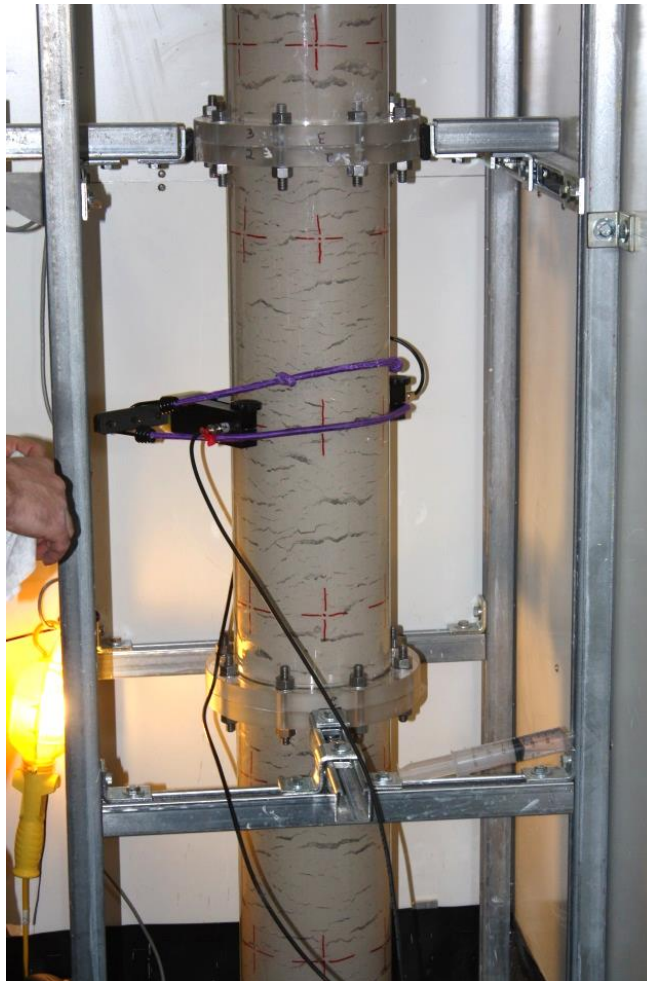

Figure 2.10.   Photograph of the Ultrasonic Transducer Fixture Installed on the Intermediate-Scale Column During an Ultrasonic Measurement

2.1.4   Photographs and Video Documentation

Digital still photographs and time-lapse video were taken during both intermediate-scale column d_{max} tests. Periodically, a Canon Model DS126181digital SLR camera with a 55-mm lens was used to photograph the west side of the column from bottom to top. When photographs were taken, three images were recorded for each column segment containing sludge simulant and/or water. These three images corresponded to the lower, middle, and upper portions of each segment. Only the west side of the column was photographed because much of the east side of the column was inaccessible due to the side walls surrounding the column on two sides. An effort was made to take each successive set of photographs at the same vertical locations with the camera oriented perpendicular to the column surface.

The digital images were used to document the size and shape of the bubbles, slits, and cracks in the simulant at selected periods during the tests. For d_{max} Test #2, photographs were taken with sufficient frequency to allow estimation of the retained-gas vertical profile in the simulant by analyzing the movement of visually identifiable bubbles between successive sets of images. This process is described in Section 3. Full sets of photographs were taken at the times/dates listed in Table 2.1 below.

Table 2.1. Times and Dates for Digital Image Sets

Test #	Date	Time
1	10/17/2013	16:00
	10/20/2013	11:00
	10/21/2013	09:00
	10/21/2013	16:30
	10/22/2013	12:45
	10/23/2013	09:15
	10/24/2013	14:30
2	11/01/2013	11:45
	11/04/2013	12:00
	11/04/2013	18:50
	11/05/2013	10:15
	11/05/2013	13:40
	11/05/2013	18:40
	11/06/2013	16:30
	11/07/2013	09:30
	11/07/2013	18:40
	11/08/2013	13:20

In addition to the still images, time-lapse video was obtained from selected elevations on the west side of the column. Initially, three Brinno Model TLC200 Pro time-lapse video cameras were mounted on the support structure of the intermediate-scale column and oriented with their 24- to 70-mm zoom lenses perpendicular to the column and focused on the ruler. These cameras were located near the midpoint of Segment #1 (i.e., approximately 0.35 m above the bottom of the column), near the midpoint of Segment #5 (i.e., approximately 3.2 m above the bottom of the column), and at the level of the liquid surface above the simulant layer (i.e., approximately 4.6 m above the bottom of the column at the start of the test). The camera viewing the liquid layer was moved as necessary to ensure that the liquid level was

in view. During d_{max} Test #2, a fourth camera was added to view the liquid level to ensure that images of the liquid level location were captured without the need to frequently move the camera. During the d_{max} tests, all time-lapse cameras were adjusted to record one image per minute.

Cameras were not employed for the open-channel-depth tests.

2.1.5   Testing Procedure

The intermediate-scale column d_{max} tests began when the prepared sludge simulant was loaded into the acrylic column. Simulant was added to the column by filling one segment at a time. The bottom-most segment was centered on the platform scale and approximately 9.5 liters of simulant added by scooping from buckets as described in Section 2.1.2. This quantity was sufficient to fill half of the segment. Next, a concrete vibrator (Multiquip Model CV-2) was operated and moved throughout the simulant until gas bubbles were no longer observed to be forming at the simulant surface (i.e., approximately 30 to 60 seconds). More simulant was then added until the segment was nearly full, and the vibrator degassing procedure repeated. The next column segment was then bolted into place and filled half-way with simulant before it was degassed with the vibrator. The vibrator was moved vertically through the simulant both to degas the simulant and to help mix the successive simulant layers. Figure 2.11 shows a test engineer operating the vibrator during simulant loading for Test #1.

Figure 2.11. Degassing the Sludge Simulant during Column Assembly

This procedure (i.e., filling the column segments with simulant and degassing) continued until the simulant surface was 4.3 m (14 ft) above the bottom of the column. Water was then carefully added to the column until the simulant was covered by a 0.3-m-thick water layer. The mass of sludge simulant and water were recorded along with the liquid level as indicated by the rulers affixed to the sides of the column. The water layer was added to the column to provide a clear indication of the volume of simulant and water contained in the column. The water/air interface was distinct and flat, which made it relatively easy to read the level as indicated by the rulers affixed to the sides of the column. The simulant/water interface, by contrast, was relatively rough and unclear.

Additional column segments were successively added and filled until all nine segments were installed. A top plate was then secured to the upper flange of the top segment. The top plate included fittings to allow the column headspace to be purged with nitrogen to remove oxygen before hydrogen generation occurred via reaction of the zerovalent iron with water. A tube was connected from the top plate and routed to near the base of the column where inverted graduated cylinders were used to collect and measure the generated gas as described in Section 2.1.1.

Once the top plate was installed and the gas-collection apparatus configured, the column for the next 7 to 8 days as the zerovalent iron reacted to produce gas throughout the sludge simulant. The liquid level in the column was monitored during this period both visually and using time-lapse cameras. Approximate measurements of the location of the simulant/water interface were also made periodically during the tests. Those measurements are considered approximate because, as noted above, the simulant/water interface was not always distinct. Because the liquid-level measurements were much more accurate, they were used to calculate the volume of gas retained in the column. In addition to the liquid- and simulant-level measurements, the volume of collected gas and ambient temperature were recorded.

Ultrasonic signal attenuation was measured as described in Section 2.1.3. Measurements were made twice per day during the portions of the test when the simulant was generating gas. In addition, measurements were made before gas generation was observed (as indicated by an increase in liquid level compared with the initial level); however, these measurements were not made twice per day because there was relatively little change between subsequent readings prior to gas generation.

The behavior of the simulant was monitored via digital photography and time-lapse cameras as described in Section 2.1.4.

Test monitoring continued until approximately 2 days after the retained-gas fraction reached a maximum. The duration of Test #1 was 9 days and the duration of Test #2 was approximately 8 days.

After the final set of liquid- and simulant-level readings, each test was declared complete. Prior to unloading the column, simulant compression tests were conducted (see Section 2.1.6). Following the compression tests, the simulant was removed from the column and the column disassembled one segment at a time. As the column was disassembled, simulant samples were collected at 0.3-m (1-ft) intervals. These samples were used for shear-strength measurements and moisture-content analysis.

2.1.6   End-of-Test Compression Measurements

Upon the completion of each d_{max} test, but before the column was emptied, a series of simulant compression tests were performed. These tests involved changing the pressure experienced by the bubble-laden column of sludge simulant and observing the resulting degree of simulant compression or expansion. The principal goal of these tests was to evaluate whether the retained-gas profile could be estimated by increasing the thickness of the water layer above the simulant and observing the resulting vertical, downward movement of the simulant. Photographs of the column were taken before and after each pressure change to allow for measurement of simulant movement at various depths throughout the column.

The compression test conducted at the end of d_{max} Test #1 involved only one change in pressure. After the column headspace was purged with nitrogen to remove hydrogen, the column top plate was removed and 24.8 kg of water carefully added to the existing water layer above the simulant. Before the water was added, a full set of digital photographs were taken of the west side of the intermediate-scale column. The time-lapse cameras were positioned to view the rulers on the west side of the column for segments 1, 3, and 5. A fourth time-lapse camera focused on the liquid-layer surface in segment 8. For these tests, the time-lapse cameras were adjusted to record one image per second.

A second set of photographs was taken 10 minutes after completion of water addition. A third set of photographs was taken 50 minutes after water addition. In addition to the photographs and time-lapse video, the heights of the water/air and simulant/water interfaces were observed and recorded before and after water addition.

The compression test at the end of d_{max} Test #2 was more extensive in that multiple changes in pressure were applied to the simulant column. The time-lapse cameras were set up in the same manner as for the Test #1 compression test and digital photographs were taken of the west side of the column before and after each change in column headspace pressure. Instead of water addition to apply the pressure changes, the column headspace was pressurized with nitrogen. After each pressurization step, the column headspace was vented back to atmospheric pressure. Using gas pressure to apply compression to the sludge simulant allowed multiple compression tests to be conducted more quickly and for application of more pressure than would be allowed by using water in the limited headspace in the intermediate-scale column.

Pressure in the column headspace was monitored using a water-based manometer mounted to the intermediate-scale column support structure. A 3-m-long ruler with millimeter-scale resolution was affixed alongside the water-filled manometer tube. One end of the manometer was connected to the column headspace and the other end was open to ambient pressure. Nitrogen was supplied to the column headspace via a separate tubing connection.

Five pressurization/vent cycles were performed for the Test #2 compression test. After each pressurization step, the column headspace was returned to atmospheric by opening a vent valve. The gas pressures applied in the column headspace were 8.6, 9.0, 18.2, 18.1, and 25.8 kPa. Upon completion of the compression tests, the simulant was removed from the intermediate-scale column and samples collected as described in Section 2.1.5. The compression test results are provided and discussed in Section 3.1.4.

2.1.7   Wall-Friction Tests in a Single Column Segment

Upon completion of the intermediate-scale d_{max} tests, a concern was raised that friction between the column wall and the simulant might significantly reduce the overburden pressure experienced by the sludge simulant at depth. If the walls provide a significant amount of vertical support, then calculation of d_{max} for the test is complicated by the fact that not all of the overburden pressure is acting to close off the gas channels as is assumed in the d_{max} theory.

A test was performed to address this concern. One of the acrylic column segments from the intermediate-scale column was loaded with sludge simulant using the same composition as was used for the d_{max} tests. The bottom of the column was first loaded with an 8.5-cm-thick layer of kaolin clay sludge simulant that did not contain iron but otherwise had the same composition as the simulant used in the d_{max} tests. The purpose of this layer was to prevent movement of gas from beneath the simulant up into the bubble-laden simulant. The initial depth of the iron-containing simulant was 38 cm; thus, the total initial depth of simulant in the column was 46.5 cm. A thin layer (1.4 cm) of water was then carefully added to the top of the simulant to aid in measurement of level changes. The simulant was then allowed to remain undisturbed in the column segment while gas was generated in the iron-containing portion of the simulant.

After gas retention peaked in the simulant, nitrogen was used to pressurize the bottom of the sludge column and force the simulant upward by approximately 10 cm. Nitrogen addition was then stopped and the gas pressure required to hold the simulant in its lifted position was measured using the manometer described in Section 2.1.6. Some of the gas from beneath the simulant was then released to allow the simulant to slip back downward by a few centimeters. The gas pressure below the simulant was then monitored using the manometer. Several of these tests were performed in which the simulant was lifted and the steady-state pressure measured before the simulant was lowered and the steady-state pressure again measured.

When the simulant was lifted, the gas pressure required to hold it in position was greater than expected. The simulant resisted movement due to friction between the simulant and the interior wall of the acrylic column. The expected gas pressure, in the absence of any wall-friction effects, was the weight of the simulant divided by the cross-sectional area of the column. The greater-than-expected pressure was due to the resistance to movement resulting from the wall-friction effect. Similarly, when the simulant is allowed to slip downward the wall-friction results in the gas pressure required to hold the simulant in its position being less than expected based on the simulant weight and column cross-sectional area. The difference between the measured pressure and the expected pressure is a measure of the magnitude of the wall-friction effect.

Figure 2.12(a) and Figure 2.12(b), repectively, show the simulant loaded in the column segment before and after it was lifted upward. The bottom-most 8.5 cm of simulant did not contain iron, which can be seen by the slightly lighter color of the iron-free layer. Results of the wall-friction tests are provided in Section 3.1.5.
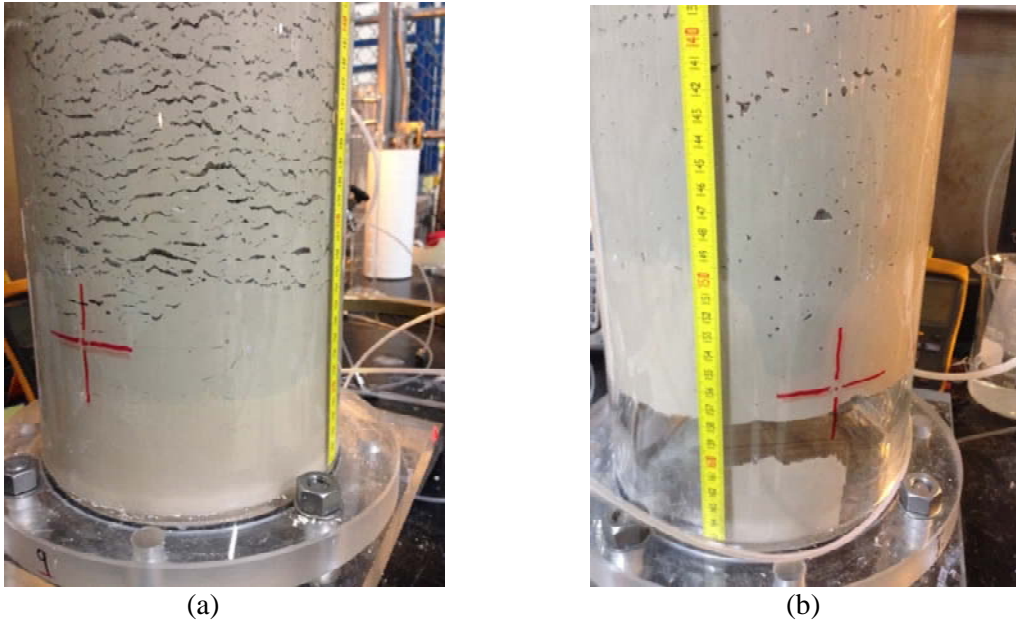
(a)   (b)

Figure 2.12. Simulant in Column Segment for Wall-Friction Testing

2.2   Open-Channel-Depth Tests

The open-channel-depth tests were designed to directly measure the depth at which a cylindrical channel is closed off by movement of the surrounding material in response to the overburden pressure. This channel close-off depth should be directly predicted by d_{max} theory (Equation 1.1); thus, the open-channel-depth tests represent a simple, direct check of the accuracy of the d_{max} theory predictions.

Relatively small-scale laboratory tests were performed in which a 2-cm-diameter vertical channel was formed in the center of sludge simulant loaded into one of the acrylic column segments from the intermediate-scale column tests.[1] An electrical-resistance-based probe was then slowly lowered through the open channel until it reached a depth where its reading changed to indicate the probe was surrounded by sludge simulant and the channel closed off. This depth was taken to be the open channel depth.

This test was conducted using sludge simulants composed of kaolin clay and biocide-treated water. No zerovalent iron was added to the sludge simulants used for open-channel-depth testing. The biocide concentration and simulant preparation was similar to that described in Section 2.1.2 with the exception that in some cases the simulants were mixed with a handheld rotary mixer rather than the mortar mixer. The mortar mixer was not necessary in some cases because the open-channel-depth tests required less simulant be prepared (especially for the low-strength tests). The sludge simulants used for the tests ranged in shear strength from approximately 80 to 2000 Pa with dried solids fraction ranging from 44.6 to 58.9 wt%, respectively.

The open-channel-depth procedure is shown schematically in Figure 2.13. Each open-channel-depth test involved first placing the channel-forming structure into the test chamber (see Figure 2.13a) and then loading the sludge simulant into the chamber and around the channel former (See Figure 2.13b). The

---

[1] One column segment provided sufficient simulant depth for all of the tests except that with the highest shear strength. For that test, two column segments were bolted together to provide the needed depth.
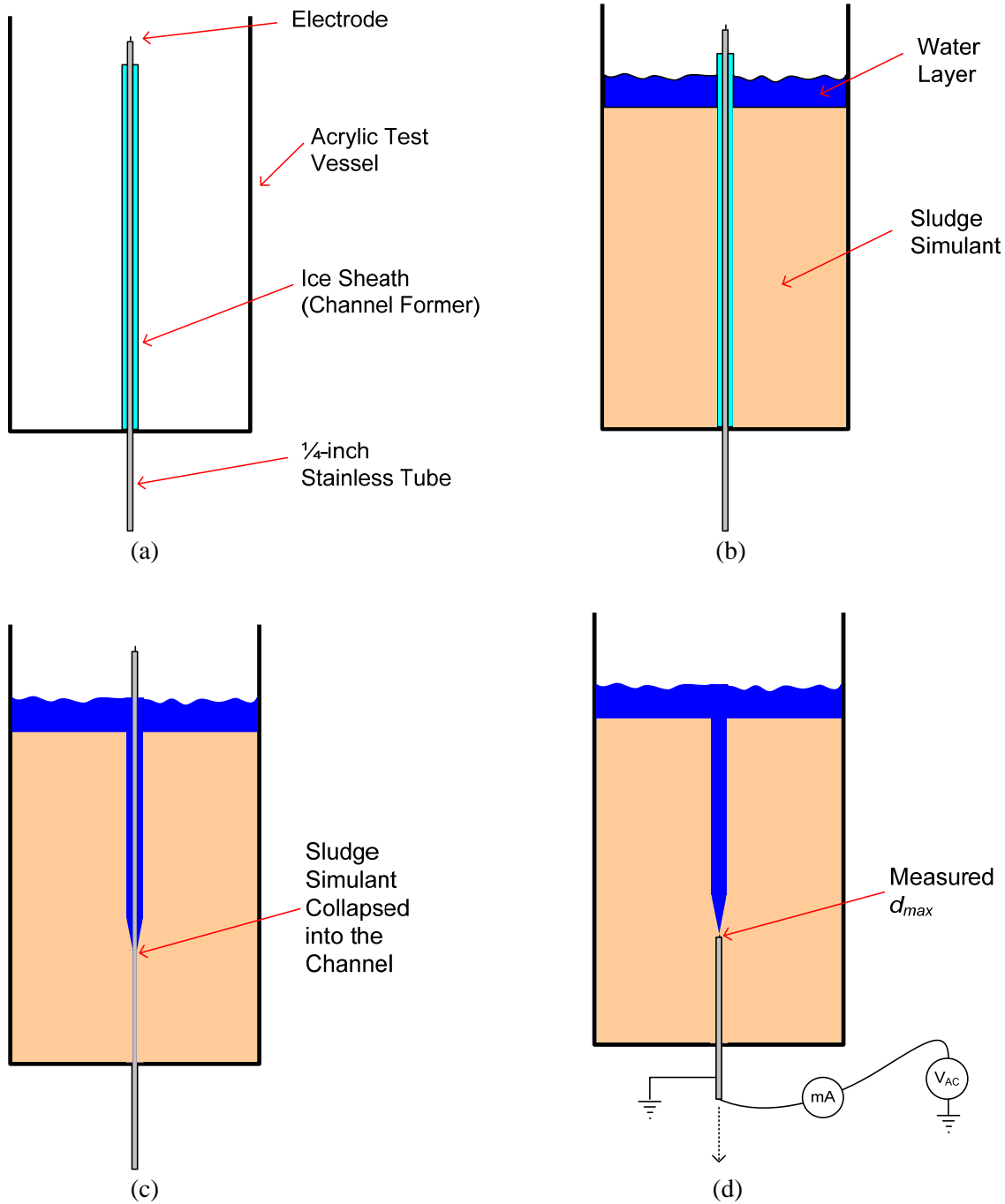
Figure 2.13. Open-Channel-Depth Testing Procedure

channel former was made from 2-cm-diameter, 10-cm-long cylinders of ice. Each cylinder had a 0.25-in.-diameter hole through its center. This hole allowed the cylinder to be positioned in the center of the test column as they were slid onto the 0.25-in.-diameter tube that supports the sludge sensor. Once the ice cylinders were in place, sludge simulant was added to a depth of at least 37 cm. Testing began with the lowest-strength simulant and proceeded with simulants of increasing shear strength. The low-strength results were extrapolated to predict the open channel depth for each stronger simulant. The

simulant depth was increased according to these predictions to ensure that a sufficient quantity of simulant was loaded for the higher-strength tests. Table 2.2 lists the shear strength, dried weight percent solids, and initial simulant depth used for each of the open-channel-depth tests.

Table 2.2. Simulant Properties and Loading

Shear Strength (Pa)	Weight Percent Solids (wt%)	Initial Simulant Depth (cm)
81	44.60	37.3
251	48.92	37.5
614	52.50	37.3
1030	55.80	43.0
1270	56.49	54.5
1980	58.87	110.5

Once the simulant was fully loaded around the ice cylinders up to the target depth, a 2.5-cm-deep layer of water was added on top to ensure that the channel remained fully filled with water once the ice melted (see Figure 2.13c). After the water layer was added, a minimum of 4 hours was allowed to pass before proceeding with the test to ensure the ice fully melted. Ice was used to form the initial channel in the sludge simulant to avoid disrupting the simulant layer. If a non-melting channel former was used (e.g., a solid rod), the simulant would be disrupted when the channel former was removed and this disruption could compromise the results. The ice-based channel formers were placed in the test vessel before the simulant to avoid imposing residual stresses on the sludge simulant as would occur if the simulant were loaded first and then the channel former pushed down through the simulant.

After the 4-hour wait period, the sludge sensor was energized with 27 VAC and the tube was slowly withdrawn vertically downward through the water layer at an average speed of 3.0 cm per minute until sludge simulant was detected in contact with the electrode at the top end of the tube (Figure 2.13d). Detection of the sludge simulant was indicated by a change in the measured current flowing through the probe. When in contact with sludge simulant, the measured electric current is higher than when in contact with water or dilute slurry. Figure 2.14 shows the sludge-sensor probe tip.

Figure 2.15 shows a plot of measured electric current through the probe versus probe depth. When the probe tip is initially located in the clear water layer above the sludge simulant the measured current is relatively low, but as the probe is submerged farther below the simulant surface the electric current increases, presumably because the channel walls have moved inward and the probe tip is closer to the sludge simulant, which has a higher electrical conductivity than the water. The clear change in electric current at a depth of 14.5 cm (as shown in Figure 2.15) indicates the probe tip was submerged in simulant at that depth. As the probe was lowered farther through the simulant, the electric current remained largely stable until the probe came within about 5 cm of the bottom of the column. At that point, the current again decreased. This behavior, which was observed in all of the tests, is attributed to there being less of the grounded 0.25-in. tube in contact with the simulant near the bottom of the column.
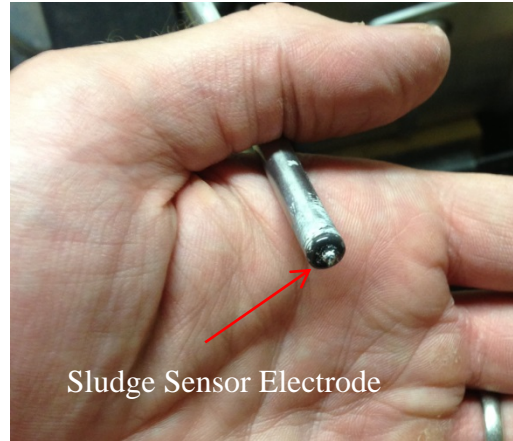
Figure 2.14. Sludge Simulant-Sensor Electrode at the End of a 0.25-in. Stainless Tube
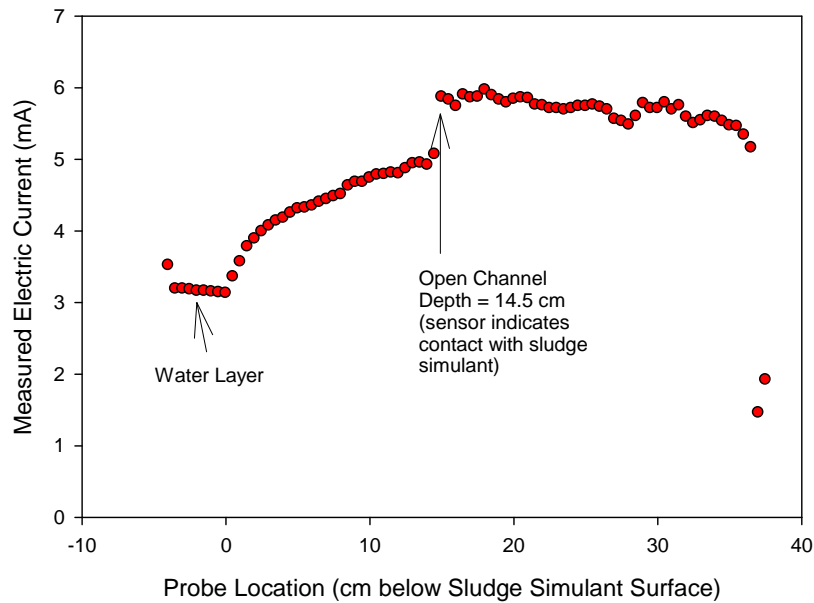
Figure 2.15. Example Sludge-Sensor Probe Data (taken from 251 Pa Test)

Figure 2.16 shows the open-channel-depth test apparatus ready for the start of a test. The sludge sensor is located in the center of sludge simulant and protruding up through the water layer. The tubing near the foreground wall was used to carefully add the water layer on top of the simulant layer and was removed before the each test commenced. Figure 2.17 shows a typical view after the test was completed and the water layer removed. The 2-cm-diameter hole is visible in the center of the column.

Figure 2.16. Open-Channel-Depth Test Apparatus

Figure 2.17. View from Above the Simulant After an Open-Channel-Depth Test

3.0   Results

This section provides the results of the intermediate-scale column d_{max} and open-channel-depth tests. The d_{max} tests did not indicate increased gas retention at depths below the calculated d_{max}. The open-channel-depth tests indicated that the overburden pressure was sufficient to close off gas channels at depths much shallower than those predicted by d_{max} theory. Taken together, these results imply that d_{max} theory does not accurately predict a change in gas-retention behavior at depths below d_{max}. Further, the open-channel-depth results show d_{max} is shallow enough that many previously conducted gas-retention tests used sludge-simulant layers deeper than d_{max} yet gas transport out of the simulant was observed in those tests even though d_{max} theory would have predicted otherwise (e.g., Gauglitz et al. 2012). Sections 3.1 and 3.2 discuss the intermediate-scale column tests and the open-channel-depth tests, respectively.

3.1   Intermediate-Scale Column d_{max} Test Results

Two tests were conducted in the intermediate-scale column with the goal of determining whether gas retention increases below a depth consistent with the predicted d_{max} (Equation 1.1). Neither test showed evidence of increased retained gas in the lower levels of the column. The detailed results of the d_{max} tests are provided in this section.

Figure 3.1 shows photographs taken at the conclusion of d_{max} Test #2 at various elevations along the column. There is no visually apparent, qualitative difference either in retained gas fraction or in the characteristics of the bubbles and cracks near the wall of the column. Visual observations made throughout both d_{max} tests were consistent with this statement and no evidence for differences above and below d_{max} was found. As discussed in Section 1.1.1, d_{max} in the intermediate-scale tests is predicted to occur at depths at or below 2.8 m. The photographs in Figure 3.1(a) and Figure 3.1(b) were taken from depths below 2.8 m.

3.1.1   Average Gas Retention and Cumulative Gas Generation

The liquid level in the column was monitored and recorded during the d_{max} tests to allow calculation of the average retained-gas fraction in the simulant. Changes in the liquid level directly reflect changes in the volume of gas retained in the sludge simulant. The initial retained-gas fraction was calculated as described in Equation 2.2 using the measured mass and volume of simulant added. As additional gas is generated by reaction of the zerovalent iron, the liquid level in the column increases and the volume associated with this level increase is a direct measure of the volume of gas retained in the sludge simulant.

Figure 3.2 shows the average retained-gas fractions for both d_{max} tests. The initial retained-gas percentages were approximately 0.6 to 0.7 percent. After the 4- to 5-day induction periods, significant gas generation was observed. Over the next 2 days, the retained-gas percentages increased to between 17 and 18 percent. After reaching their peaks, the retained-gas fractions decreased over the remaining 2 days.

(a)

(b)

(c)

(d)

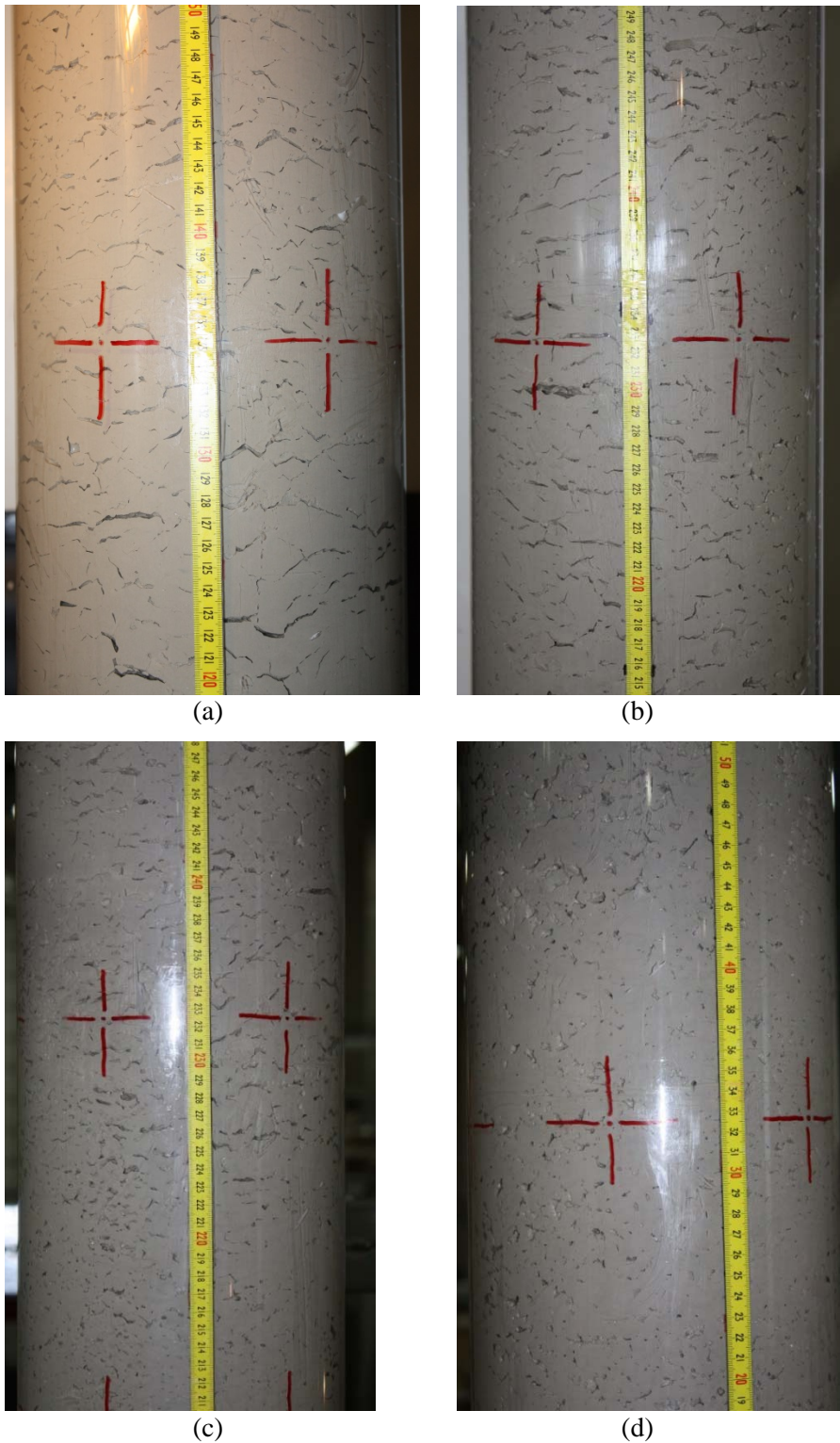**Figure 3.1**. Photographs of the Simulant in the Intermediate-Scale Column at Four Elevations at the Conclusion of d_{max} Test #2 (time = 187 h). The vertical centers of the photographs are at the following elevations and simulant depths: (a) elevation = 0.35 m, depth = 4.65 m; (b) elevation = 1.75 m, depth = 3.25 m; (c) elevation = 3.1 m, depth = 1.9 m; (d) elevation = 4.6 m, depth = 0.4 m.
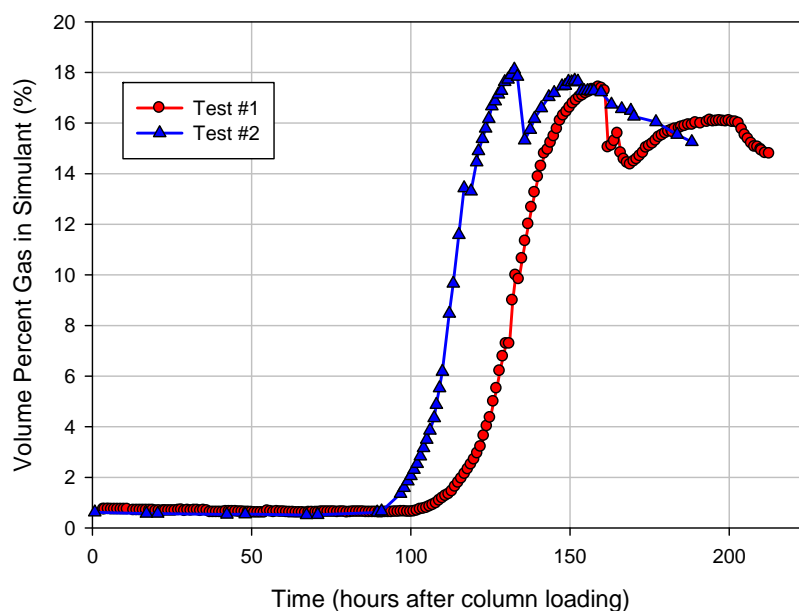
Figure 3.2. Volume Percent Retained Gas vs. Time for d_{max} Tests #1 and #2

Figure 3.3 and Figure 3.4 show the retained-gas volume in the sludge simulant along with the total gas generated during d_{max} Tests #1 and #2, respectively. The retained-gas volume is determined directly from the volume increase indicated by the liquid-level increase during the tests. The total gas generated is the volume of gas released from the column headspace during the test. As described in Section 2.1.1, the volume of gas released from the headspace was monitored continually throughout the tests by collection of gas in inverted, water-filled, graduated cylinders. All gas volumes reported in this section are referenced to 20°C and 1.0 atm pressure.

Figure 3.3 and Figure 3.4 show that for approximately the first 20 hours after gas generation begins, the volume of gas retained in the simulant is approximately equal to the volume of gas released from the column headspace. Relatively little gas is released from the simulant during this period because the bubbles, slits, and cracks forming in the simulant have not yet formed an interconnected network that allows vertical transport of gas up to the simulant/water interface where the gas is released to the column headspace. However, after the initial 20-hour period the total gas generated continues increasing while the retained-gas volume levels off at 20 to 25 L. During both tests, in excess of 80 L of gas was expelled from the column headspace. The total gas generated was roughly four times the volume of gas retained in the sludge simulant; thus the maximum retained-gas fraction was clearly not limited by insufficient gas generation and the quantity of zerovalent iron added to the simulant was sufficient to ensure that the true maximum retained-gas fraction was achieved.

Figure 3.5 shows the gas-generation rate for both d_{max} tests. In general, the gas-generation rates are in the 1-to-2 L/hr range and show a decreasing trend after a maximum is reached at a time corresponding roughly with the time at which the simulant reached its maximum retained-gas fraction.
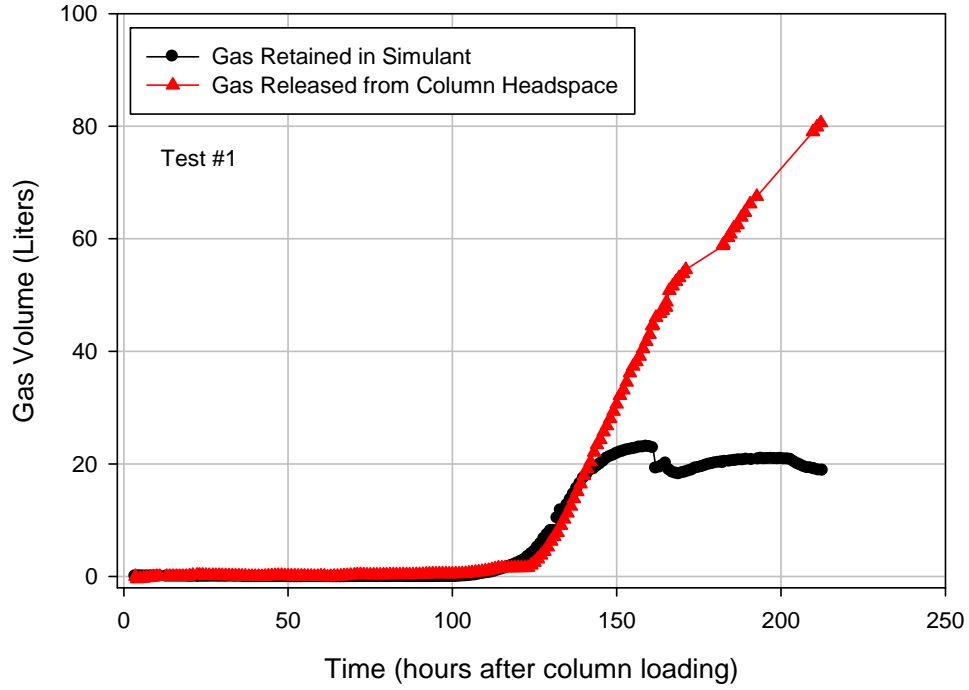
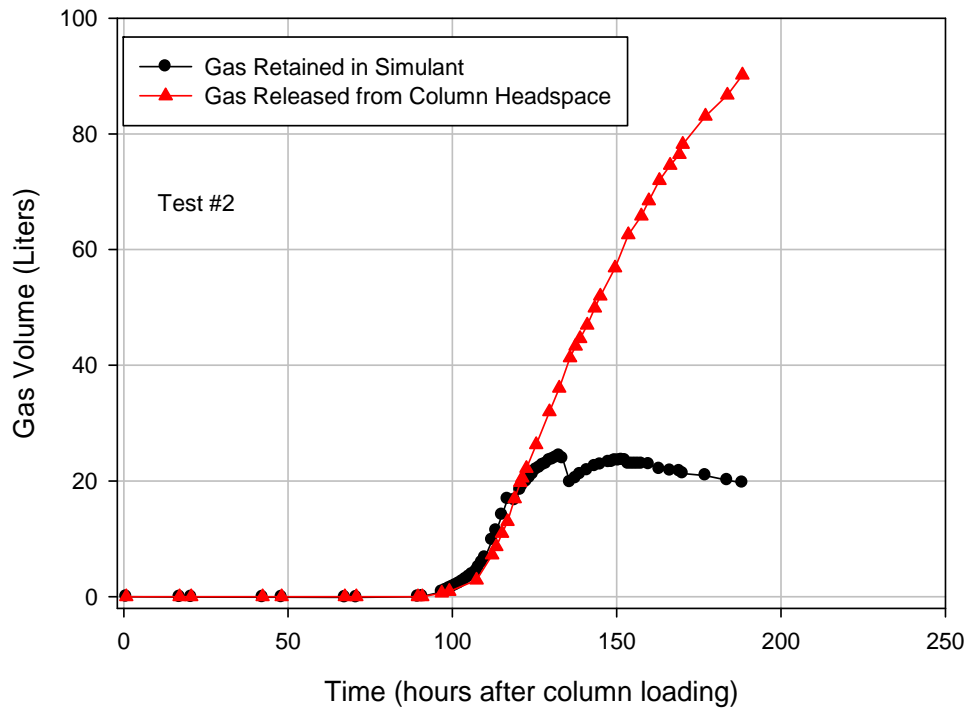**Figure 3.3**. Retained-Gas Volume and Total Gas Volume for d_{max} Test #1

Figure 3.4. Retained-Gas Volume and Total Gas Volume for d_{max} Test #2
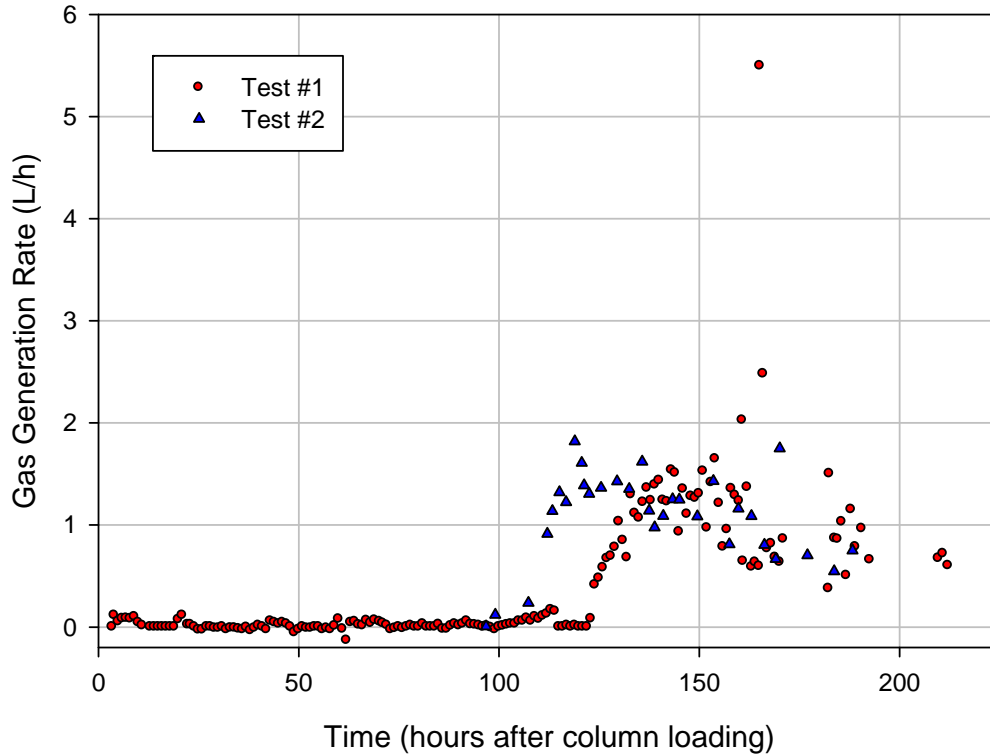
Figure 3.5. Gas-Generation Rate during d_{max} Tests

3.1.2   Sludge Simulant Characterization

The physical properties of the sludge simulants were measured before and after each d_{max} test. These measurements were made to allow calculation of d_{max} based on the actual simulant shear strength for each test to ensure that the calculated d_{max} was less than the depth of the simulant in the intermediate-scale column. The principal goal of the intermediate-scale d_{max} tests was to determine whether gas retention increases at depths below d_{max}; to satisfy this goal, the tests required the calculated d_{max} to be less than the initial 4.3-m (14-ft) simulant depth.

Samples of the sludge simulants used in Tests #1 and #2 were collected at the beginning of each test, as the intermediate-scale column was loaded. The vane shear strength and moisture content of the samples were measured. For Test #1, the initial weight percent solids was 51.81 wt% and the shear strength was 380 Pa. For Test #2, the initial weight percent solids was 51.87 wt% and the shear strength was 330 Pa. The same simulant composition was used for both tests, so the shear strength and weight percent solids values were, as expected, similar for both tests.

Some consolidation of the sludge simulant was expected during the tests, because overburden weight tends to force water from the simulant in the lower levels of the column. Consolidation of the simulant was a concern because as the simulant solids fraction increases there is a corresponding increase in shear strength.

Upon completion of each d_{max} test, simulant samples were taken at 0.3-m (1-ft.) intervals as the column was disassembled and emptied. These samples were subjected to shear strength and weight

percent solids measurements. The purpose of these measurements was to verify that the simulant did not consolidate during the test and reach a point where its strength would predict that d_{max} is deeper than the initial simulant depth (4.3 m). Figure 3.6 shows the post-test sample analysis results for Test #1. Some consolidation is evident in both the weight percent solids and shear strength values. The initial values are shown on the plots for comparison as a vertical dashed line. In addition to the gravity-driven consolidation effects, reaction of zerovalent iron with water during the test results in a small increase in the solids fraction. If all of the iron reacts, the increase in solids content is approximately less than or equal to 0.16 wt%.

The shear strength values shown in Figure 3.6 for the three samples collected nearest the column bottom were estimated based on the measured weight percent solids corresponding to those locations. The shear strength measurements for those three samples were inaccurate due to moisture loss from the samples before measurement. The post-test samples continued to generate gas via the zerovalent iron reaction and the containers for the three samples in question were inadvertently filled too near the top of the 0.5-L sample container. Gas generation expanded the simulant inside the container and forced water out from under the sample-container cover before the shear strength measurements were made. No other samples were affected by this issue. For Test #2, the sample-collection procedure was adjusted to ensure that all sample containers were filled with less simulant to guard against water loss resulting from continued gas generation.

Figure 3.7 shows the post-test sample analysis results for Test #2. As in Test #1, the Test #2 data show that some consolidation is evident because most of the data values are increased compared with the initial weight percent solids and shear strength measurements.

As expected, a small amount of sludge simulant consolidation occurred during both d_{max} tests. However, the change in simulant properties due to consolidation was not sufficient to increase the calculated d_{max} to a level greater than the initial simulant depth. The quantity of water loss from the sludge simulant associated with the observed consolidation is small and not sufficient to result in significant erosion of the gas-channel walls (see Section 1.1). Further, the change in simulant physical properties resulting from the consolidation during the test was not sufficient to result in d_{max} exceeding the sludge simulant depth used for the d_{max} tests.

According to Figure 1.1, even if the conservative parameters are used in the d_{max} calculation, the simulant shear strength must exceed about 530 Pa before d_{max} exceeds 4.0 m (13.1 ft). If the "expected parameter values" are used instead, the shear strength must exceed 1060 Pa before d_{max} exceeds 4.0 m. The 4.0-m depth corresponds to the depth of the sample collected at the 0.3-m height in the column.[1] For both tests, the shear strength measured at this elevation is well below these limiting values: For Test #1 the shear strength for the 0.3-m sample was 450 Pa, and for Test #2 the shear strength for the 0.3-m sample was 400 Pa. Because the shear strengths of the consolidated, post-test samples were lower than the limits implied by the d_{max} theory for a d_{max} of 4.0 m, we conclude that the initial simulant loading in the column was sufficiently deep to ensure a shift in gas-retention behavior would have been detected if d_{max} theory were correct.

---

[1] The bottom-most sample shows the highest post-test shear strength for both d_{max} tests and these shear strengths imply larger d_{max} values than the samples at the 0.3-m and higher elevations. However, the properties of the bottom-most sample are not relevant to the evaluation of the d_{max} theory in this case because the test arrangement did not allow quantification of the retained gas fraction at the very bottom of the column.
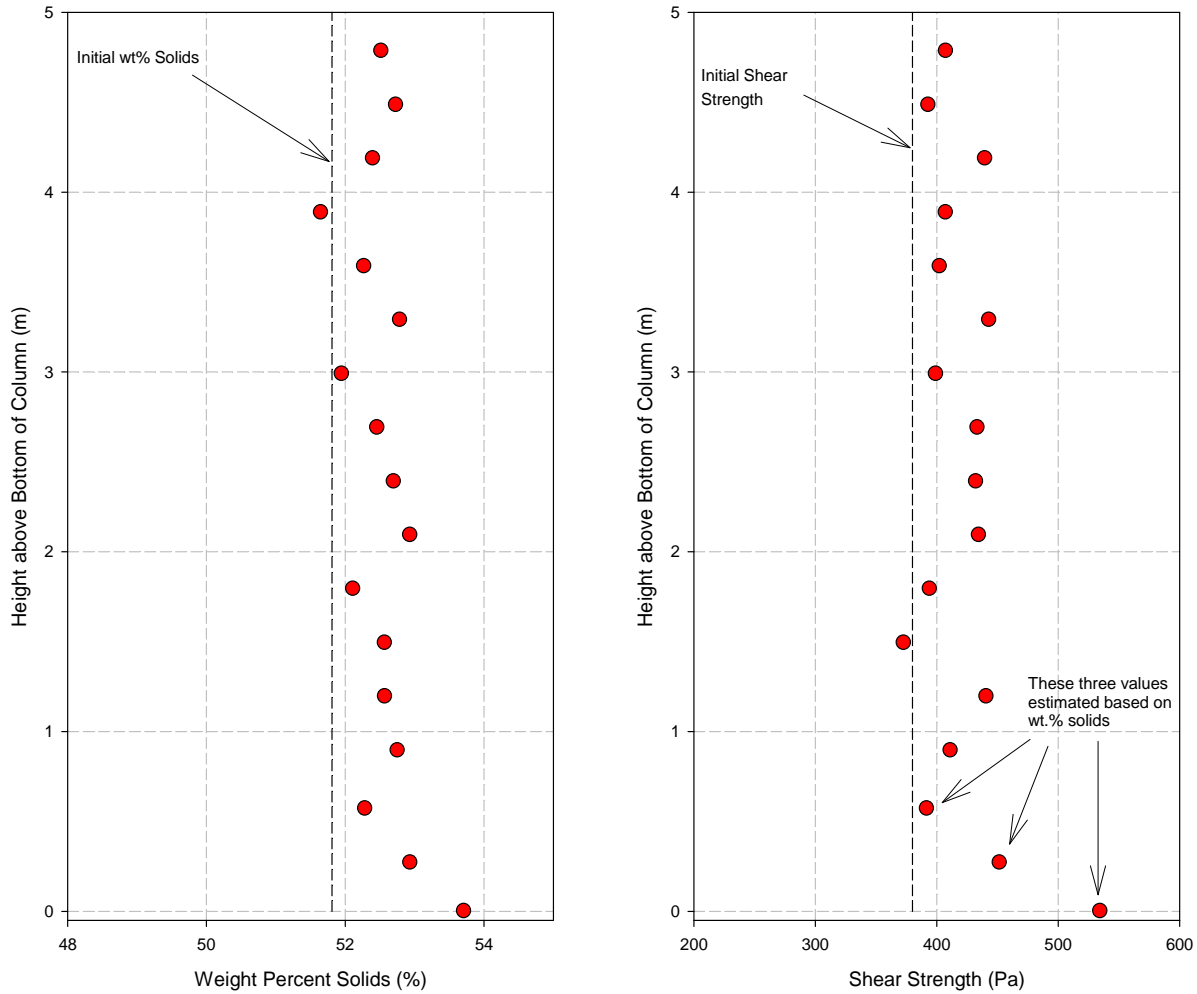
Figure 3.6. Post-Test Simulant Weight Percent Solids and Shear Strength Profiles for Test #1

3.1.3   Retained-Gas-Fraction Profile

As described earlier, the average retained gas fraction can be determined by measuring the change in height of the liquid/gas interface during the d_{max} tests. However, evaluating the accuracy of the d_{max} theory requires an understanding of the retained-gas fraction variation as a function of simulant depth. The d_{max} theory predicts a significant increase in retained-gas fraction at depths below d_{max}, so evaluating d_{max} theory requires determining whether the retained gas fraction is higher than the overall average retained-gas fraction at depths below d_{max}. The overall average retained-gas fraction is calculated from the changes in liquid-level height, but determining how the retained-gas fraction varies vertically through the column requires additional measurement techniques.
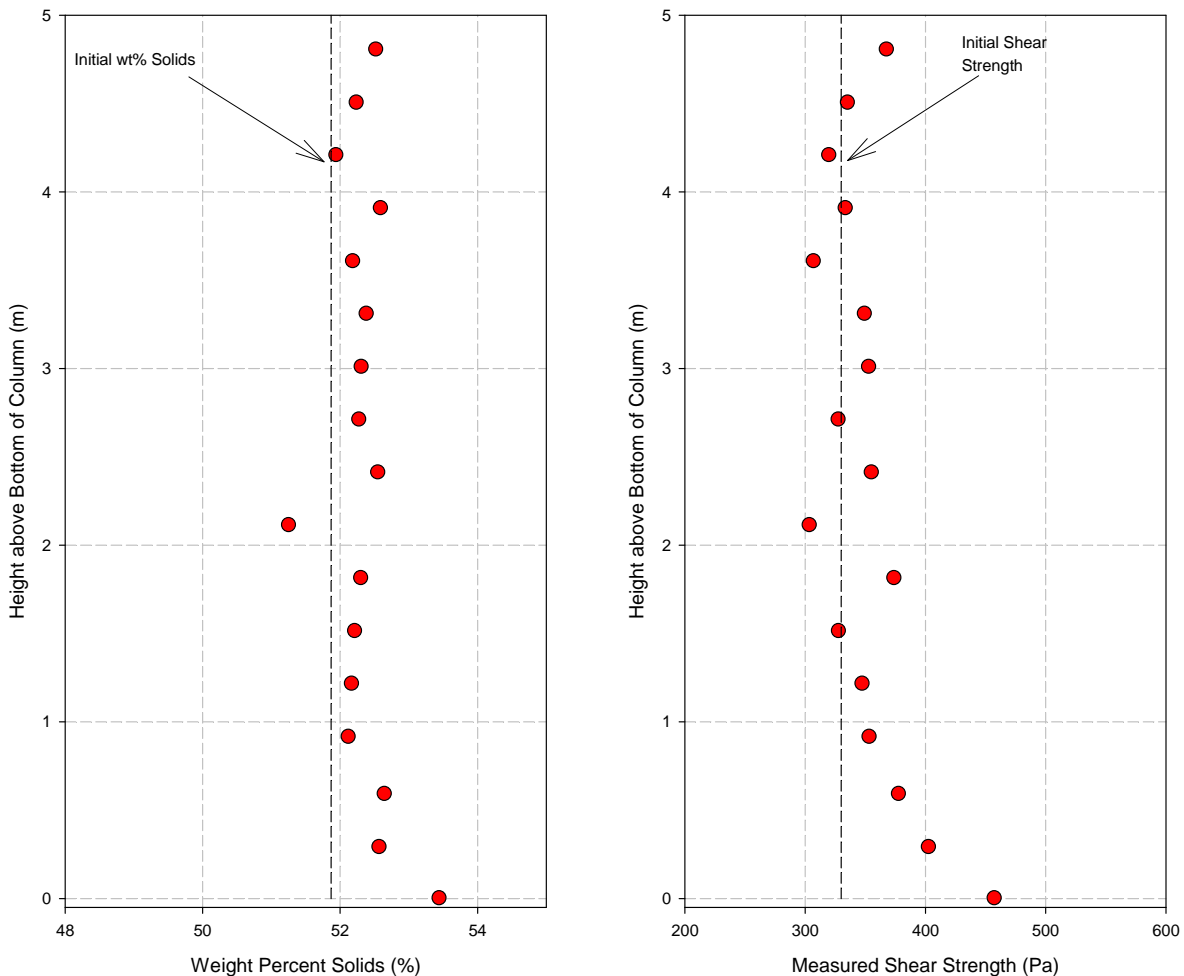
Figure 3.7. Post-Test Simulant Weight Percent Solids and Shear Strength Profiles for Test #2

Two techniques were used to determine the vertical, retained-gas-fraction profile for the d_{max} tests. The first technique involved visual analysis of photographs and time-lapse video to directly measure the changes in simulant height during the test at selected vertical locations. The second technique was measurement of ultrasonic attenuation as described in Section 2.1.3.   The results of these two analysis techniques are described in the subsections below.

3.1.3.1   Retained-Gas-Fraction Profile from Photographs and Time-Lapse Video

The average retained-gas fraction in the simulant column is estimated based on the observed change in level of the liquid/air interface throughout the test. The initial average retained-gas fraction (ϕ_{init}) is calculated based on the as-loaded density of the simulant (see Section 2.1.2). The initial retained gas fraction is assumed to be uniformly distributed throughout the simulant. The volume of the initially retained gas is equal to the initial simulant volume multiplied by ϕ_{init}. As gas is generated thereafter and the liquid level rises, the volume associated with that level rise is a direct measure of the quantity of gas

retained within the simulant. The average volume fraction of gas is calculated by adding the initial gas volume to the volume indicated by the level rise and then dividing by the total simulant volume.

A similar approach can be used to determine how the retained gas fraction varies vertically in the column. Suppose, at the beginning of a d_{max} test, a visually distinct tracer particle is loaded into the simulant column at a level h above the bottom of the column. As the test proceeds, the level of the tracer particle varies with time from its initial level (h_{init}) and the tracer level changes by $\Delta h(t)$, which is given by this equation:

$$\Delta h(t) = h - h_{init} \tag{3.1}$$

The average retained-gas fraction in the simulant between the bottom of the column and level h can be calculated[1] by:

$$\phi_{avg}(t) = \frac{\phi_{init} h_{init} + \Delta h(t)}{h_{init} + \Delta h(t)} \tag{3.2}$$

where $\phi_{avg}(t)$ =   average retained-gas fraction up to level h
        ϕ_{init} =   initial gas volume fraction in the simulant (assumed uniform)

Testing d_{max} theory requires an assessment of whether the *local* retained-gas fraction increases at depths below d_{max}. Values for the local retained-gas fraction (ϕ_{local}) can be computed between any two depths (h_1 and h_2) based on their respective values of ϕ_{avg} using the equation:

$$\phi_{local} = \frac{(\phi_{avg,h_2}) h_2 - (\phi_{avg,h_1}) h_1}{h_2 - h_1} \tag{3.3}$$

This equation provides the average retained-gas fraction between depths h_1 and h_2. To illustrate use of this equation, consider a hypothetical case where, at some time during a d_{max} test analysis of the movement of visually distinct tracer particles yields $\phi_{avg} = 0.1$ for $h = 0.5$ m and $\phi_{avg} = 0.15$ for $h = 1.0$ m. Using these values in Equation 3.3 yields $\phi_{local} = 0.2$. Again, this value is the average retained-gas fraction in the column between 0.5 and 1.0 m.

In the intermediate-scale column d_{max} tests, no visually distinct tracer particles were loaded into the sludge simulant. However, when the column was loaded with simulant, some small bubbles were present due to entrained air that was not removed by application of the concrete vibrator during loading. Further, once gas generation began, bubbles and cracks formed in the simulant that could be tracked as they moved vertically in response to changing quantities of retained gas. Figure 3.8 shows an example of visibly identifiable bubble/crack shapes. These photographs were taken 5 hours apart during d_{max} Test #2 (i.e., 1:40 pm and 6:40 pm on 11-5-2013). As is evident in the photographs, the crack in the left-hand photograph at the 240-cm level (indicated by the white arrow) has moved to the 245-cm level in the right-hand photograph.

---

[1] The equations in this section apply specifically to the case where the simulant is contained in a column of constant cross-sectional area. The cross-sectional area of the intermediate-scale column is constant.
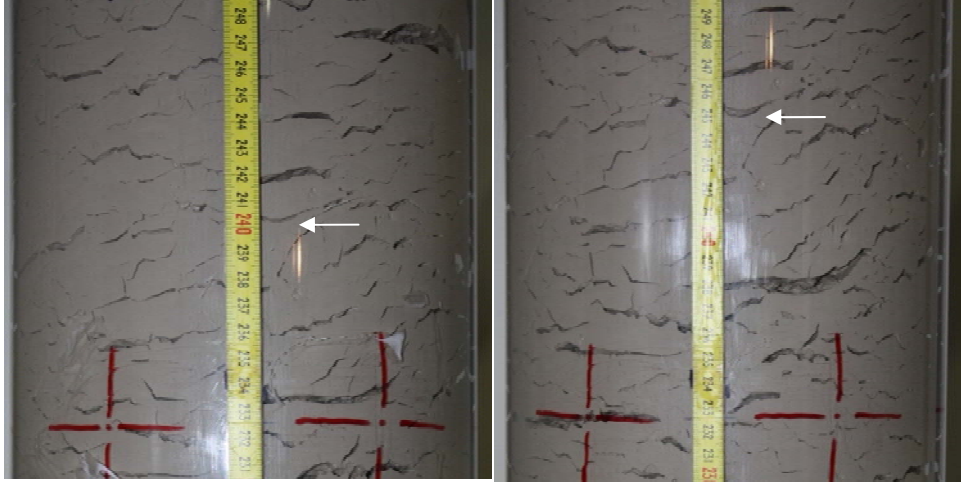
Figure 3.8. Example Bubble/Crack Movement Between Subsequent Photographs

For the analysis of photographs and video images, the measured bubble/crack elevations had to be corrected for parallax errors. The rulers used to quantify elevation changes were affixed to the exterior of the column. The 0.95-cm (0.375-in.) thickness of the acrylic column walls introduces a parallax error when measuring movement of simulant features on the inside wall of the column via a ruler affixed to the outside wall of the column. The parallax correction was made by photographing one of the empty column segments with a ruler affixed to the inside wall of the segment and lined up with the ruler on the outside wall. This dual-ruler column was then photographed using the same camera settings and distances as were used during the d_{max} tests. The parallax shift for each camera was then determined directly and accurately by comparing the readings from the ruler on the outside wall with the readings on the inside wall.

The digital photographs and time-lapse video for both intermediate-scale d_{max} tests were carefully reviewed to identify features in the simulant that could be used to measure the vertical elevation changes of the features throughout the tests. Fewer digital photographs were taken during the rapid-growth phase of Test #1 because much of the growth occurred during night-time hours when staff qualified to operate the scissor lift were not present. Due to the height of the column, a scissor lift was required to access the upper half of the column and take high-quality photographs. During Test #2, photographs were taken more often during the rapid-growth period and this greatly facilitated tracking of bubbles and cracks between subsequent photographs.

For Test #1, generation of a full, vertical retained-gas profile based on the bubble/crack-tracking method described above was not completed because of the smaller number of photographs available. The Test #2 photographs, however, were sufficient to develop the desired vertical retained-gas profile.

Evaluation of d_{max} theory is the principal goal of this work. Knowledge of the full retained-gas profile in the column is not required to evaluate d_{max} theory; the primary interest is in determining if, at depths below d_{max}, the retained-gas fraction is significantly greater than the average retained-gas fraction. If the retained-gas fraction at depths below d_{max} is no greater than the overall average for the entire column of simulant, then the predictions of d_{max} theory are not supported by the experimental observations.

For Test #1, the time-lapse camera focused on the 0.3-m level above the column bottom was used to generate estimates for ϕ_{avg} at $h = \sim 0.3$ m throughout the duration of the test. Those data were compared with the overall average retained-gas fraction calculated based on the liquid-level measurements. Figure 3.9 shows the results of this analysis. The triangular data points in Figure 3.9 represent the values of ϕ_{avg} (expressed as a percentage) based on the observed, parallax-corrected movement of a crack that appeared initially at the 0.315-m level. The circular data points represent the overall average retained-gas percentage in the simulant based on movement of the water/air interface near the top of the column. The retained-gas percentage estimated based on the video images is, at all times during the test, significantly *lower* than the overall average for the entire column of simulant. Based on these data, the prediction from d_{max} theory that the retained-gas fraction should be higher at depths deeper than d_{max} is not supported.
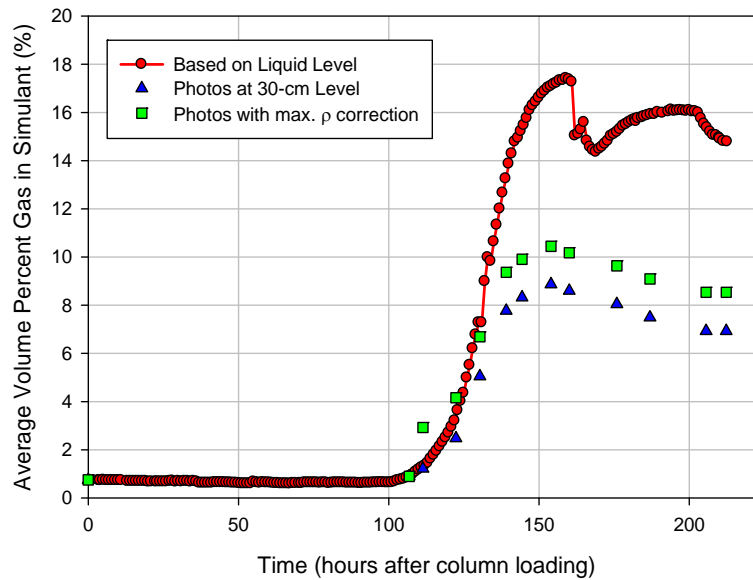

Figure 3.9. Test #1 Retained-Gas Percentage at $h = 0.3$ m Compared with the Overall Average

The image-based method for estimating retained gas fraction is affected by changes in simulant consolidation during the test. As described earlier (Section 3.1.2), the simulant near the bottom of the column experienced the greatest degree of consolidation over the course of each test. Consolidation has the effect of reducing the magnitude of the upward movement of bubbles and cracks, so in the absence of consolidation effects the observed Δh values would be larger than those actually observed. Larger Δh values imply greater volume of generated gas, so ignoring the consolidation effect results in an underestimation of the retained-gas fraction.

The square data points in Figure 3.9 represent the photo-based estimates for ϕ_{avg} at $h = \sim 0.3$ m with a correction applied for simulant consolidation. The consolidation-corrected data points were generated using the non-corrected data points and then assuming that the maximum observed degree of consolidation in Test #1 was applied to all the simulant at the $h = \sim 0.3$ m level and below. The sample taken from the very bottom of the column exhibited the greatest increase in weight percent solids during Test #1. For the purpose of generating the square data points in Figure 3.9, the simulant at $h = \sim 0.3$ m and below was assumed to consolidate to the density of the simulant at the very bottom of the column. This adjustment was applied to all the Δh values following the initial appearance of the crack at the

0.315-m level. Applying the consolidation adjustment at this point has the effect of maximizing the magnitude of the adjustment. The actual value of ϕ_{avg} for h = ~0.3 m likely lies between the two sets of data points (triangles and squares) shown in Figure 3.9 for the photo-based retained-gas measurements.

Even with application of the maximum credible adjustment for consolidation, the average retained-gas fraction at the h = ~0.3-m level and below is significantly less than the overall retained-gas fraction for the full simulant column. This result is in direct contradiction with the predictions of d_{max} theory.

Analysis of the photographs from Test #2 was more extensive because the greater frequency at which the photos were taken during the rapid-growth period allowed bubbles/cracks to be tracked at most elevations throughout the test. Features were identified and tracked between each subsequent set of photographs (refer to Table 2.1 for a list of all digital photograph sets). The elevation of each feature was determined from the parallax-corrected reading obtained from the ruler in the each photograph.

Very few bubbles/cracks can be consistently identified throughout all the sets of photographs. Particularly in the higher elevations of the column, the simulant experiences enough vertical movement during the test that many bubbles and cracks are deformed or eliminated from view. A visually identifiable crack that appears in one set of photographs might be unrecognizable or missing in the next set of photographs. To address this problem, a relatively large number of corresponding features were identified in each pair of subsequent photographs. Where possible, a feature used in a preceding pairing of photographs was also used in subsequent photograph pairings. However, where this was not possible, an interpolation approach was employed.

The interpolation approach is most clearly explained using a hypothetical example. Assume sets of photographs are taken at 6-hour intervals and that each set of photographs provides images covering the entire height of the simulant in the column. Starting with the photographs taken at 0 and 6 hours, visually identifiable, corresponding features are located that appear in both sets of photographs. The crack indicated by the white arrows in Figure 3.8 is an example of a typical corresponding feature. Each identified feature has an elevation that can be determined based on the ruler reading with an appropriate parallax correction. While examining all the photographs taken at 0 and 6 hours, a table of data can be created to show the elevation of each identified feature at 0 and 6 hours. Next, a similar exercise can be performed using corresponding features in photographs taken at 6 and 12 hours. Where possible, the same features identified in the 0- to 6-hour comparisons can be re-used. Presumably, because relatively few of these early features survive, new corresponding features will also be identified. As all 6- and 12-hour photographs are examined, another table of data will be created, containing the beginning and ending elevations for each of the features.

Similar tables of beginning-and-ending elevation data can be constructed by comparing the 12- and 18-hour photographs, the 18- and 24-hour photographs, the 24- and 30-hour photographs, and so on until the last pair of photograph sets is examined. At this point, the aforementioned interpolation approach can be applied.

Suppose the 0- to 6-hour photograph comparison identifies a feature with an elevation of 50 cm at 0 hours and 54 cm at 6 hours. Suppose a different feature in the same set has an elevation of 60 cm at 0 hours and 68 cm at 6 hours. Neither of these hypothetical features appears in the photographs taken at 12 hours, but a feature at 58 cm in the 6-hour photographs appears in the 12-hour photographs at 60 cm. If the elevation change is assumed linear with respect to elevation between each set of points in the 0- to

6-hour data set, interpolation can be used to determine what the elevation of the 58-cm/6-hour feature would have been if it had also been present in the 0-hour photographs. The linear assumption implies that between 0 and 6 hours, the elevation change varies linearly from +4 at 54 cm final elevation to +8 at 68 cm final elevation. This information can be used to estimate what the elevation of the 58-cm/6-hour feature would have been, if it had been visible in the 0-hour photograph set. Interpolating between the elevation change at 54 and 68 cm to find the expected elevation change at 58 cm gives 5.14 cm. If the retained-gas-fraction profile for the 0-hour features is known, the interpolated elevation change can be used to estimate the retained gas fraction for the 58-cm/6-hour feature even though it did not appear in the 0-hour photograph.

The basic approach described above was applied for the analysis of the Test #2 column photographs. The first set of photographs was taken less than 18 hours after the column was loaded, so the retained-gas fraction in the simulant at that time was known based on the measured mass and volume of simulant loaded in the column. The initial retained-gas fraction was assumed to be uniformly distributed throughout the column. Subsequent photographs were then used to track the elevation changes of visually identifiable features and the retained-gas fraction calculated as described above.

Figure 3.10 shows how the calculated ϕ_{avg} values at the end of d_{max} Test #2 vary with elevation above the bottom of the column. The data in this figure were corrected for consolidation using the post-test moisture-content analyses and interpolating linearly as necessary. The black data points connected by the red line are the estimated ϕ_{avg} values (expressed as a percentage in the graph). The vertical dashed line at 15.1 percent represents the average retained-gas percentage calculated based on the changes in the water/air interface level during the test. Ideally, the top-most ϕ_{avg} value calculated from analysis of the photographs (14.8 percent) should match the 15.1 percent value indicated by the liquid level. Agreement between the two values is acceptably good.

A visual inspection of the variation of the ϕ_{avg} profile shown in Figure 3.10 clearly shows that the local retained-gas fraction at deeper elevations is lower than the average retained-gas fraction. This observation is consistent with the results of Test #1, which showed that the retained-gas fraction does not increase at depths deeper than d_{max}.

The data in Figure 3.10 can be used to generate a plot of the local retained-gas fraction (ϕ_{local}) by application of Equation 3.3. The Figure 3.10 data were used to generate Figure 3.11, which shows the local retained-gas percentage profile. Values from the Figure 3.10 data were used at roughly 50-cm intervals along with Equation 3.3 to calculate values for ϕ_{local}. The data are plotted such that each calculated ϕ_{local} is assumed to apply to the average elevation used in the calculation. For example, values of ϕ_{avg} for $h_1 = 99$ cm and $h_2 = 150$ cm were used to calculate ϕ_{local} and that value is plotted at an elevation of about 124.5 cm in the figure.

The data in Figure 3.11 clearly show that the local retained-gas fraction does not increase at depths below d_{max}, as is predicted by d_{max} theory. This result is consistent with the results of Test #1.
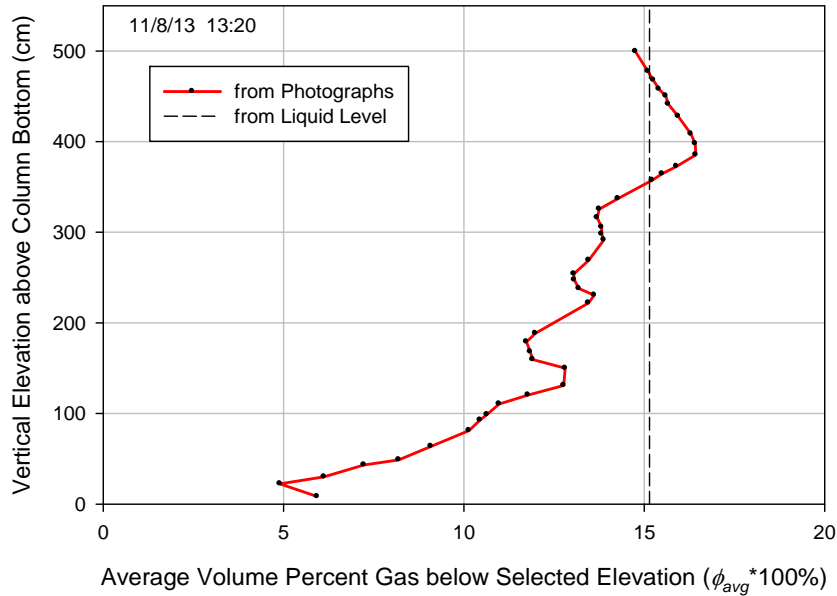
Figure 3.10. End-of-Test Vertical Profile for ϕ_{avg} Estimated from Test #2 Photographs (time = 187 h)
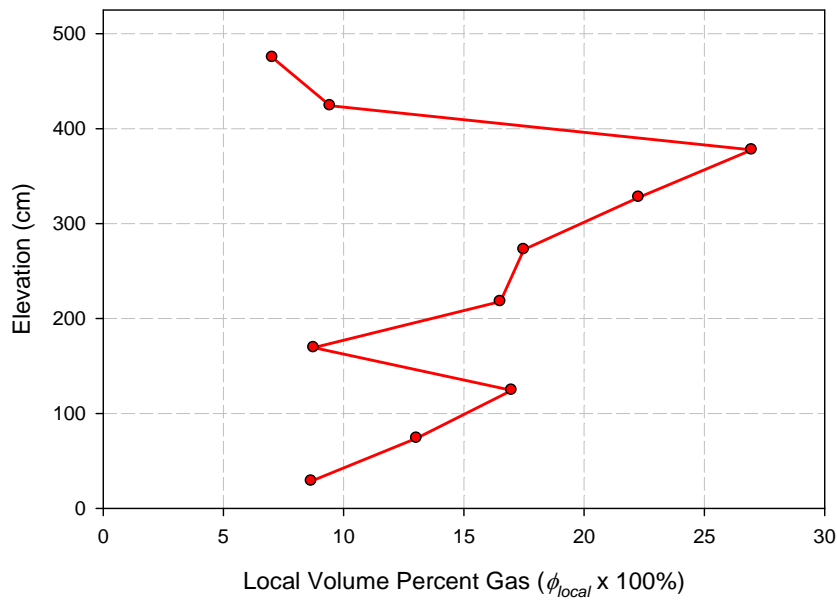

Figure 3.11. Local Volume Percent Gas Profile at the End of dmax Test #2 (time = 187 h)

3.1.3.2   Retained-Gas-Fraction Profile from Measurement of Ultrasonic Attenuation

Two ultrasonic-to-GVF correlation tests were conducted, which will be referred to as Ultrasonic Correlation Test #1 and Ultrasonic Correlation Test #2. Ultrasonic measurements were performed each time the water level changed in the test section by 0.5 cm during Ultrasonic Correlation Test #1. This test

yielded a kaolin shear strength of 360 Pa and maximum GVF of 14.5 vol%. Overall, the test data showed a logarithmic increase in ultrasonic attenuation with increasing GVF; however, the correlation data were relatively low in resolution due to the time between 0.5-cm water level changes. The data also indicated a decreasing trend in attenuation after 10 vol% retained gas.

To determine if the decrease in attenuation after 10 vol% GVF was real and repeatable, a second ultrasonic correlation test was performed. Data were collected every 10 to 30 minutes during Ultrasonic Correlation Test #2, with measurements being made more frequently during gas-growth phases. Ultrasonic Correlation Test #2 was conducted in parallel with d_{max} Test #2 and the test section was filled with the same simulant as that loaded into the intermediate-scale column for d_{max} Test #2. The simulant had an initial shear strength of 330 Pa (see Section 3.1.2). Although the same simulant mixtures were loaded into the ultrasonic test section and the intermediate-scale column at the same time and in the same laboratory location, the maximum GVF reached in each test was different. The maximum GVF reached in the ultrasonic test section was 21.5 vol%; however, the maximum GVF reached in the intermediate-scale column during d_{max} Test #2 was only 17.5 vol% (see Figure 3.2).

Gas generation continued in the test section until the average retained-gas percentage reached approximately 20.5 vol%, whereupon the average GVF began to fluctuate, as shown in Figure 3.12. One first significant fluctuation occurred before the maximum 21.5 vol% GVF was reached in the test section. The GVF fluctuated several more times after this point, reaching a maximum once more. This phenomenon may explain the apparent decrease in attenuation after 10 vol% GVF in Ultrasonic Correlation Test #1. Data were only collected after every 0.5-cm water level change during Ultrasonic Correlation Test #1. GVF fluctuations could have occurred between net 0.5-cm water-level changes and data collected during the GVF fluctuation phase may have more uncertainty due to a less even gas distribution within the test section. The water level also becomes difficult to read during the GVF fluctuation phase due to bubble adhesion at the acrylic/water interface, as shown in Figure 3.13.

Ultrasonic attenuation decreased early in the test (i.e., approximately the first 70 hours) as the simulant settled and slightly decreased in volume at the start of Ultrasonic Correlation Test #2. Ultrasonic attenuation then increased with increasing GVF and began to fluctuate when the GVF began to fluctuate, as shown in Figure 3.14. Attenuation is expressed on a logarithmic scale, so a difference of 6 dB in attenuation is a factor of two difference in signal amplitude, a difference of 20 dB represents a factor of 10, a difference of 40 dB represents a factor of 100, and a difference of 60 dB represents a factor of 1000.

Due to the increased uncertainty of the gas distribution in the test section and the difficult-to-measure bubbly water layer during the GVF fluctuation phase, only data during the gas-growth phase up to the first significant GVF fluctuation were used for developing the mathematical correlation between ultrasonic attenuation and GVF. The mathematical correlation for Ultrasonic Correlation Test #2 was based on the data collected up to 20.5 vol%. The GVF and attenuation data after 20.5 vol% appeared to track relatively well during the GVF fluctuation phase; however, the attenuation data for the 15- and 30-cm elevations are in less agreement and indicate an uneven distribution of gas in the test section.
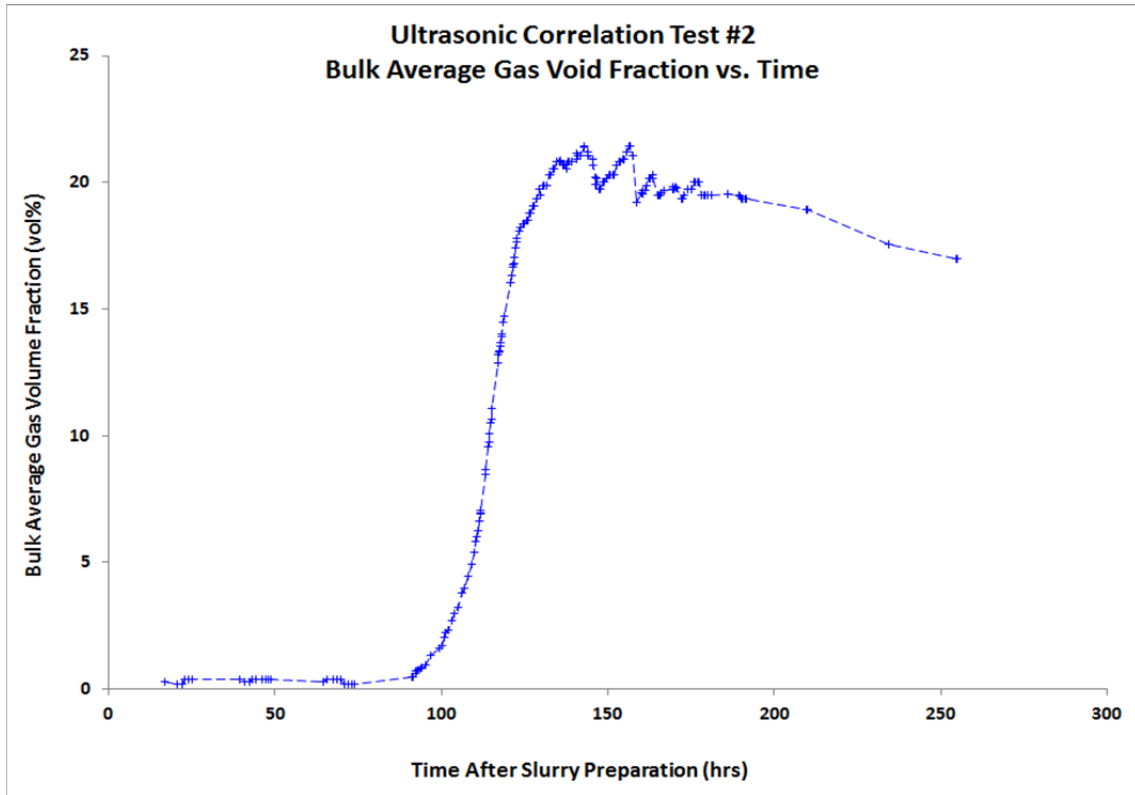
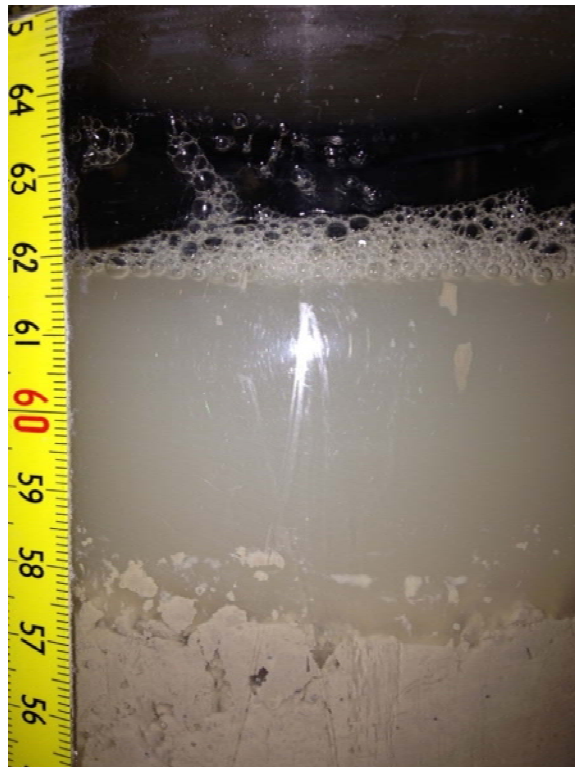**Figure 3.12**. Bulk GVF vs. Time for Ultrasonic Correlation Test #2

Figure 3.13. Photograph of Bubble Adhesion at the Acrylic/Water Interface in the Ultrasonic Test
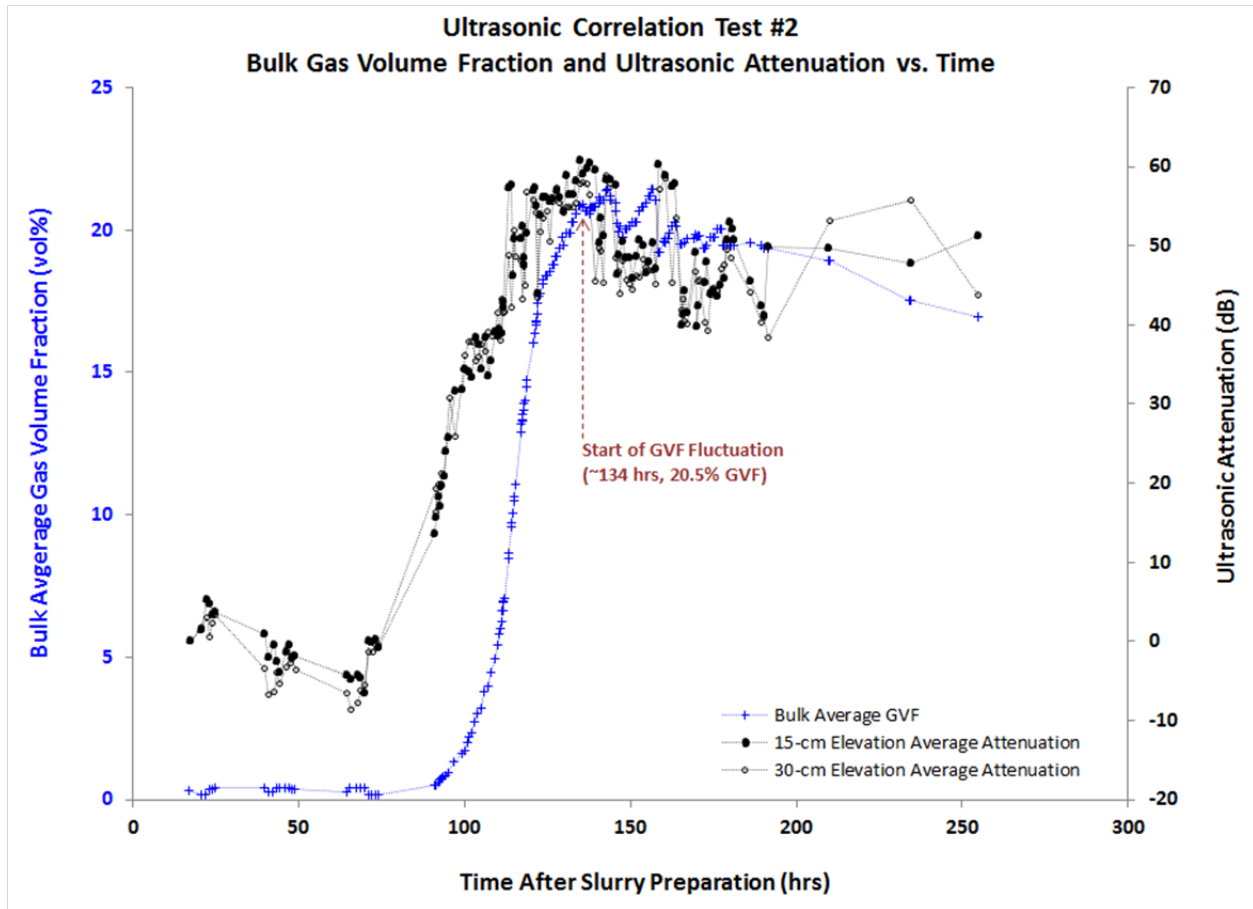Section

Figure 3.14. Bulk GVF and Ultrasonic Attenuation vs. Time for Ultrasonic Correlation Test #2

    The ultrasonic attenuation as a function of bulk GVF for Ultrasonic Correlation Test #1 and Ultrasonic Correlation Test #2 are provided in Figure 3.15. The data for the 15- and 30-cm elevations are plotted separately and the trendlines for each series are displayed. Ultrasonic Correlation Test #1 data are shown in red (open and solid red diamonds) and Ultrasonic Correlation Test #2 data are shown in black (open and solid black dots). The maximum GVF measured for Ultrasonic Correlation Test #1 was only 14.5 vol%; however, the trendlines for Ultrasonic Correlation Test #1 are extrapolated to 20.5 vol% to demonstrate the good agreement between extrapolated data for Ultrasonic Correlation Test #1 and the collected data for Ultrasonic Correlation Test #2.

    A nominal ultrasonic correlation equation from the 15- and 30-cm trendlines from Ultrasonic Correlation Test #2 was found by averaging the trendlines for the 15- and 30-cm data. The nominal correlation equation was used to relate the attenuation to GVF for both d_{max} tests in the intermediate-scale column. The nominal equation for Correlation Test #2 was selected because Ultrasonic Correlation Test #2 contains the highest resolution data and the data trend is in generally good agreement with that of Correlation Test #1. The nominal correlation equation from Ultrasonic Correlation Test #2 was $y=13.217\ln(x)+17.5$ where x is the calculated GVF and y is the measured attenuation. A plot of the nominal correlation equation (blue solid dots) is shown in Figure 3.16.
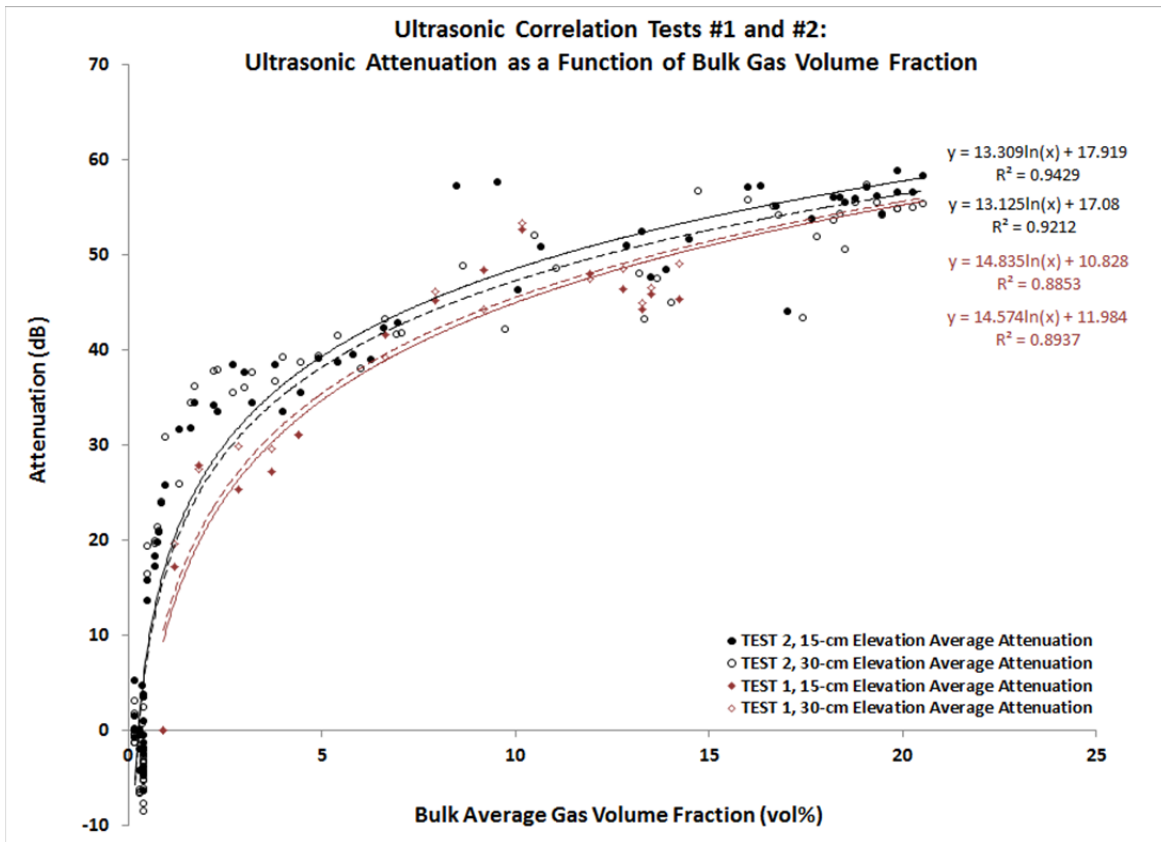
3.17

Figure 3.15. Plots of Ultrasonic Attenuation as a Function of GVF for Ultrasonic Correlation Test #1 and Ultrasonic Correlation Test #2

Ultrasonic data were collected during d_{max} Test #1 and d_{max} Test #2 in a similar fashion to the ultrsaonic correlation development tests. Each segment of the intermediate-scale column had three different measurement elevations. Ultrasonic measurements were performed at three circumferential orientations at each elevation and averaged to generate one measurement for each elevation. Ultrasonic measurements from each d_{max} test were used to calculate the GVF at each elevation along the intermediate column using the nominal correlation equation. The ultrasonically determined GVF profiles from d_{max} Test #1 and d_{max} Test #2 are shown in Figure 3.17 through Figure 3.20. Data are plotted as ultrasonically determined GVF vs. test time for each column elevation as well as column height vs. ultrasonically determined GVF for each measurement interval in time.

The ultrasonically determined, localized GVFs for d_{max} Test #1 and d_{max} Test #2 are higher than the bulk average GVF measured via water level changes for d_{max} Test #1 and d_{max} Test #2 (see Figure 3.2). The source of the discrepency between the GVF measurements from the two methods has not been determined, but the bulk average GVF estimates made based on the liquid-level changes are known to be accurate because simulant volume changes are due to changes in the volume of gas retained in the simulant (i.e., the water and gas-free simulant volumes remained constant throughout the d_{max} tests). Consequently, the discrepancy between the ultrasonically determined, localized GVFs and the liquid-level-determined bulk average GVF for each d_{max} test must be due to inherent differences between the conditions in the intermediate-scale column and the ultrsonic test section used to develop the nominal correlation equation. The cause of the discrepancy has not been identified.
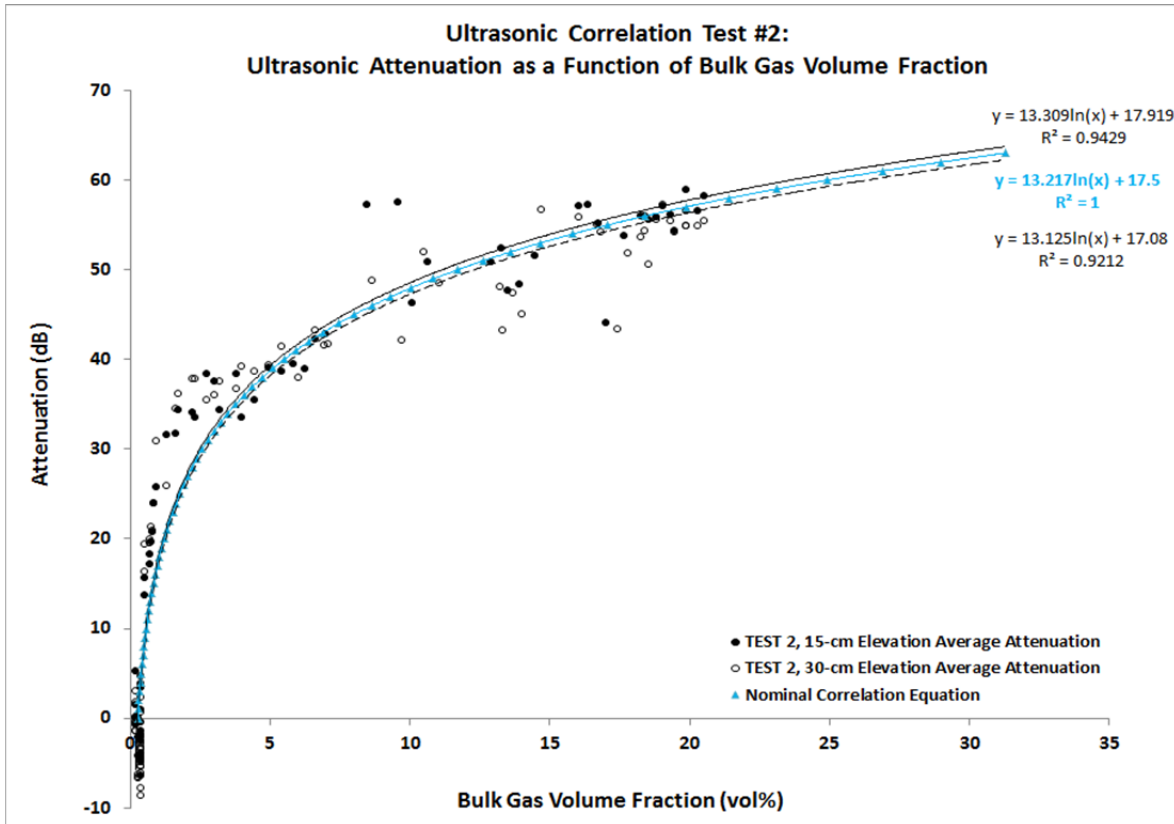
3.18

Figure 3.16. Nominal Correlation Equation (shown in solid blue triangles) from Correlation Test #2

Despite the discrepencies between the absolute values of the bulk average GVFs and the localized GVFs, the relative differences in ultrasonically determined GVFs along the column height for each d_{max} test are within 10 percent for the majority of the test durations. Exceptions to this statement are: (1) the 138-hour measurement interval for d_{max} Test #1 where the GVF is significantly lower in the lower portion of the column than in the upper portions of the column; (2) the 146-hour measurement interval for d_{max} Test #1 where the GVF is higher in the top one-third of the column than in the lower portions of the column; and (3) the 112-hour measurement interval for d_{max} Test #2, where the GVF is significantly lower in the bottom one-quarter of the column than in the upper portions of the column. In none of the measurement intervals was the GVF higher in the bottom portions of the column than in the upper portions as would be predicted by d_{max} theory.

Figure 3.17. Ultrasonically Determined GVF as a Function of Test Time for d_{max} Test #1

Figure 3.18. Column Height as a Function of Ultrasonically Determined GVF for d_{max} Test #1

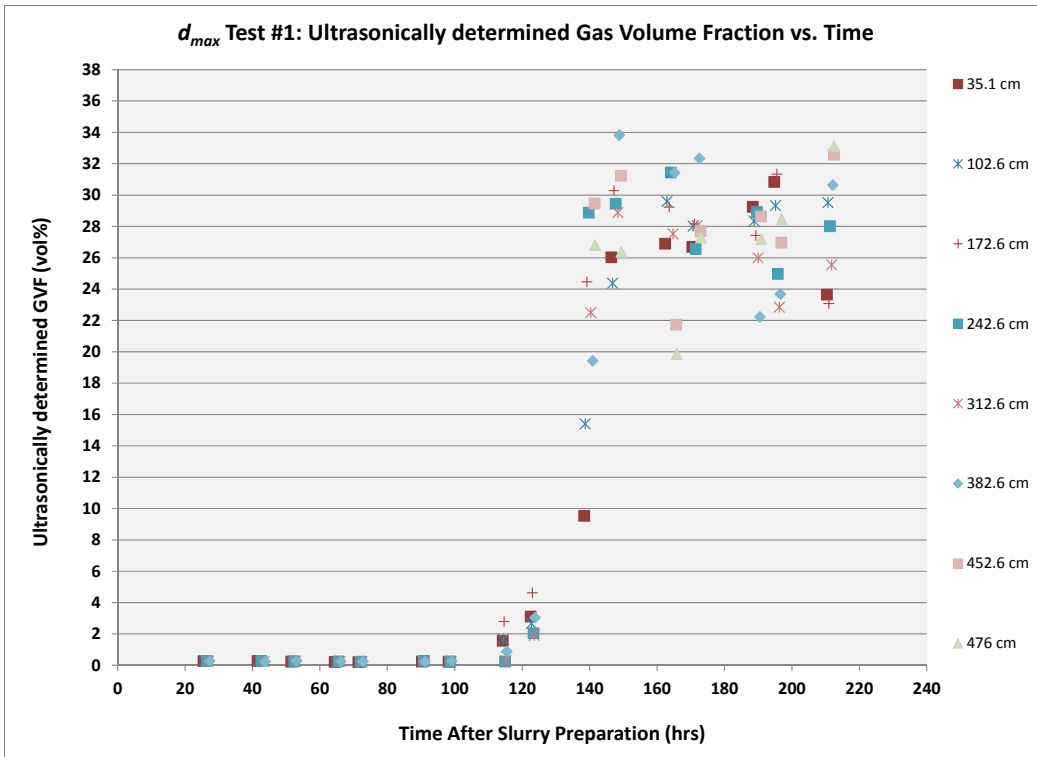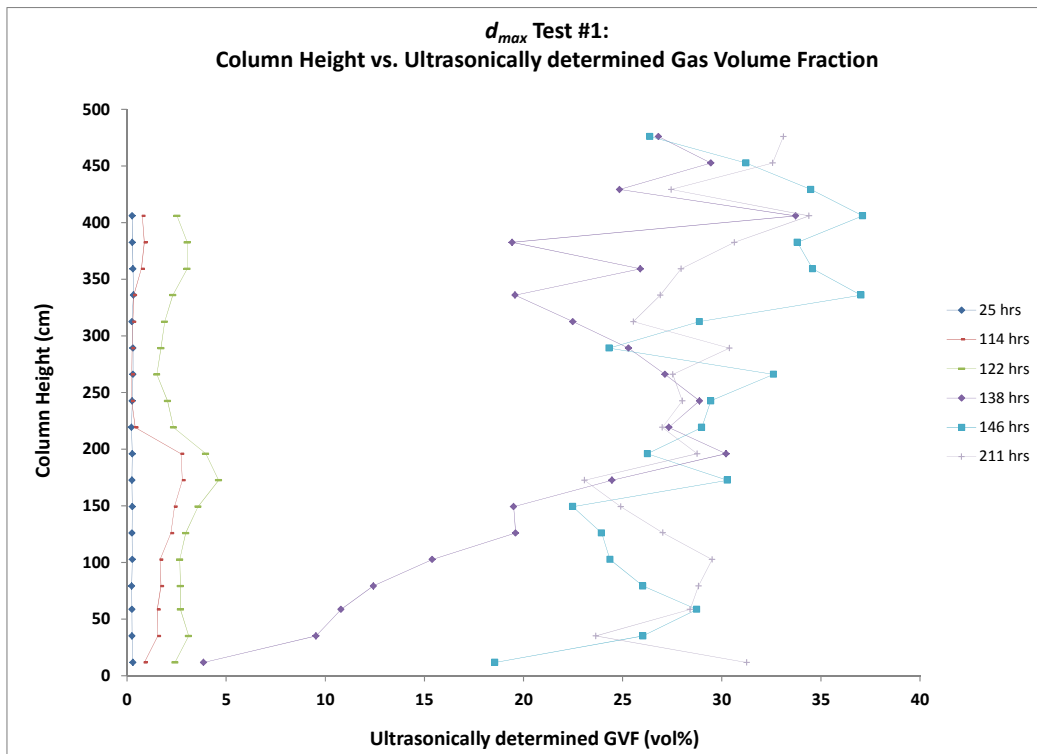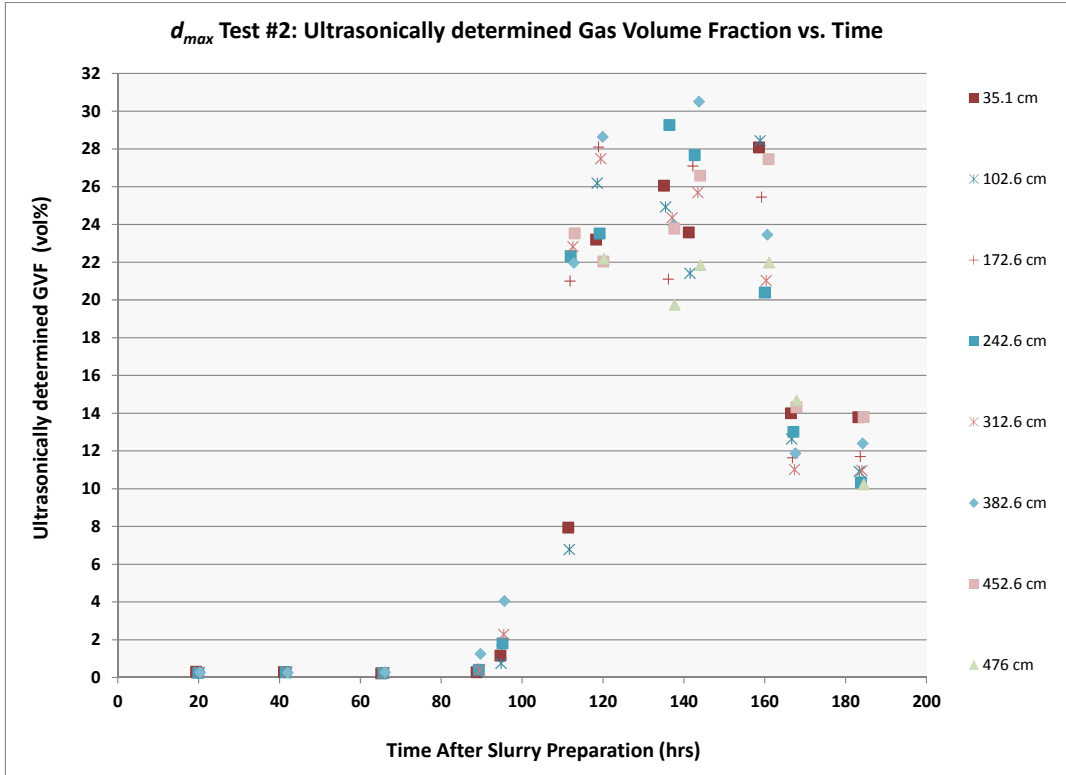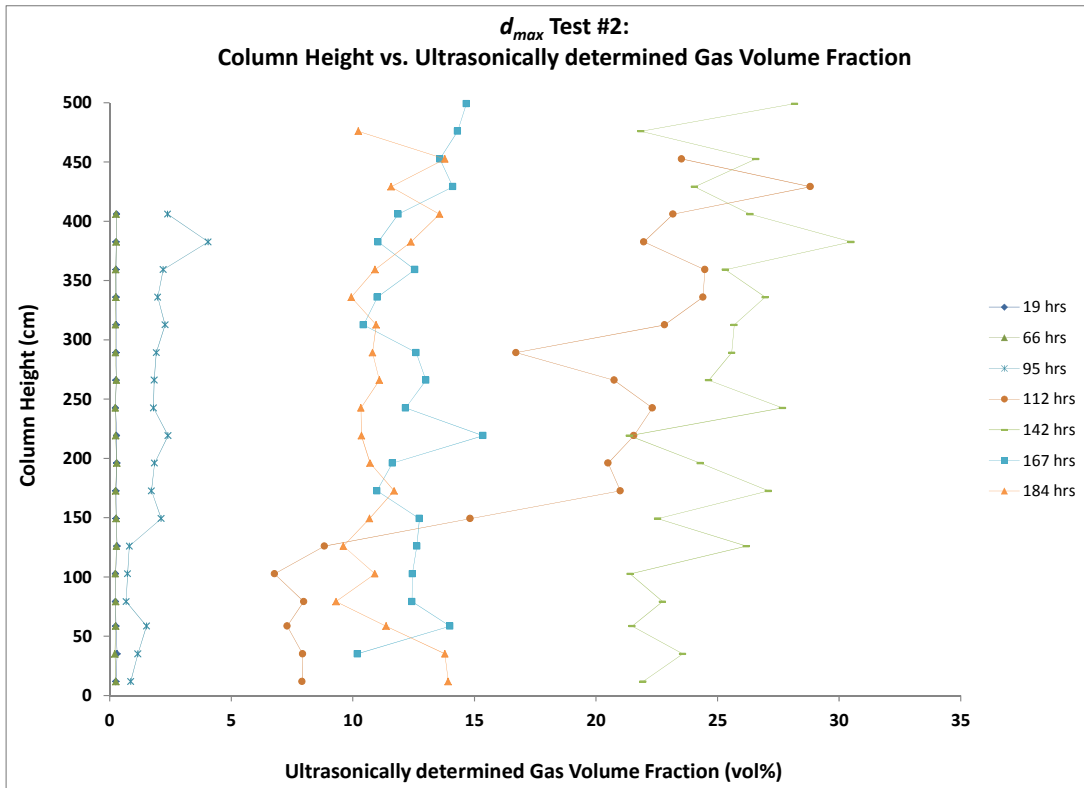**Figure 3.19**. Ultrasonically Determined GVF as a Function of Test Time for d_{max} Test #2

Figure 3.20. Column Height as a Function of Ultrasonically Determined GVF for d_{max} Test #2

3.1.4   Compression Tests

As described in Section 2.1.6, simulant compression tests were performed once each of the two d_{max} tests were declared complete. After d_{max} Test #1, water was added to the top of the column to increase the hydrostatic load on the sludge simulant. After d_{max} Test #2, the column headspace was repeatedly pressurized with nitrogen gas and then vented to atmospheric pressure. Before and after each change in hydrostatic load or gas pressure in the column, sets of digital photographs were taken. In addition, several time-lapse cameras recorded the movement of sludge simulant within the column in response to the changes in pressure/load.

The goal of this effort was to determine whether the average retained-gas fraction and/or the local retained-gas-fraction vertical profile can be estimated by observing the relative movement of simulant at various vertical locations in response to the applied compressive load at the top of the column. The photographs and video were reviewed to measure the pressure-induced changes in elevation for selected bubbles and cracks. Elevation measurements were made based on ruler readings and all readings were corrected for parallax effects as described in Section 3.1.3.

Upon completion of d_{max} Test #1, 24.8 kg of 19°C water was added to the top of the column. This additional hydrostatic load resulted in measured compression of the sludge simulant as indicated both by the liquid level near the top of the column and by the downward movement of simulant. If there had been no compression of the simulant, the liquid level should have increased by 92.7 cm in response to the water addition, but only an 89.4-cm increase in liquid level was observed.[1] This result implies the water/simulant interface moved downward by 3.3 cm from its initial elevation of 495 cm.

Figure 3.21 shows the amount of simulant movement throughout the column in response to the water addition. Circular data points were obtained by analysis of the before-and-after-compression photographs. The triangular data point reflects the amount of movement at the top surface of the simulant (3.3 cm) implied by the discrepancy between the observed liquid-level increase (89.4 cm) and the amount of increase expected based on the volume of water added to the column (92.7 cm).

The compression test results show, as expected, greater simulant movement at higher elevations within the column. The dashed line in Figure 3.21 shows the expected magnitude of simulant movement if the simulant is assumed to have a uniform retained-gas fraction of 0.146 and to behave as a yield-free fluid with entrained gas bubbles. The assumed value for ϕ_{avg} of 0.146 is based on the known average retained-gas fraction in the simulant at the beginning of the compression test calculated from the observed liquid level in the column. The observed compression is significantly smaller than the expected compression. It is not clear at this time why the observed compression differs from the expected compression, but candidate explanations include the effects of friction between the column wall and the simulant as well as potential effects of the simulant yield stress acting to restrict bubble/crack shape changes within the bulk of the simulant. If similar compression tests are to be used for the tall-column d_{max} experiments to determine the ϕ_{local} vertical profile, then additional analysis will likely be required to determine how best to interpret the compression test results. At this point, it is not clear how to accurately determine the ϕ_{local} vertical profile based on the compression test results.

---

[1] A level-volume correlation test was performed before d_{max} testing began. This test established the effective inside diameter of the intermediate-scale column to be 18.47 cm (7.27 in.).
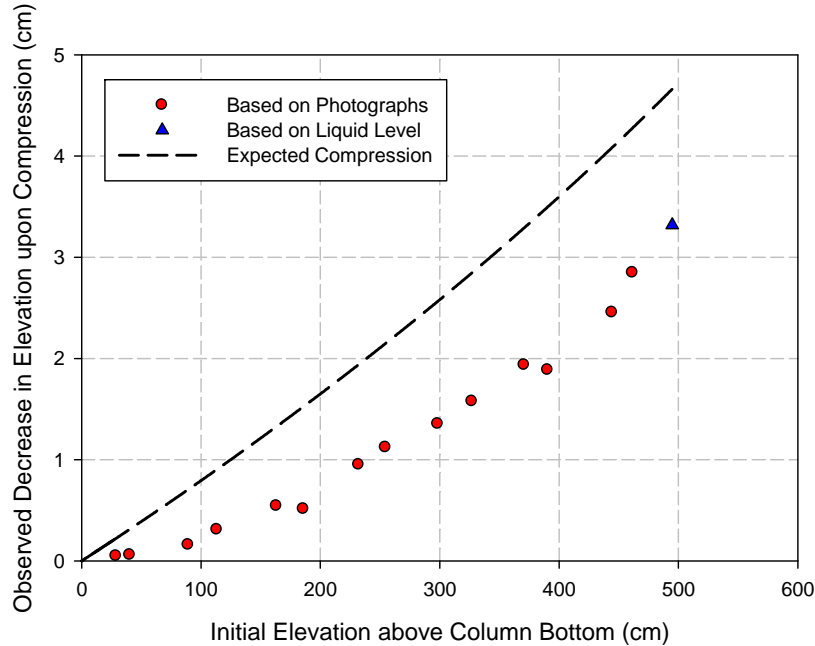
Figure 3.21. Compression Test Results from d_{max} Test #1

A more extensive set of compression tests were performed at the end of d_{max} Test #2. Five pressurization/vent cycles were performed for the Test #2 compression test. After each pressurization step, the column headspace was returned to atmospheric by opening a vent valve. The gas pressures applied in the column headspace were 8.6, 9.0, 18.2, 18.1, and 25.8 kPa. At the start of the compression-test sequence, the average retained-gas percentage in the simulant was 15.2 percent, based on the liquid level in the column. Figure 3.22 shows the variation in column headspace pressure with time. All pressures are referenced to atmospheric pressure (i.e., the plotted values are gauge pressures). The first pressurization (to 8.6 kPa) occurred at time = 88 minutes on the plot. The increase in pressure at time = 13 minutes was associated with disconnection of the gas-collection system (inverted, water-filled graduated cylinder), which was applying 3.8 kPa of vacuum to the column headspace. After the gas-collection system was disconnected and the column headspace vented to atmospheric pressure, the simulant was allowed to stabilize at the new pressure for 75 minutes before the compression tests were initiated. The column was allowed a minimum of 5 minutes to respond to each change in pressure before proceeding with the next pressure change. This 5-minute wait period was determined to allow sufficient time for the column to respond based on the observed lack of additional simulant movement after the first 2 minutes in response to the first pressure change.

The liquid level in the column changed in response to the applied headspace gas pressure. Variation of the liquid level (height above the column bottom) is shown in Figure 3.23. As expected, the liquid-level varies in a manner inversely related to the column headspace pressure.
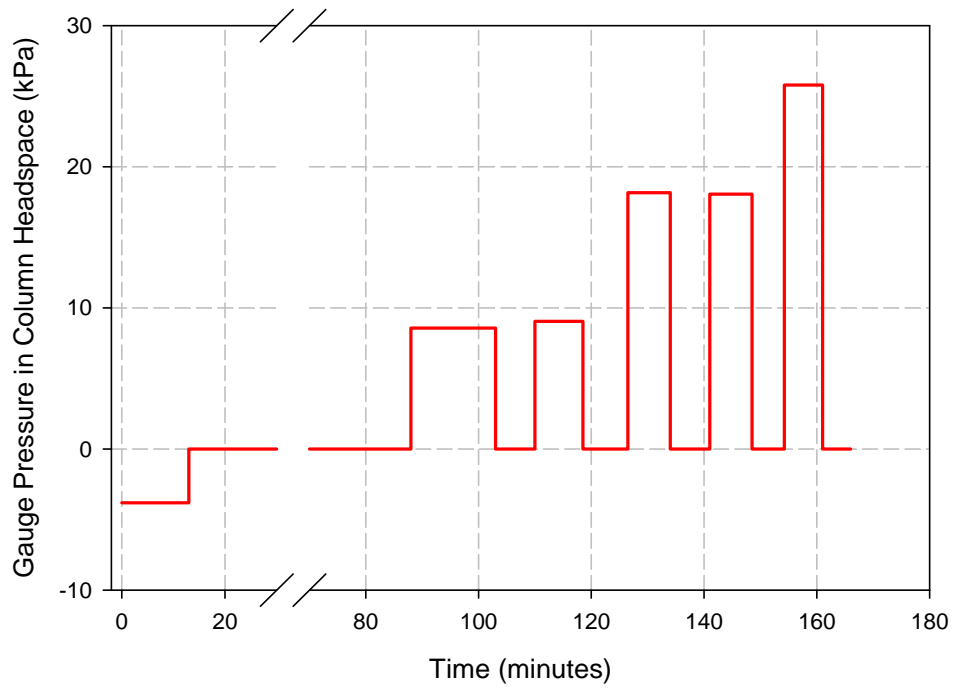
Figure 3.22. Variation of Test #2 Column Headspace Pressure during Compression Test
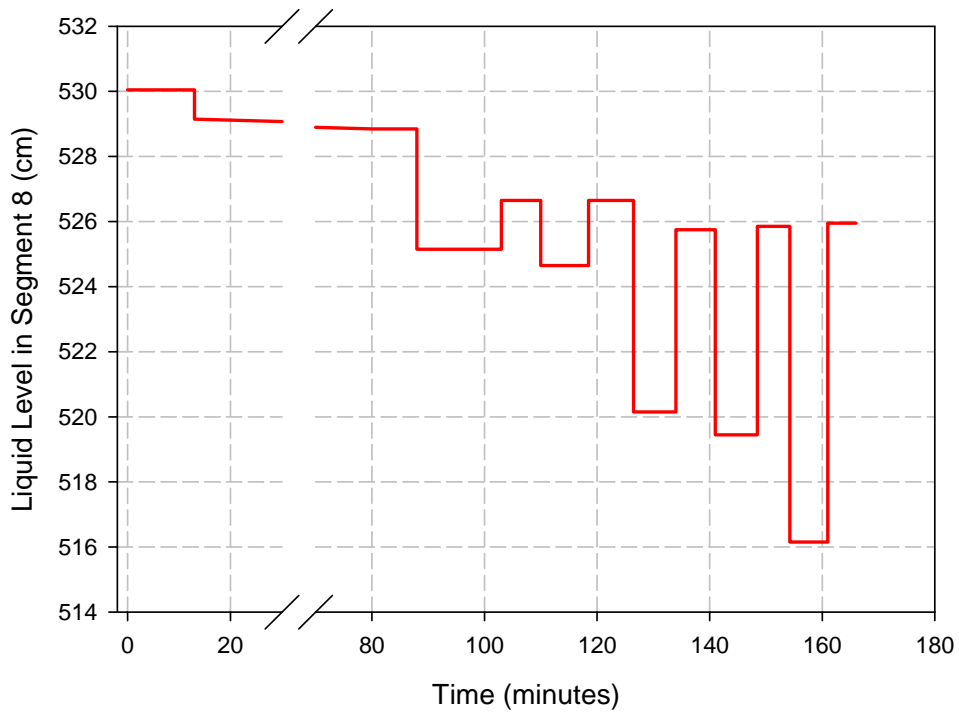

Figure 3.23. Variation of Test #2 Liquid Level during Compression Test

3.24

Seven distinct bubbles/cracks were identified in the photographs taken before and after each pressure change. These same seven features were tracked through all the pressure changes shown in Figure 3.22. Figure 3.24 through Figure 3.28 show the observed changes in elevation for the seven features. Each plot shows the decrease in elevation resulting from the applied pressure (red circles). The triangular data points show the net downward movement of each feature once the headspace was returned to atmospheric pressure. If all the bubbles/cracks returned to their starting elevations, then the triangular data points would show zero decrease in elevation. For each plot, the starting elevation for the seven bubbles/cracks is the starting elevation just before the pressurization occurred. The starting elevations for the second pressurization, for example, are the ending elevations from the first pressurization. Similarly, the starting elevations for the third pressurization are the ending elevations from the second pressurization and so on.

The compression test results shown in Figure 3.24 are particularly interesting because they show the simulant in the deeper regions of the column responded to the initial pressurization but then did not rebound at all toward their initial positions once the pressure was returned to atmospheric. During the first and third pressurizations (8.6 and 18.2 kPa), gas was observed bubbling up through the liquid layer on top of the simulant. The quantity of gas released during these periods is unknown, but based on the number and size of the bubbles the volume was likely on the order of 1 L or more. Possibly this pressure-induced gas release affected the compression test results. As shown in Figure 3.4, the total volume of gas retained in the simulant at the beginning of d_{max} Test #2 compression tests was approximately 20 L, so even a 1-L gas loss would have had a measureable effect on the average retained-gas fraction. The lack of rebound for the bubbles/cracks at the lower depths might be related to the observed gas release or it might indicate the impacts of simulant yield-stress effects.

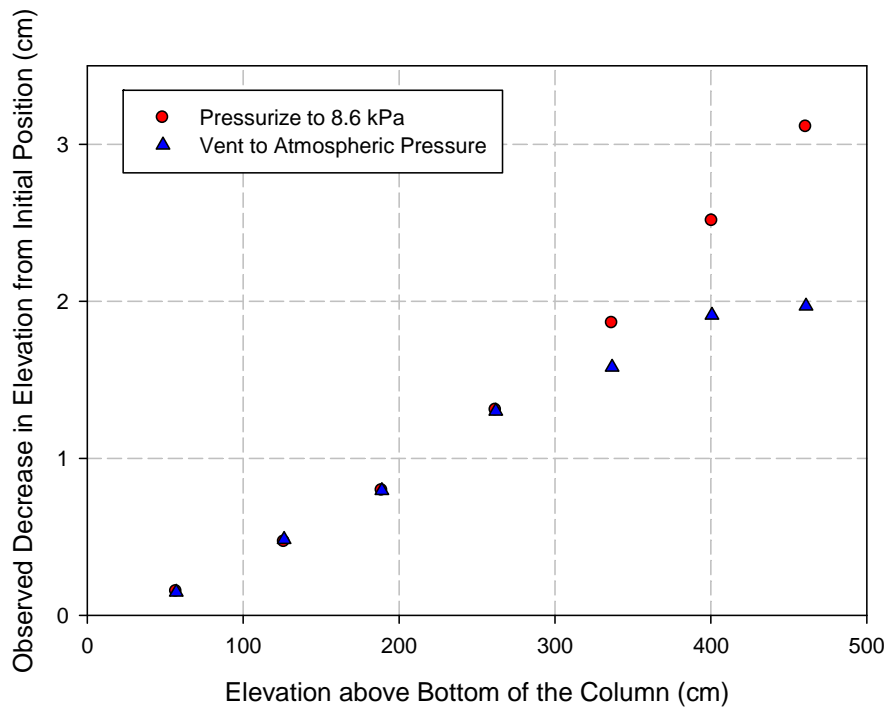**Figure 3.24**. Simulant Compression for First Pressurization/Vent Cycle
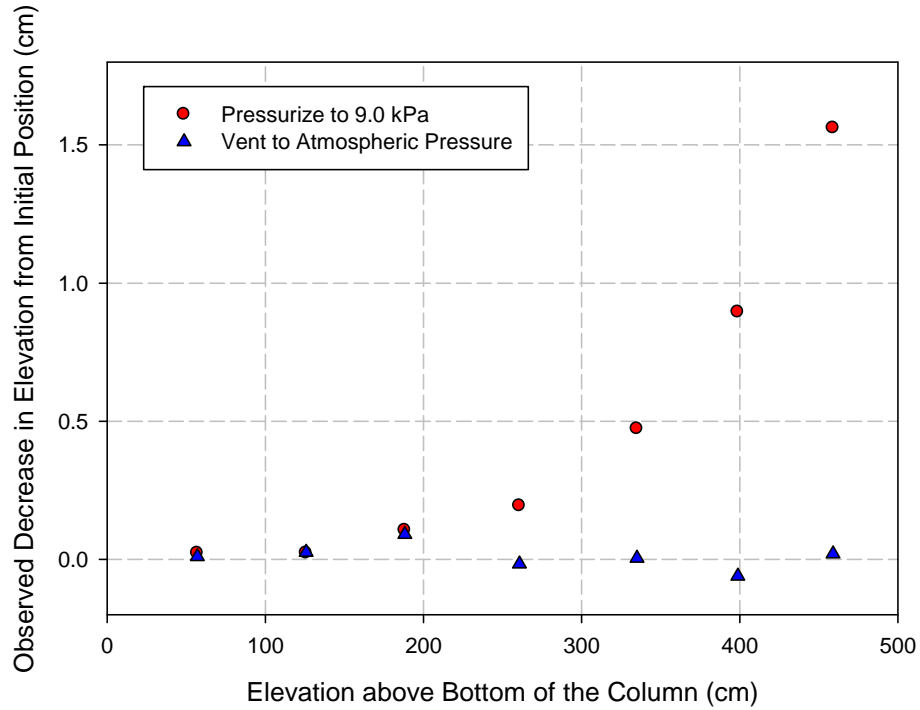
Figure 3.25. Simulant Compression for Second Pressurization/Vent Cycle

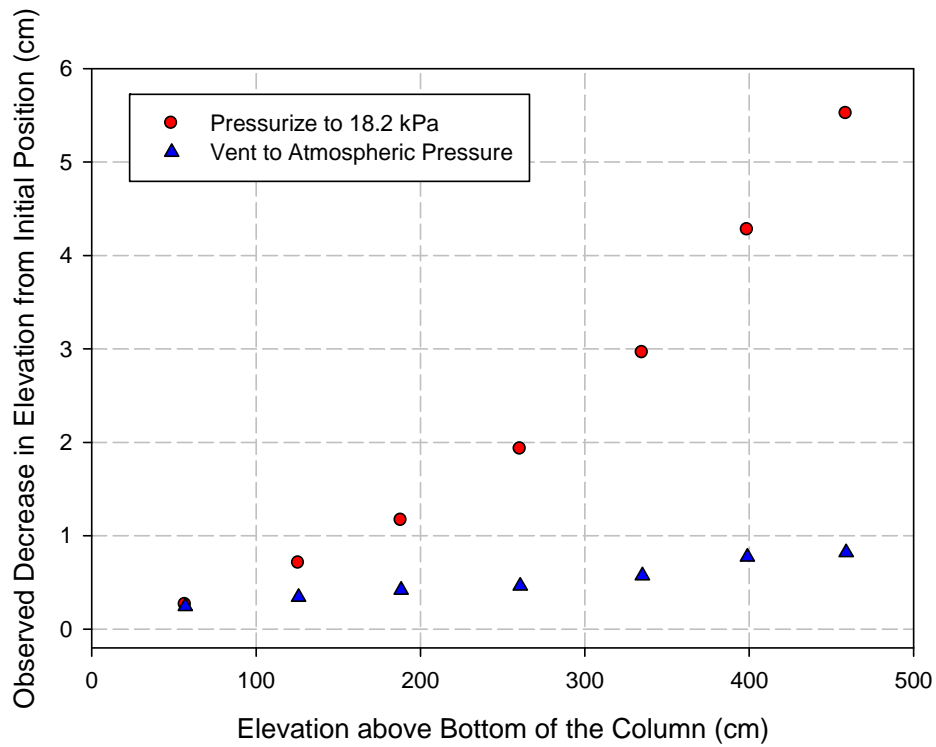**Figure 3.26**. Simulant Compression for Third Pressurization/Vent Cycle
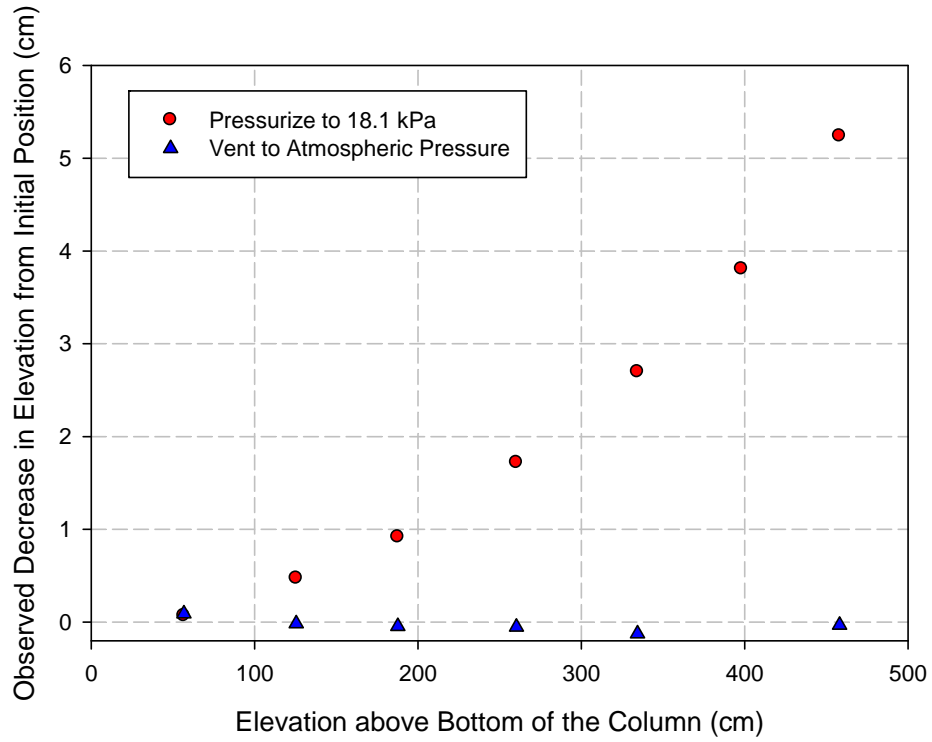
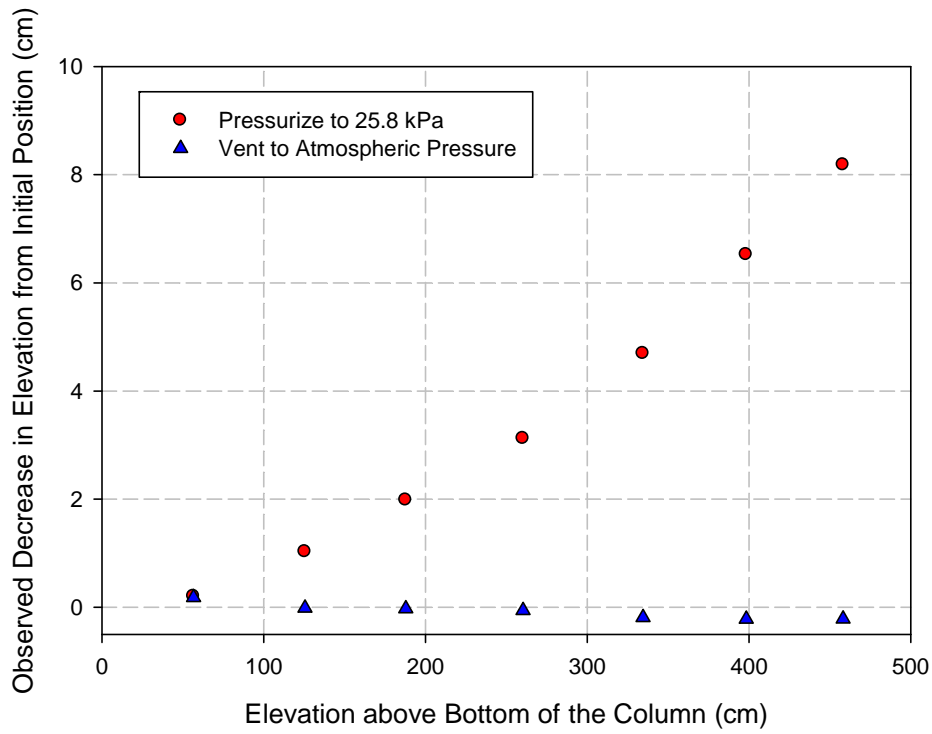**Figure 3.27**. Simulant Compression for Fourth Pressurization/Vent Cycle

Figure 3.28. Simulant Compression for Fifth Pressurization/Vent Cycle

After the first pressurization cycle, the bubbles/cracks return largely to their initial elevations after each pressurization cycle is complete. The third pressure cycle is a possible exception to this statement as the bubbles/cracks did not quite rebound to their initial locations in that test. Again, it is possible that this lack of complete rebound is associated with gas release because gas bubbles were observed exiting the liquid layer during the third pressurization.

As was discussed earlier, it is unclear at this time how to apply the compression test results toward the goal of estimating the vertical ϕ_{local} profile. The data are included here to aid in future efforts aimed at understanding the compression behavior of bubble-laden simulants similar to the kaolin-clay-based simulants used in this test program.

The data from the first compression in each of the two tests can be used estimate the average retained-gas fraction in the simulant. Equation 3.4 relates the average retained gas fraction to the measured simulant compression and compression-test conditions. This equation assumes zero friction between the acrylic column and the simulant. In addition, the retained gas is assumed to compress as an ideal gas in response to changes in the combined lithostatic/hydrostatic load without any interference from the yield strength of the simulant. The average retained gas fraction implied by the compression test is given by:

$$\phi_{avg} = \frac{1}{\Delta P}\left[\frac{\Delta h_c \rho_{gf}(1-\phi_{avg})g}{\ln\left(\frac{P_{atm}+P_{hyd}+\Delta P+\rho_{gf}(1-\phi_{avg})gh_s}{P_{atm}+P_{hyd}+\Delta P}\right)}\right] \tag{3.4}$$

where Δh_c = measured elevation change of simulant surface upon compression, m
ρ_{gf} = gas-free density of the sludge simulant, kg/m^3
g = gravitational acceleration, 9.81 m/s^2
ΔP = change in pressure at simulant surface upon compression, Pa
P_{atm} = atmospheric pressure, Pa
P_{hyd} = hydrostatic head above simulant surface before compression, Pa
h_s = simulant depth before compression, m

Note that Equation 3.4 is not explicitly solved for ϕ_{avg}, so finding ϕ_{avg} requires an iterative approach wherein the calculated ϕ_{avg} value is repeatedly substituted into the equation until the value converges.

In the compression test following d_{max} Test #1, the simulant-layer thickness before compression was 4.95 m, and there was a 0.31-m-thick water layer on top of the simulant.[1] The gas-free density of the simulant was 1,476 kg/m^3. Water was added to increase the hydrostatic pressure on the simulant by 9,080 Pa, and, in response, the simulant surface elevation decreased by 0.033 m. This observed compression implies, according to Equation 3.4, a ϕ_{avg} of 10.4 percent.

In the compression test following d_{max} Test #2, the simulant-layer thickness before compression was 4.98 m, and there was a 0.31-m-thick water layer on top of the simulant. The gas-free density of the simulant was 1,476 kg/m^3. Nitrogen was used to increase the pressure in the column headspace from atmospheric pressure to 8,560 Pa above atmospheric pressure. In response, the simulant surface elevation

---

[1] The simulant, water layer, and all added water were equilibrated with the laboratory room temperature, which ranged from 19 to 20°C during both sets of compression tests.

decreased by 0.037 m. This observed compression implies, according to Equation 3.4, a ϕ_{avg} of
12.2 percent. The ϕ_{avg} values estimated based on the compression tests are summarized in Table 3.1. For
comparison, the liquid-level-based estimate for ϕ_{avg} is included in the right-most column of the table. The
estimates for ϕ_{avg} based on the compression tests are lower than the liquid-level-based values. The
liquid-level-based values are more accurate, so the discrepancy is likely due to one of the complicating
effects that were assumed insignificant in the derivation of Equation 3.4 (e.g., negligible wall friction, the
retained gas is at hydrostatic/lithostatic pressure, and simulant yield stress does not affect the compression
test result). However, despite this discrepancy the compression-test-based ϕ_{avg} values are reasonably
consistent with those determined based on liquid-level measurements.

Table 3.1. ϕ_{avg} Estimated from Compression Tests

Test Number	Observed Compression (m)	Applied Pressure (Pa)	ϕ_{avg} based on Compression Test (%)	ϕ_{avg} based on Liquid Level (%)
1	0.033	9,080	10.4	14.6
2	0.037	8,560	12.2	15.1

3.1.5 Wall-Friction Measurements

Measurements were made to characterize the apparent friction between the simulant and the inside
walls of the acrylic column. A concern was raised that friction between the simulant and the column
walls could result in the simulant experiencing significantly less than the full hydrostatic/lithostatic load.
If the column walls significantly reduce the overburden load transmitted down through the simulant, then
the level at which gas channels are closed off, as predicted by d_{max} theory, would be significantly deeper
than predicted by Equation 1.1. The wall-friction measurements were performed in an effort to address
this concern.

Gas-generating sludge simulant was loaded into a single segment of the acrylic column used for the
intermediate-scale column d_{max} tests (see Section 2.1.7 for a more detailed description of the experimental
procedure). Once the retained-gas fraction in the simulant had peaked, nitrogen was introduced beneath
the simulant layer to lift it upward by approximately 10 cm. The nitrogen pressure required to maintain
the simulant in its lifted position was then measured. Nitrogen was released from beneath the simulant to
lower the simulant layer by several centimeters before the venting was ceased and the measurements
made of the pressure required to maintain the simulant in its new position. This same cycle of raising and
then lowering the simulant was then repeated.

Figure 3.29 shows the measured nitrogen gas pressure during this process. The triangular data points
indicate the gas pressure measurements made after the simulant was raised. The circular data points
indicate the gas pressure measurements made after the simulant was lowered. The horizontal dashed line
in the plot shows the hydrostatic/lithostatic head at the bottom of the simulant. This line indicates the gas
pressure expected if there is no friction between the simulant and the inside wall of the column. Raising
of the simulant layer is resisted by friction between the simulant and the acrylic wall, so the pressure
required to raise the simulant is greater than the no-friction gas pressure. Conversely, lowering the
simulant results in some of the simulant weight being supported by the wall friction, so the gas pressure
after lowering the simulant is less than the no-friction gas pressure.

After raising the simulant layer, the pressure stabilizes at between 82 and 85 cm of water head. This gas pressure is roughly 15 percent greater than the expected no-friction gas pressure of 72.5 cm. This result implies that wall friction between the simulant and the acrylic wall could support about 15 percent of the simulant weight with the remaining roughly 85 percent of the weight being transmitted down through the simulant.

Lowering the simulant layer gives a more complicated and harder-to-interpret result. When the simulant layer is lowered, the gas pressure required to support the simulant decreases to about 55 cm before slowly increasing on a timescale of hours. Eventually, the gas pressure exceeds the no-friction pressure before rapidly decreasing and then again slowly increasing. This behavior is likely due to the buildup and release of gas pressure from within the simulant. The generated gas is unlikely to be in direct contact with the nitrogen below the simulant because, as described in Section 2.1.7, a layer of gas-free simulant separates the nitrogen from the bubble-laden simulant. Gas generated in the simulant is not necessarily released immediately. Instead, the gas releases appear to be episodic, occurring every few hours. Gas accumulating in the simulant increases the pressure in the bubbles/cracks and in response the simulant attempts to expand within the column. Expansion of the simulant in the upward direction tends to decrease the residual wall-friction stress, which results in more pressure transmitted through the simulant and into the nitrogen. Expansion of the simulant in the downward direction also tends to increase the nitrogen pressure by reducing its volume. In both directions, then, expansion of the simulant results in increased nitrogen pressure. Eventually, the generated gas is rapidly released and the simulant contracts, thereby resulting in a rapid reduction in the nitrogen pressure.

Figure 3.30 shows the continuation of this pressure-variation behavior over a 23-hour period. The first data point represents the time at which the simulant was initially lowered. The pressure variations that follow are the result of gas-generation-induced changes in the apparent wall friction.
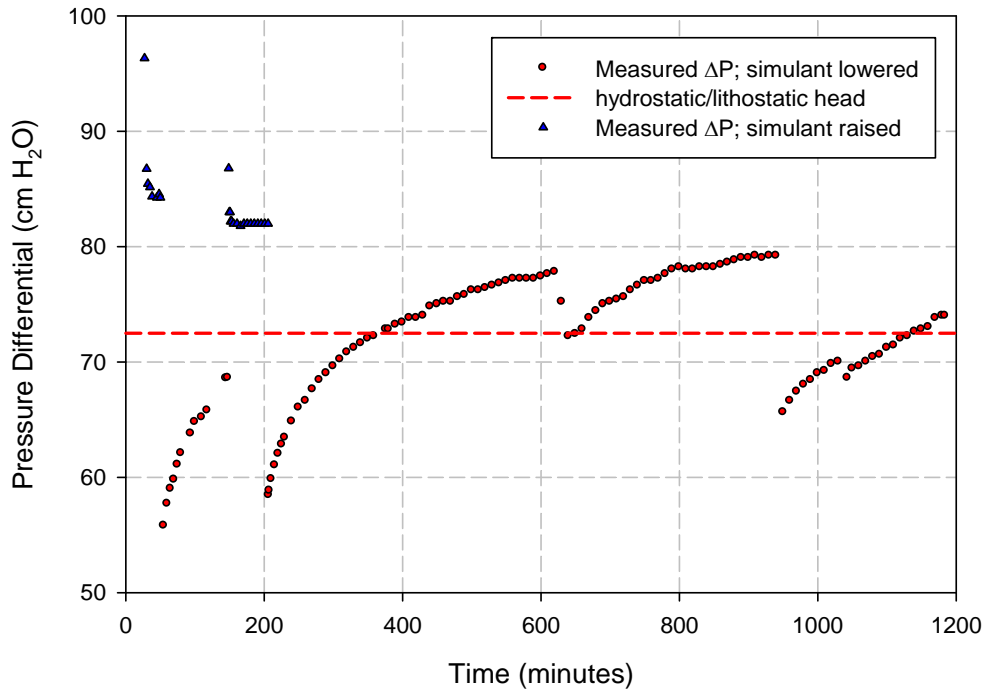
Figure 3.29. Gas Pressure Supporting Simulant; Simulant Raised and Lowered
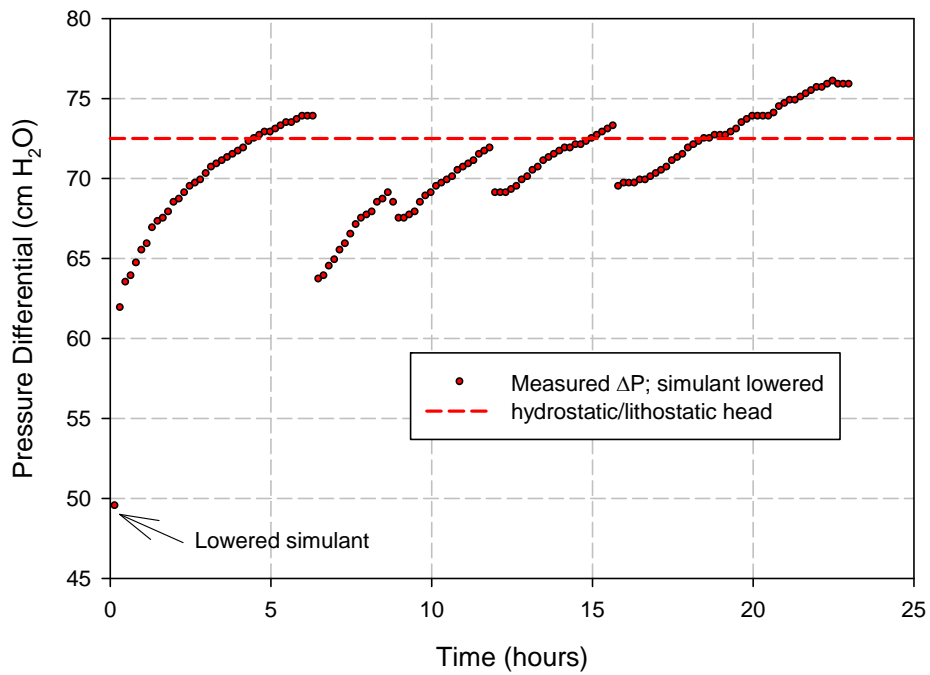

Figure 3.30. Gas Pressure Supporting Simulant; Simulant Lowered

The results of the wall-friction tests help address the concern that wall friction may have adversely affected the intermediate-scale column d_{max} tests. First, a wall-friction effect appears to exist, and the data collected when raising the simulant layer implies it amounts to about 15 percent of the simulant weight. Second, because the gas generation and release behavior of the simulant results in continual expansion and contraction of the simulant it is likely that the magnitude of the wall-friction effect varies with time. When the simulant layer is rising in the column, the wall-friction effect tends to *increase* the pressure transmitted down through the simulant to levels that are higher than the simulant hydrostatic/lithostatic head. After the retained gas fraction reaches its peak and begins to decrease, the simulant layer tends to move downward in the column and this movement, combined with the wall-friction effect, is expected to result in a decrease in the pressure transmitted through the simulant. However, the continuing gas generation and release effects are likely to result in the transmitted pressure varying slightly above and slight below the hydrostatic/lithostatic head as was observed in Figure 3.30.

In summary, the wall-friction tests demonstrate that the overburden load is effectively transmitted down through the simulant and the wall effects are relatively minor. Consequently, the intermediate-scale column d_{max} tests were not adversely affected by the wall effects and the depth of simulant used for the tests (4.3 m) was sufficient to ensure that observations of retained-gas fraction could be made at depths well below the calculated d_{max}.

3.2 Open-Channel-Depth Test Results

Open-channel-depth tests were conducted to directly measure the predictions of d_{max} theory. Equation 1.1 allows direct calculation of the predicted maximum depth to which a circular channel will be closed off by the action of overburden pressure on the sludge. The open-channel-depth tests were conducted as described in Section 2.2. This section provides the results of the tests.

Table 3.2 lists the results of the open-channel-depth tests. Simulant shear strength varied from less than 100 Pa to nearly 2000 Pa and the measured open channel depths varied from 7 to 92 cm

Table 3.2. Open-Channel-Depth Test Results

Shear Strength (Pa)	Weight Percent Solids (wt%)	Open Channel Depth (cm)
81	44.60	7
251	48.92	15
614	52.50	26
1030	55.80	38
1270	56.49	49
1980	58.87	92

The open-channel-depth results are compared with d_{max} theory predictions for kaolin clay sludge simulant in Figure 3.31. Two sets of d_{max} theory predictions are provided in the figure. The black line represents the predictions that result when conservative assumptions are made for the Equation 1.1 input parameters. The red dashed line represents the predictions when the expected parameter values are used. Please refer to Section 1.1 for a discussion of the conservative and expected parameter values. If the d_{max} theory predictions are accurate, the open-channel-depth test results should be consistent with the calculated d_{max} values. The open-channel-depth results in Figure 3.31 clearly show the measured open

channel depths are significantly shallower than predicted by d_{max} theory. The difference between the predicted and measured values is approximately an order of magnitude. Clearly, d_{max} theory greatly overestimates the maximum open channel depth.

There are three important implications of these results. First, according to Figure 3.31, the measured d_{max} for a sludge simulant with a shear strength of 400 Pa is approximately 22 cm. The intermediate-scale column d_{max} tests used sludge simulants with shear strengths lower than 400 Pa; thus, the d_{max} in those tests should have been approximately 22 cm or less. Per d_{max} theory, both intermediate-scale column d_{max} tests, which used an initial simulant depth of 4.3 m, should have seen increased gas retention in the deeper simulant layers. A 4.3-m simulant depth is nearly 20 times the measured 22-cm d_{max} indicated in Figure 3.31. As discussed in Section 3.1.3, no increase in retained-gas fraction in the lower simulant layers was observed.

The second implication of this result is that Equation 1.1 significantly over-predicts d_{max}. It is beyond the scope of this document to diagnose the reason for this discrepancy, but there clearly is adjustment needed to d_{max} theory before it can be said to predict d_{max} with a useful degree of accuracy.

The third implication of this result is that d_{max} theory apparently does not correctly describe the mechanism by which gas is released and retained from gas-generating sediments. The results of the testing described in this report and previously by others (e.g., Gauglitz et al. 2012) show that gas is released from depths much deeper than the measured d_{max}. If gas-retention behavior actually changed at depths deeper than the d_{max} measured by the open-channel-depth tests, that change in behavior should have been observed by previous investigators as well as during the tests described in this report.

According to d_{max} theory, an interconnected network of gas flow channels forms at depths shallower than d_{max} and these channels allow more-or-less continuous release of the generated gas. Further, visual observations made during the d_{max} testing as well as the wall-friction test results (Section 3.1.5) imply that gas release tends to occur episodically rather than continuously. This difference in gas-release behavior may imply that a conceptually different model is needed to accurately describe and predict gas retention in sludge layers.
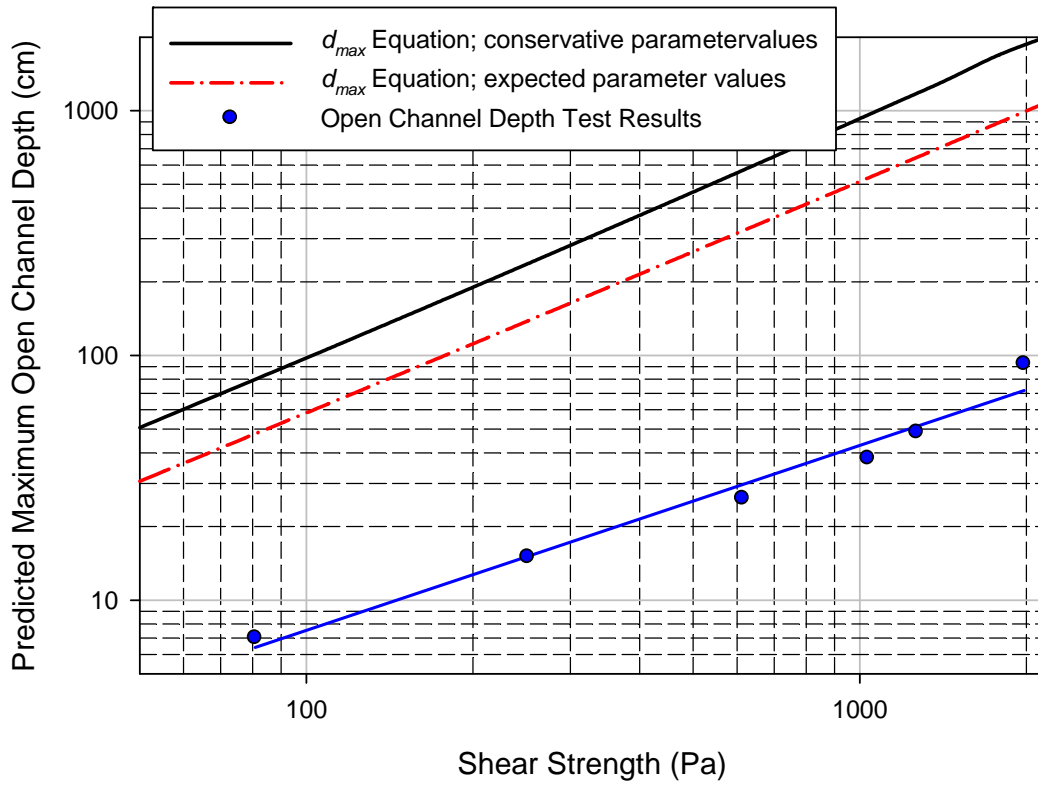
Figure 3.31. Open-Channel-Depth Results Compared with d_{max} Theory Predictions

4.0   Conclusions

The work described in this document was focused on the goal of evaluating the accuracy of d_{max} theory as it pertains to predicting gas retention in gas-generating sludge layers within the double-shell tanks at the Hanford Site. Based on this work, the following conclusions can be drawn:

- The d_{max} tests conducted in the intermediate-scale column demonstrated no increase in retained-gas fraction at depths below d_{max}. This result is in direct contradiction with the predictions of d_{max} theory.

- The open-channel-depth tests revealed that d_{max} theory significantly overestimates d_{max}.

- The d_{max} depths measured by the open-channel-depth testing are sufficiently shallow that the change in gas retention predicted by d_{max} theory should have been readily observed, not only in the intermediate-scale column d_{max} tests, but also in similar, but shallower experiments conducted by others (e.g., Gauglitz et al. 2012).

Taken together, these conclusions imply that d_{max} theory does not accurately reflect the actual gas-retention behavior in sludge layers. Further, the core prediction of d_{max} theory that gas retention increases significantly at depths deeper than d_{max} appears to be incorrect.

In addition to the conclusions listed above, the testing revealed a need for additional work to improve understanding of both the simulant compression tests and the use of ultrasonic attenuation for characterization of retained-gas fraction. Both the simulant compression test and ultrasonic attenuation measurements are planned for use in the tall-column d_{max} experiments. Based on our current level of understanding, the simulant compression tests are not likely to directly yield estimates for the retained-gas-fraction profile. The utility of ultrasonically measured GVF was not demonstrated to a sufficiently accurate level in the present test column. However, this shortcoming may be due largely to the effect of the intermediate-scale column's relatively small diameter. Testing in larger-diameter columns (e.g., the tall column d_{max} tests) may prove the ultrasonic technique to be both useful and sufficiently accurate to characterize the retained-gas profile.

5.0   References

Anderson AL and LD Hampton. 1980. "Acoustics of gas-bearing sediments I: Background." *Journal of the Acoustical Society of America.* **67**:1865-1889.

Bontha JR, JJ Jenks, GP Morgen, TJ Peters, WA Wilcox, HE Adkins, CA Burns, MS Greenwood, PJ MacFarlan, KM Denslow, PP Schonewill, J Blanchard, and EB Baer. 2010. *Evaluation of Slurry Transfer Line Critical Velocity Measurement Instruments.* PNNL-19441 Rev. 0, Pacific Northwest National Laboratory, Richland, Washington.

Crosato A. 1998. "Non-Homogeneous Mud Structure at Consolidation." Report DM16. *Drainage System Behavior.* August 2005, z2313.10. Delft Hydraulics.

Gauglitz PA, WC Buchmiller, SG Probert, and AT Owen. 2012. *Strong-Sludge Gas Retention and Release Mechanisms in Clay Simulants.* PNNL-21167 Rev 0, EMSP-RPT-013, Pacific Northwest National Laboratory, Richland, Washington.

Kepkay PE and RC Cooke. 1978. "Velocity of Sound as a Function of Bubble Distribution in Gas-bearing Sediments." *Geophysical Research Letters.* **5**:1071-1073.

Lide DR, editor. 2003. *Handbook of Chemistry and Physics.* CRC Press, New York.

van Kessel T and WGM van Kesteren. 2002. "Gas Production and Transport in Artificial Sludge Depots." *Waste Management.* **22**:19-28.

Wells BE, JJ Jenks, G Boeringa, NN Bauman, and AD Guzman. 2010. *Lateral Earth Pressure at Rest and Shear Modulus Measurements on Hanford Sludge Simulants.* PNNL-19829, Pacific Northwest National Laboratory, Richland, Washington.

Wichman BGHM, GC Sills, and R Gonzalez. 2000. "Experimental validation of a finite strain theory for gassy mud." *Can. Geotech. J.* **37**:1227-1240.

Wilkens RH and MD Richardson. 1998. "The influence of gas bubbles on sediment acoustic properties: in situ, laboratory, and theoretical results from Eckernforde Bay, Baltic sea." *Continental Shelf Research* **18**:1859-1892.

Wilson PS, AH Reed, WT Wood, and RA Roy. 2008. "The low-frequency sound speed of fluid-like gas-bearing sediments." *Journal of the Acoustical Society of America Express Letters*. **123**:EL99-EL104.

Distribution

No. of **Copies**		No. of **Copies**	

OFFSITE

1   M Epstein
     Fauske and Associates, LLC
     1118 3rd Street, #308
     Santa Monica, CA 90403

1   G Terrones
     Applied Physics Division (X-4)
     MS: T086
     Los Alamos National Laboratory
     Los Alamos, NM 87545

3   Savannah River National Laboratory
     Savannah River Site
     Aiken, SC 29808
     D Koopman
     C Nash
     B Wilmarth

1   RD Holtz
     Civil & Environmental Engineering
     University of Washington
     201 More Hall, Box 352700
     Seattle, WA 98195-2700

ONSITE

1   **DOE Office of River Protection**

     BJ Stickney   H6-60

7   **Washington River Protection Solutions**

     WB Barton   S7-90
     R Calmus   H8-04
     JM Grigsby   S7-90
     NW Kirch   R2-58
     DB Little   R2-58
     JE Meacham   R2-58
     TL Sams   R2-52

19   **Pacific Northwest National Laboratory**

     RC Daniel   P7-22
     JM Davis   K6-24
     KM Denslow   K5-26
     CM Fischer   K6-24
     PA Gauglitz (5)   K7-15
     DJ Heldebrant   K2-44
     MR Powell   K6-24
     M Prowant   K5-26
     SD Rassat   K6-28
     DR Rector   K7-15
     S Sande   K6-01
     PP Schonewill   P7-25
     MR Telander   K3-80
     BE Wells   K7-15
     Project Records

Pacific Northwest
NATIONAL LABORATORY

Proudly Operated by **Battelle** *Since 1965*

U.S. DEPARTMENT OF
ENERGY

902 Battelle Boulevard
P.O. Box 999
Richland, WA 99352
1-888-375-PNNL (7665)
www.pnl.gov